Energy Research and Development Division
FINAL PROJECT REPORT

OPTIMIZING CONCENTRATING SOLAR POWER WITH THERMAL ENERGY STORAGE SYSTEMS IN CALIFORNIA

Final Report

Appendix A-G

Prepared for: California Energy Commission
Prepared by: DNV GL

DECEMBER 2014
CEC-500-2015-078-AP

APPENDICES

Appendix A: KERMIT Model.....

Appendix B: Production Cost Modeling .....

Appendix C: Renewable Generation Modeling.....

Appendix D: Thermodynamic Plant Models.....

Appendix E: Detailed Results from Thermodynamic Plant Model Simulations.....

Appendix F: MGO - Operational Optimization Model.....

Appendix G: Input Data for MGO 2020 Simulations.....

Appendix A:
KERMIT Model

KERMIT Model Architecture

KERMIT is DNV GL's proprietary software to study the impact of non-dispatchable resources, energy storage and new technologies on electric power systems. The model incorporates AGC response to non-fault events such as generator trips, sudden load rejection, and volatile renewable resources (wind and solar). The input includes data on power plants, wind and solar production, daily load, hourly generation schedule, interchange schedules, system inertias and interconnection model, balancing and regulation, as well as new technologies such as Energy Storage. The output includes ACE, power plant output, area interchange frequency deviation, real-time dispatch requirements and results, and numerous other dynamic variables. A conceptual overview of the KERMIT dynamic model is shown in Figure 92, while Figure 93 shows a representation of the KERMIT Simulink Graphical User Interface (GUI). Blocks 1 to 8 aim to balance any mismatch between hourly schedule and actual load. Block 2 takes hourly generation schedules from both conventional and renewable plants along with the actual real-time load (block 1) to calculate the actual import requirements. Block 4 represents the AGC in which up and down regulation requirements are obtained comparing scheduled generation and import, with their respective actual quantities (block 3). The third balancing entity (block 6) is to obtain 5-min load-following requirements. This load-following block takes scheduled renewable generation and its forecast as inputs (block 5) and gives load-following requirements up and down. Finally, a 5-min market balancing model (block 8) is used to compute the increase or decrease of each plant to their scheduled generation, taking into account scheduled generation and import, actual generation and import, and generation bids for increase or decrease (block 7). In KERMIT, the dynamics of conventional generations are modeled using Institute of Electrical and Electronics Engineers (IEEE) standards (block 10). This block takes inputs of up/down regulation requirements, up/down load-following signals, and requests for increase/decrease of each plant to schedules (block 9), and according to the dynamics of each plant, determines what the actual MW output of each plant type would be. Dynamic variables obtained through this simulation, such as actual generation and ACE, can be further post-processed to study different aspects of the performance of system such as average ACE, maximum ACE, CPS1, CPS2, and so forth. It should be noted that KERMIT is a system dynamics simulation tool, which is run for consecutive time intervals over a specified time horizon, typically 24 hours.

Figure 1: Conceptual Overview of KERMIT

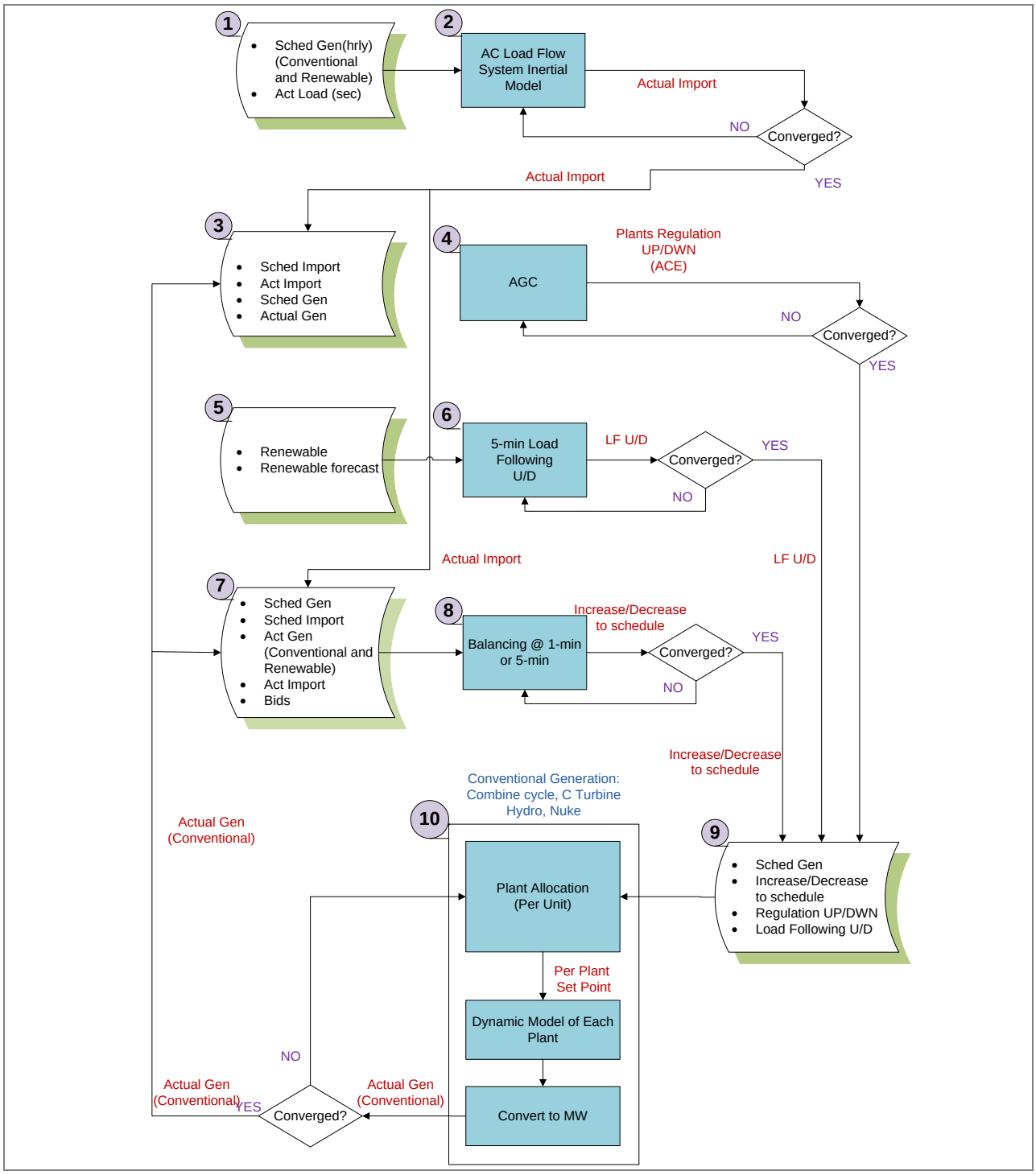

Source: DNV GL

Figure 2: Schematic Representation of KERMIT Simulation

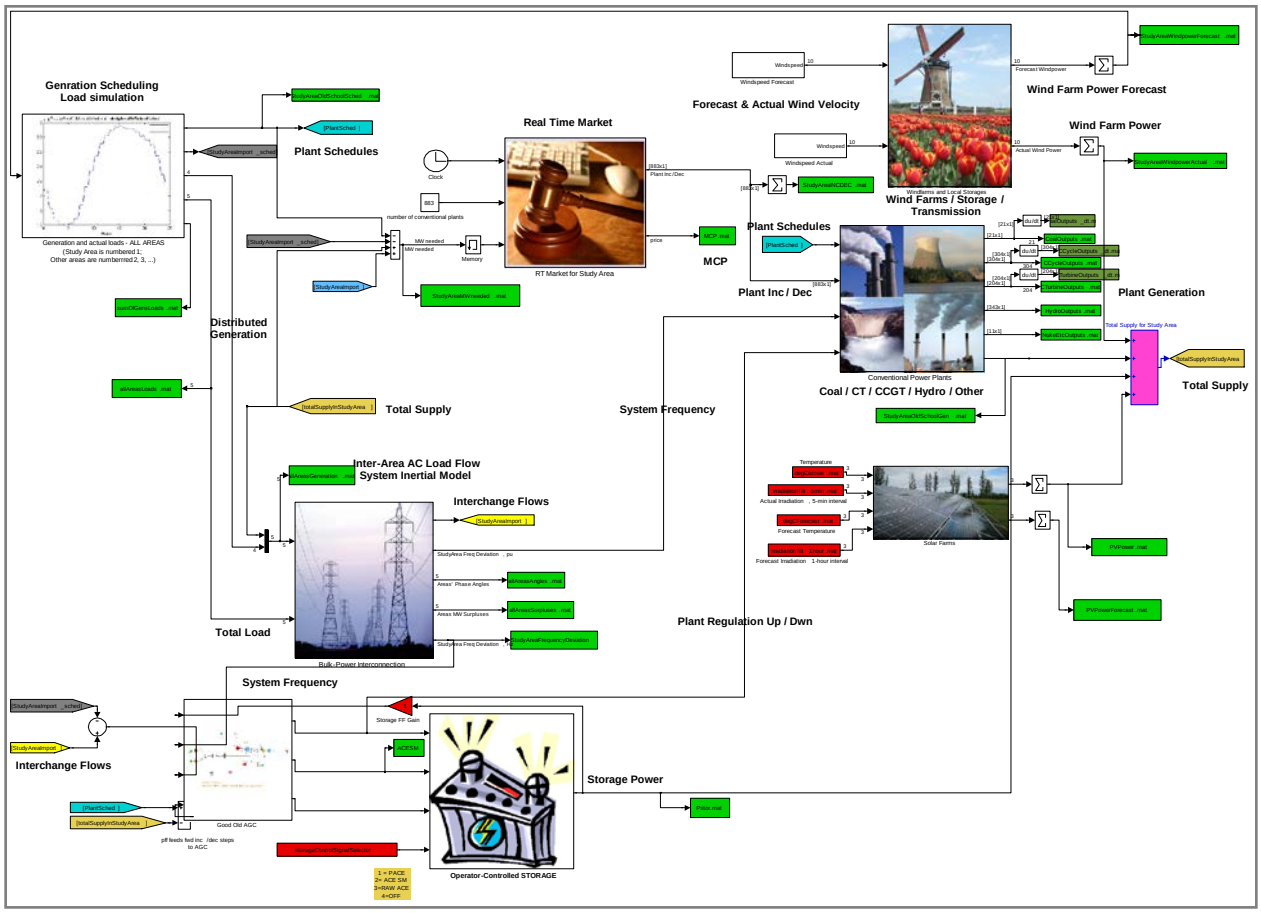

Source: DNV GL

Modeling CSP-TES in KERMIT

In this section, the methodology used to model CSP-TES systems in MATLAB Simulink is described (see Figure 94 for an overview of the CSP-TES model). Each sub-section roughly corresponds to a sub-block in the Simulink model. In the following sub-sections, the relevant underlying thermodynamic equations and simplifying assumptions are presented.

Figure 3: Flowchart of CSP-TES Model in KERMIT

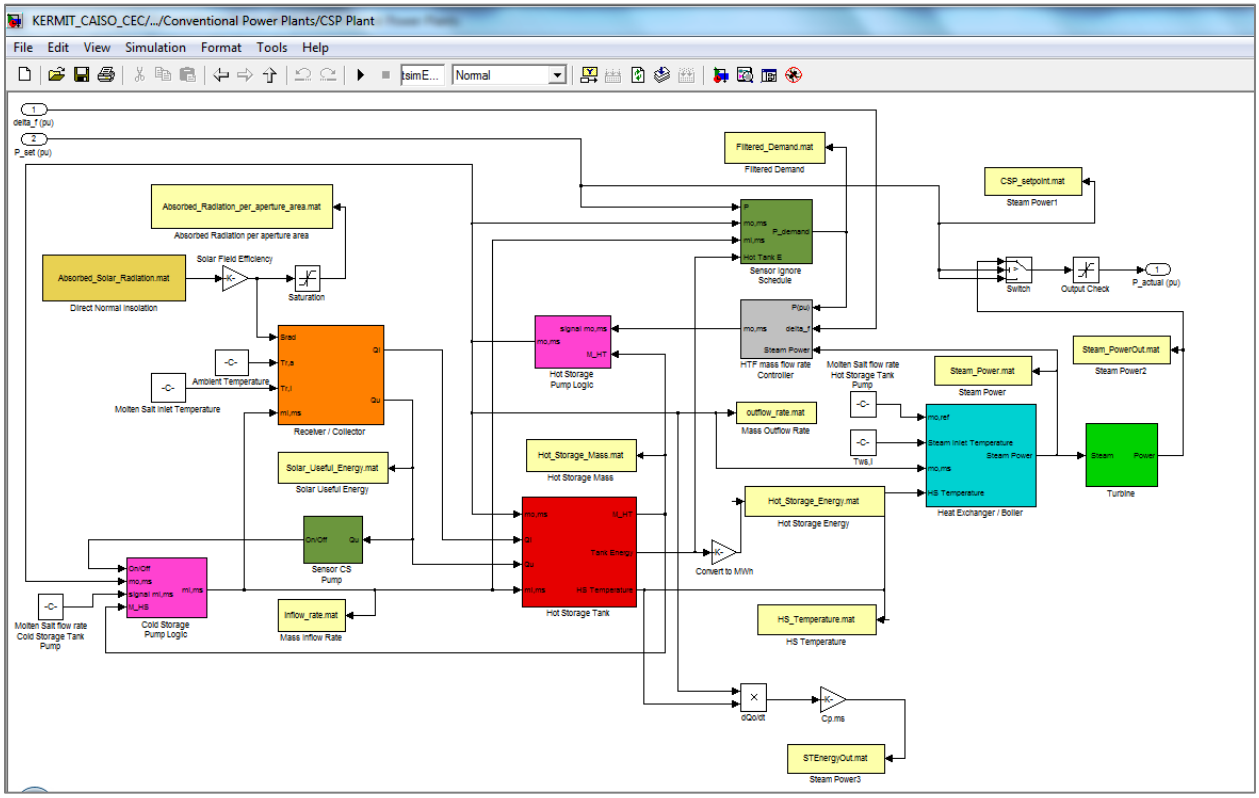

Source: DNV GL

The CSP-TES model used for the first phase of this study consists of a collector field and a tower receiver on the CSP side, and two-tank direct storage on the TES side. The heat transfer fluid (HTF) is molten salt. Molten salt, at 290°C (554°F), is pumped from a "cold" storage tank through the receiver where it is heated to 565°C (1,049°F) and then into a "hot" tank for storage. When power is needed from the plant, the HTF is pumped from the “hot” tank to a steam generating system for a conventional Rankine-cycle turbine/generator system, and then to the "cold" storage tank, and eventually cycles to the receiver again for heating. In a typical installation, solar energy collection occurs at a rate that exceeds the maximum required to provide steam to the turbine and, therefore, the storage system can be charged at the same time that the plant is producing power at full capacity.

Solar Field Model

Extraterrestrial solar radiation follows a direct line from the sun to the earth. Upon entering the earth’s atmosphere, some solar radiation is diffused by air, water droplets, and dust within the atmosphere. The direct normal insolation (DNI), denoted by I_a, represents the portion of solar radiation reaching the surface of the earth that has not been scattered or absorbed by the atmosphere. It can be defined as the rate at which direct radiant energy is incident on a surface per unit area of surface with units of [W/m^2].

The radiation absorbed by the receiver, denoted by S [W/m²], is some fraction of the DNI, adjusted for incidence angle, row shading, solar field availability, collector cleanliness, and the collector field surface properties. In other words, it is the difference between the DNI and the optical losses. In our model, this effect is simplified to only one efficiency factor named "Solar Field Efficiency" in the control panel, or η_{opt}. Thus,

$$S = \eta_{opt} I_a \qquad (1)$$

The collector includes the receiver and concentrator. The receiver is the element where the radiation is absorbed and converted to some other energy form. The concentrator is the element that directs radiation onto the receiver. The aperture of the concentrator is the opening through which the solar radiation enters the concentrator.

The performance of a concentrating collector is described by the differential equation that governs the energy balance,

$$\dot{Q}_u = F_r \left(\dot{Q}_{opt} - \dot{Q}_{loss} \right) \qquad (2)$$

where $\dot{Q}_u$ [W] is the collector/receiver useful gain, which can be interpreted as the rate of useful energy extracted by the collector/receiver, $\dot{Q}_{opt}$ [W] is the rate of optical radiation incident on the receiver, $\dot{Q}_{loss}$ [W] is the rate of thermal energy loss from the receiver, and F_r is a flow correction factor to account for temperature gradients along the receiver, set to 0.95 in our Simulink model. The flow factor allows us to use the inlet fluid temperatures in subsequent energy balance calculations.

The solar energy collection efficiency η is defined as the ratio of the rate of useful thermal energy leaving the collector, to the solar irradiance falling on the aperture area:

$$\eta = \frac{\dot{Q}_u}{A_a I_a} \qquad (3)$$

where A_a [m²] is the aperture area of the collector and I_a [W/m²] is the solar DNI falling on collector aperture area.

The optical efficiency of a solar collector, denoted by η_{opt}, is defined as the ratio of the rate of optical energy reaching the receiver to the solar radiation falling on the collector aperture area. Thus,

$$\eta_{opt} = \frac{\dot{Q}_{opt}}{A_a I_a} \qquad (4)$$

where A_a [m²] is the aperture area of the collector and I_a [W/m²] is the solar DNI falling on collector aperture area. Substituting (1) into (4) and rearranging, the equation obtained is

$$\dot{Q}_{opt} = \eta_{opt} I_a A_a = SA_a \qquad (5)$$

Using the appropriate equations for the thermal losses, the equation obtained is

$$\dot{Q}_{loss} = A_r U_L \left(T_i - T_a^R\right) \qquad (6)$$

where A_r [m²] is the receiver area, A_a [m²] is the aperture area, T_i [K] is the inlet temperature of the HTF, and T_a^R [K] is the ambient temperature surrounding the receiver, assumed to be constant at 25°C. The loss coefficient, U_L, must be estimated based on the area of the receiver. Since high temperatures are encountered in the concentrating collectors, the loss coefficient becomes temperature dependent and its calculation is complex. In our model assumes U_L is a constant value. It is estimated according to

$$U_L = \frac{(1-\eta_{rcvr})C_r}{A_r(T_i - T_a^R)} \qquad (7)$$

where η_{rcvr} is the receiver efficiency and C_r [MWt] is the receiver capacity.

Substituting (5) and (6) into (2), the following equation is obtained for the useful gain:

$$\dot{Q}_u = F_R A_a \left[S(t) - \frac{A_r}{A_a} U_L \left(T_i - T_a^R\right) \right] \qquad (8)$$

By defining the concentration ratio as $C = A_a / A_r$ the final expression is obtained for the useful gain, which is used in the Simulink model, as

$$\dot{Q}_u = F_R A_a \left[S(t) - \frac{U_L}{C} \left(T_i - T_a^R\right) \right] \qquad (9)$$

Another source of power that passes through the receiver originates from the HTF from the cold tank, which is expressed as

$$\dot{Q}_i = \dot{m}_i C_{p,HTF} T_i \qquad (10)$$

where $\dot{m}_i$ [kg/s] is the mass flow rate of the HTF from the cold storage tank through the receiver, and $C_{p,HTF}$ [J/(kgK)] is the specific heat at constant pressure of the HTF. The tower model built in Simulink is illustrated in Figure 95.

Figure 4: Tower Model; Simulink

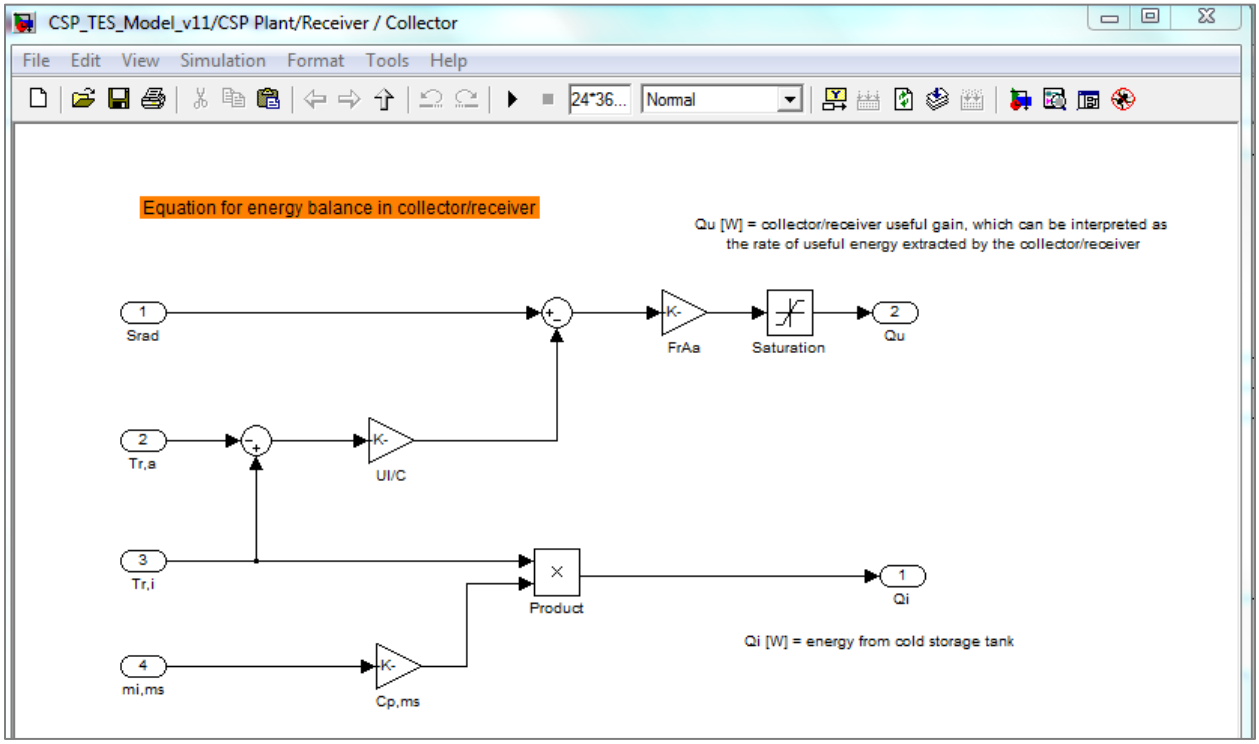

Source: DNV GL

Energy Storage

To model the energy stored in the hot tank, the energy and mass balances due to inflows and outflows of the HTF is considered. The energy in the hot storage tank is governed by the following differential equation:

$$\dot{Q}_H = \dot{Q}_{in} - \dot{Q}_{out} = \dot{Q}_i + \dot{Q}_u - \dot{Q}_{out} \qquad (11)$$

where $\dot{Q}_H$ [W] represents the net rate of change in energy in the hot storage tank, $\dot{Q}_{in}$ [W] represents the power into the tank as a result of input HTF from the solar receiver, and $\dot{Q}_{out}$ [W] represents the power leaving the tank as a result of output HTF to the heat exchanger. $\dot{Q}_i$ [W] and $\dot{Q}_u$ [W] are defined by (9) and (10) as wel as in Figure 95. Moreover, $\dot{Q}_{out}$ is expressed as

$$\dot{Q}_{out} = \dot{m}_o C_{p,HTF} T_H \qquad (12)$$

where $\dot{m}_o$ [kg/s] is the mass flow rate of the HTF out of the hot storage tank and T_H [K] is the temperature of the HTF at the exit of the hot storage tank. Substituting (12) into (11), the equation obtained is

$$\dot{Q}_H = \dot{Q}_i + \dot{Q}_u - \dot{m}_o C_{p,HTF} T_H \qquad (13)$$

which is integrated to obtain the energy stored in the hot tank at each time step of the simulation. Thus,

$$Q_H = \int_0^{t_f} \dot{Q}_i + \dot{Q}_u - \dot{m}_o C_{p,HTF} T_H dt, \;\; Q_H(0) = 0 \qquad (14)$$

Commensurate with the zero energy initial condition, it is assumed the mass of the HTF inside the hot storage tank is also zero at simulation start. A mass balance is applied to obtain the mass of the HTF in the hot storage tank at each time step during the simulation. The mass balance is governed by the following differential equation:

$$\dot{m}_H = \dot{m}_i + \dot{m}_o \qquad (15)$$

Integrating, the equation obtained is

$$m_H = \int_0^{t_f} \dot{m}_i + \dot{m}_o dt, \;\; m_H(0) = 0 \qquad (16)$$

It is assumed that the storage unit is fully mixed and unstratified, hence it operates at uniform temperature, T_H, which can now be solved as

$$T_H = \frac{Q_H}{m_H C_{p,HTF}} \qquad (17)$$

The hot tank modeled in Simulink is shown in Figure 96.

Figure 5: Hot Tank Model; Simulink

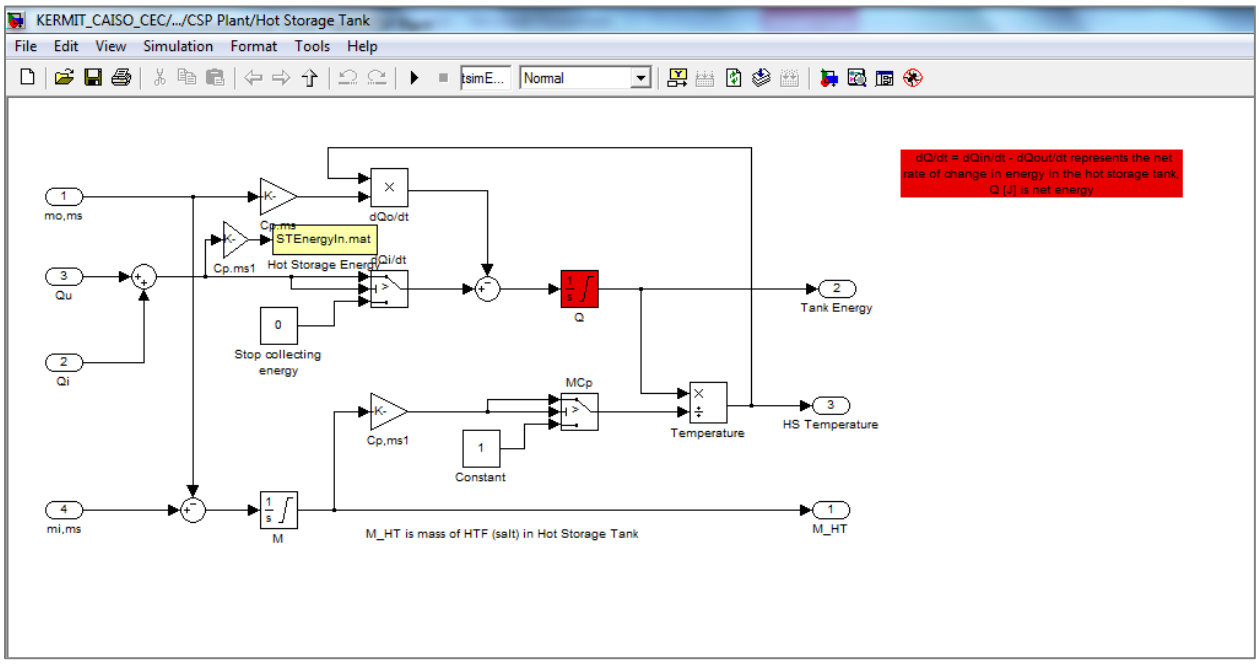

Source: DNV GL

Cold Storage Pump Logic

The HTF discharge rate from the cold tank is assumed equal to the HTF charge rate into the hot tank, which is denoted by $\dot{m}_i$. The nominal HTF charge rate, denoted by $\dot{m}_i^n$, is calculated based on the capacity of the receiver (in other words, the rate of energy transfer in the receiver limits the HTP flow rate) as follows:

$$\dot{m}_i^n = \frac{0.7C_r}{C_{p,HTF}(T_H - T_C)} \qquad (18)$$

where T_C [K] represents the temperature of the cold storage tank. The constant 0.7 is, for the present, hardcoded into the control panel and represents the losses that occur through the piping as the HTF travels from the cold storage to the receiver.

The cold storage pump, then, adheres to the following logic:

1. If hot storage is full, $\dot{m}_i = \dot{m}_o$

   If hot storage is not full $\dot{m}_i = \dot{m}_i^n$
2. If useful gain $\dot{Q}_u > 0$, $\dot{m}_i$ remains unchanged from previous logic statement

   If useful gain $\dot{Q}_u \leq 0$, $\dot{m}_i = 0$

The current implementation of mass flow rate is a simplification; the flow rate should vary continuously to achieve some design objective via a closed-loop control.

Hot Storage Pump Logic

The maximum amount of energy that can be stored in the hot tank, denoted as $E_{\max}$, is where M_H [kg] is the maximum amount of HTF that the hot storage can contain. In the current implementation, the hot storage does not begin discharge until $0.5E_{\max}$ is reached. The tank is allowed to discharge until only $0.05E_{\max}$ remains in the tank. These threshold values are user-defined.

$$E_{\max} = M_H C_{p,HTF} T_H \qquad (19)$$

The outflow control is more complicated as it varies the rate of flow continuously to achieve some design objective via a closed-loop proportional-integral (PI) control scheme. The HTF outflow is controlled by tracking the steam power output from the heat exchanger stage (as explained later) to the reference power requested for the CSP.

Heat Exchanger (Boiler and Condenser)

Boilers and condensers are examples of heat exchangers. For instance, the heat exchanger provides means for transferring heat from the "hot" to the "cold" fluid that will propel the turbine, namely steam. The heat transfer usually involves convection in each fluid and conduction through the "wall" that separates the two fluids.

The total resistance of the heat exchanger, considering the individual resistances due to convection and conduction through the pipes and walls and the exchanger geometry, is given by

$$R_{Total} = R_i + R_{wall} + R_o = \frac{1}{h_i A_i} + \frac{\ln(d_o/d_i)}{2\pi kL} + \frac{1}{h_o A_o} \qquad (20)$$

where d [m] is the tube diameter, L [m] is the length, h [$Jm^{-2}s^{-1}K^{-1}$] is the convection coefficient, k [$Jm^{-1}s^{-1}K^{-1}$] is the thermal conductivity of the "wall", and A [m^2] is the area normal to the heat flow. The subscripts $i, o, wall$ refer to inner, outer and wall resistances.

The total thermal resistance is expressed as a function related to the overall heat transfer coefficient U [$Jm^{-2}s^{-1}K^{-1}$]

$$Q = K_Q \Delta T = \frac{\Delta T}{R_{Total}} = UA\Delta T \quad \Leftrightarrow \quad R_{Total} = \frac{1}{UA} \qquad (21)$$

Here, UA is referred to as the overall heat transfer conductance-area product. The UA for the heat exchanger at the reference state is provided as a parameter to the exchanger model. At partial loads, the UA decreases with decreasing flow rates of the fluid streams. The UA can be calculated from a reference full-load state, the data for which would be provided with the heat exchanger, according to the following relationship:

$$\frac{UA}{UA_{ref}} = \left(\frac{\dot{m}_o}{\dot{m}_{o,ref}} \right)^{0.8} \qquad (22)$$

The method chosen to obtain the rate of heat transfer is the effectiveness-NTU (number of transfer units) method. It is based on the heat transfer effectiveness ε, defined as

$$\varepsilon = \frac{\dot{Q}}{\dot{Q}_{\max}} \qquad (23)$$

Where $\dot{Q}$ is the actual heat transfer rate and $\dot{Q}_{\max}$ is the maximum possible heat transfer rate. The effectiveness also facilitates comparison between different types of heat exchangers for the purposes of selecting the best one to accomplish a particular heat transfer objective.

To evaluate $\dot{Q}_{\max}$, the heat capacitance rate of each fluid stream is defined. The heat capacitance rate of a given stream is expressed as a product of its mass flow rate and its specific heat, hence, the capacitances of the HTF and the steam are expressed as

$$\dot{C}_C = \dot{m}_{steam} C_{p,steam} \qquad (24)$$

$$\dot{C}_H = \dot{m}_o C_{p,HTF} \qquad (25)$$

where $\dot{C}_C$ [W/K] denotes the capacitance rate of the cold side fluid (steam) and $\dot{C}_H$ [W/K] denotes the capacitance rate of the hot side fluid (HTF).

Define $\dot{C}_{\min} = \min(\dot{C}_C, \dot{C}_H)$, then the maximum heat transfer possible between streams is

$$\dot{Q}_{\max} = \dot{C}_{\min} \left(T_{HTF,in} - T_{steam,in} \right) \qquad (26)$$

The effectiveness-NTU method involves the dimensionless number of transfer units NTU and capacity ratio which are defined as

$$NTU = \frac{UA}{\dot{C}_{\min}} \qquad (27)$$

$$c = \frac{\dot{C}_{\min}}{\dot{C}_{\max}} \qquad (28)$$

For a shell-and-tube Heat Exchanger, the most commonly used in solar power plants,

$$\varepsilon = \frac{2}{\left[1 + c + \sqrt{1+c^2}\,\frac{1+e^{-NTU\sqrt{1+c^2}}}{1-e^{-NTU\sqrt{1+c^2}}}\right]} \qquad (29)$$

and therefore,

$$NTU = -\frac{1}{\sqrt{1+c^2}} \ln\left(\frac{\frac{2}{\varepsilon} - 1 - c - \sqrt{1+c^2}}{\frac{2}{\varepsilon} - 1 - c + \sqrt{1+c^2}}\right) \qquad (30)$$

In changing phase from saturated liquid to saturated vapor, the heat capacitance of the feedwater/steam is infinite. Therefore, the minimum capacitance of the two fluids is always the capacitance of the hot side fluid ($\dot{C}_{\min} = \dot{C}_H$). Accordingly, $c \to 0$. Thus (29) and (30) simplify to

$$\varepsilon = 1 - \exp(-NTU) \qquad (31)$$

and

$$NTU = 1 - \ln(1 - \varepsilon)$$

Substituting (31) , (26), and (25) into (23) and rearranging, the final expression is obtained for the actual heat transfer rate as

$$\dot{Q} = [1 - \exp(-NTU)]\dot{m}_o C_{p,HTF}\left(T_{HTF,in} - T_{steam,in}\right) \qquad (32)$$

where

$$NTU = \frac{UA}{\dot{C}_{\min}} = \frac{UA}{\dot{m}_o C_{p,HTF}} = \left(\frac{\dot{m}_o}{\dot{m}_{o,ref}}\right)^{0.8} \frac{UA_{ref}}{\dot{m}_o C_{p,HTF}} \qquad (33)$$

$$= \left(\frac{\dot{m}_o}{\dot{m}_{o,ref}}\right)^{0.8} \frac{NTU_{ref}\dot{m}_{o,ref} C_{p,HTF}}{\dot{m}_o C_{p,HTF}} = \left(\frac{\dot{m}_{o,ref}}{\dot{m}_o}\right)^{0.2} NTU_{ref}$$

In the Simulink model, as shown in the diagram below, $\dot{m}_0$ acts as a control signal to vary the steam flow rate and consequently power output.

To simplify the model, the condensate tank is assumed an infinite heat sink that is able to cool the steam and HTF to desired cold side temperatures. Thus, the condenser is not modeled at present.

Figure 97 illustrates the Simulink sub-block of heat exchanger.

Figure 6: Heat Exchanger Logic; Simulink

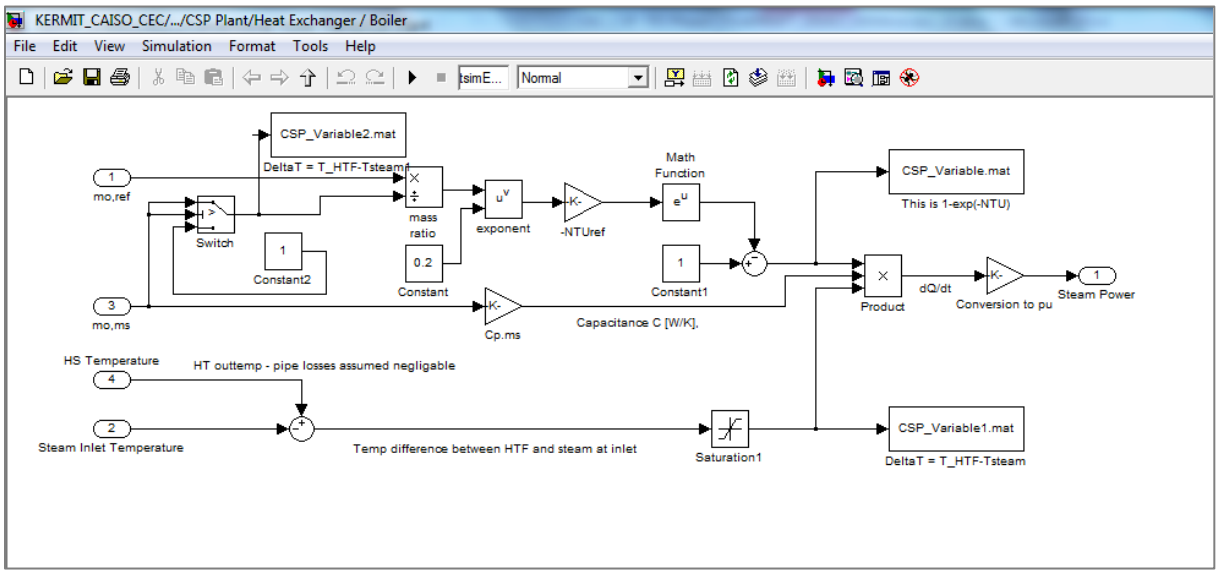

Source: DNV GL

Controller Logic

As mentioned in previous sub-section $\dot{m}_o$ acts as a control signal to vary the steam flow rate and consequently power output. Desired set-point and actual steam power is passed through the governor and a proportional-integral-derivative (PID) controller to obtain the required mass flow rate to be discharged from the hot tank storage and to be sent to the heat exchanger to generate steam for the turbine (see Figure 98).

Figure 7: Mass Flow Rate Controller Model; Simulink

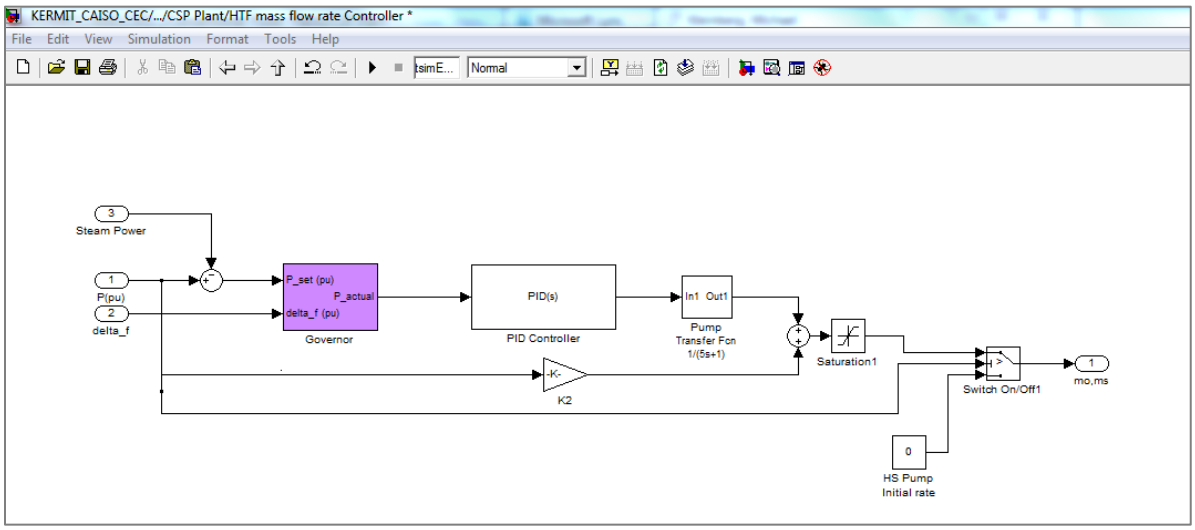

Source: DNV GL

Appendix B:
Production Cost Modeling

Modeling CSP-TES in PLEXOS

The conceptual CSP-TES plant modeled in PLEXOS consists of a power block, solar field, and thermal storage tank. As PLEXOS does not have a plant model developed for coupled CSP-TES, CSP-TES plants are modeled by adapting the pumped hydro unit object models. The input energy for the CSP plant is detailed in the same hourly fashion as hydro inflow schedules for a pumped storage facility. Production cost assumptions are specific to the CSP-TES plants however, so for instance, the conversion efficiencies of the thermal heat storage to electric energy through the steam system is CSP specific and different than the conversion of hydraulic energy to electricity in a hydro turbine, and emissions and fuel consumption are assumed negligible (gas co-firing to extend daily operation is not assumed in this phase). This will allow PLEXOS to develop dispatch schedules for the CSP-TES plants that honor limitations of the thermal storage unit and minimize peak generation cost by replacing expensive peaking units with energy from the CSP-TES plant.

Our method for modeling CSP-TES follows Denholm and Hummon.[1] Each of the original fixed CSP profiles is used as the input to a storage tank. If the tank has room and the optimization deems it prudent, energy is added to the tank. If not, the energy goes directly to the turbine. This allows the unit to provide generation as soon as it has sufficient energy, and also does not force the unit to store energy at the beginning of the day if that is not economical. The difference between the original fixed profile and the result with storage is shown in Figure 99. As noted earlier, the available hourly energy is equivalent in all cases; the storage just allows it to be saved for a later, more economical dispatch. This allows for reductions in total system costs by providing additional generation during peak price periods.

[1]Denholm and Hummon, November 2012, Simulating the Value of Concentrating Solar Power with Thermal Energy Storage in a Production Cost Model, http://www.nrel.gov/docs/fy13osti/56731.pdf.

Figure 8: Generation Dispatch of CSP-TES

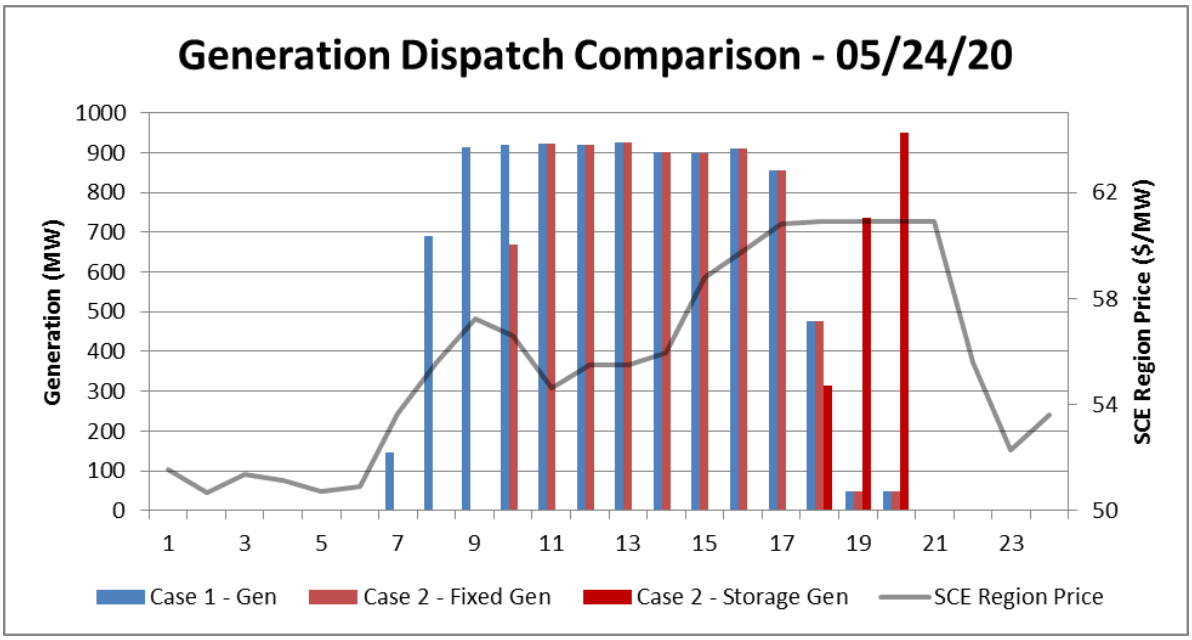

Source: DNV GL

Appendix C:
Renewable Generation Modeling

This appendix describes the methodology for developing renewable production data, representing CSP, PV, and wind power.

Variability and Forecast Error

Variability and forecast error have different characteristics depending on which resource is modeled (wind, PV, or CSP without TES), whether the resources are central or distributed, and how large an area is captured as geographical diversity will affect variability. For the purposes of this study, variability is defined as the variable intra-hour power output while forecast error is the mismatch in energy produced compared with the forecast. For this study, the relevant timeframe for forecast error is the hourly energy. The renewable generation profiles were created with hourly forecast errors aligning with CAISO recommendations,[2] outlined in Table 30. Forecast errors modeled in the current study are detailed in Table 31.

Table 1: CAISO Recommended Forecast Error for Future Studies

Wind	Forecast	Hours	Spring	Summer	Fall	Winter
Upper Limit	Persistent (T-1)	All	8.40%	7.10%	5.30%	3.90%
Lower Limit	Persistent (T-30)	All	2.90%	2.30%	1.80%	1.40%
Large PV	**Forecast**	**Hours**	**0<=CI<0.2**	**0.2<=CI<0.5**	**0.5<=CI<0.8**	**0.8<=CI<=1**
Upper Limit	(T-1) + 20%	Hours 12-16	4.20%	8.28%	6.72%	2.76%
Lower Limit	(T-1) -20%	Hours 12-16	2.80%	5.52%	4.48%	1.84%
CSP	**Forecast**	**Hours**	**0<=CI<0.2**	**0.2<=CI<0.5**	**0.5<=CI<0.8**	**0.8<=CI<=1**
Upper Limit	(T-1) + 20%	Hours 12-16	7.20%	13.08%	12.96%	3.60%
Lower Limit	(T-1) -20%	Hours 12-16	4.80%	8.72%	8.64%	2.40%

Source: CAISO, Renewables Integration Study Update, February 10 2012.

[2] CAISO, Renewables Integration Study Update, February 10, 2012.

Table 2: Forecast Errors Modeled for Renewable Generation

CSP	PV	Wind
12%	5.5%	4-6%

Source: DNV GL

The variability of the simulated renewable generation data was verified by comparing the power spectral density (psd) of real, measured data for renewable generation with the psd of the simulated data. The psd gives an indication of the amount of energy carried at different frequencies. Preserving this characteristic, or "power finger print", allows a fair representation of variability typical of a specific resource. Figure 100 shows an example of the psd of real data versus the simulated data used in this study, for a time series of PV generation.

Figure 9: PSD of Real versus Simulated PV Generation Output

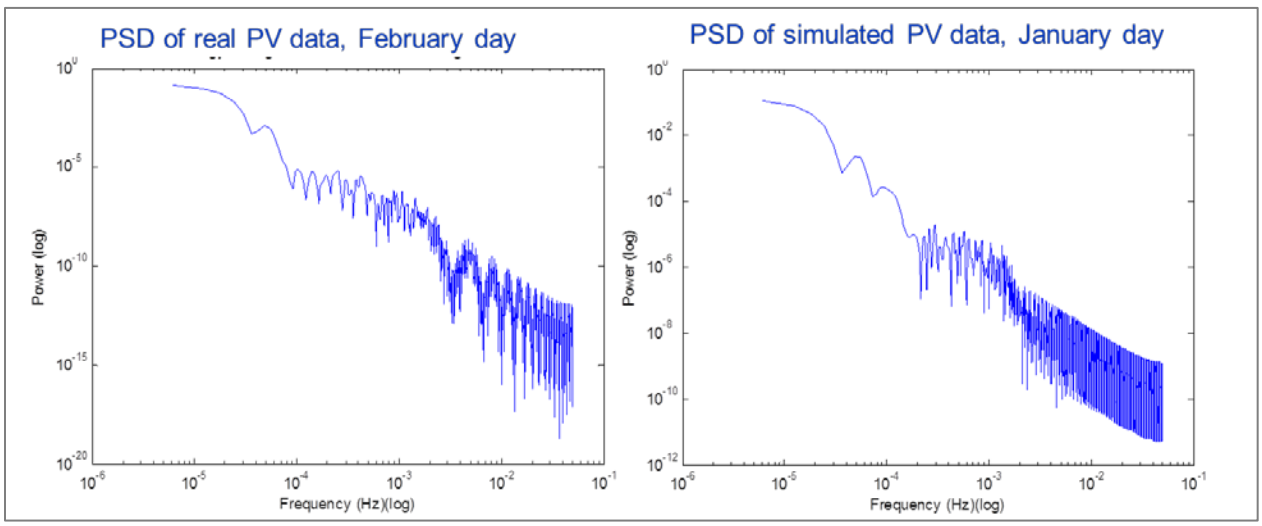

Source: DNV GL

Using these two techniques, two different profiles were developed; one with minimal forecast error, one with forecast error typical of the generation type with today's forecasting methods (following CAISO recommendations). Separating the forecast error and variability will allow for analysis of different mitigating strategies; larger capacity and longer durations are needed in order to address forecast error, while quick response times is crucial for smoothing intra-hour variability. Depending on the timeframe, different system control strategies are needed and different benefits can be realized. The study also aims to evaluate the capability of CSP-TES technologies in smoothing variability and reducing forecast error. The following figures show the 1-second profiles generated from the hourly schedules in PLEXOS. The smooth profile to the left has no variability or forecast error. In the 1-second profile to the right, variability was added at different intra-hour time intervals, mimicking the psd of real PV output data, while total

energy over each hour and over 24 hours was conserved. Hence, Figure 101 represents a profile with no forecast error but with variability representative of CSP without storage for a cloudy day. This profile was derived from the hourly schedules from PLEXOS for renewable generation in the CAISO Trajectory scenario.

Figure 102 shows the same thing for a PV plant. Note that the variability for a PV plant tends to be more rapid than for a CSP plant, due to the thermal energy stored in the steam generator.

Figure 10: Simulated Intra-Hour Variability of CSP Output

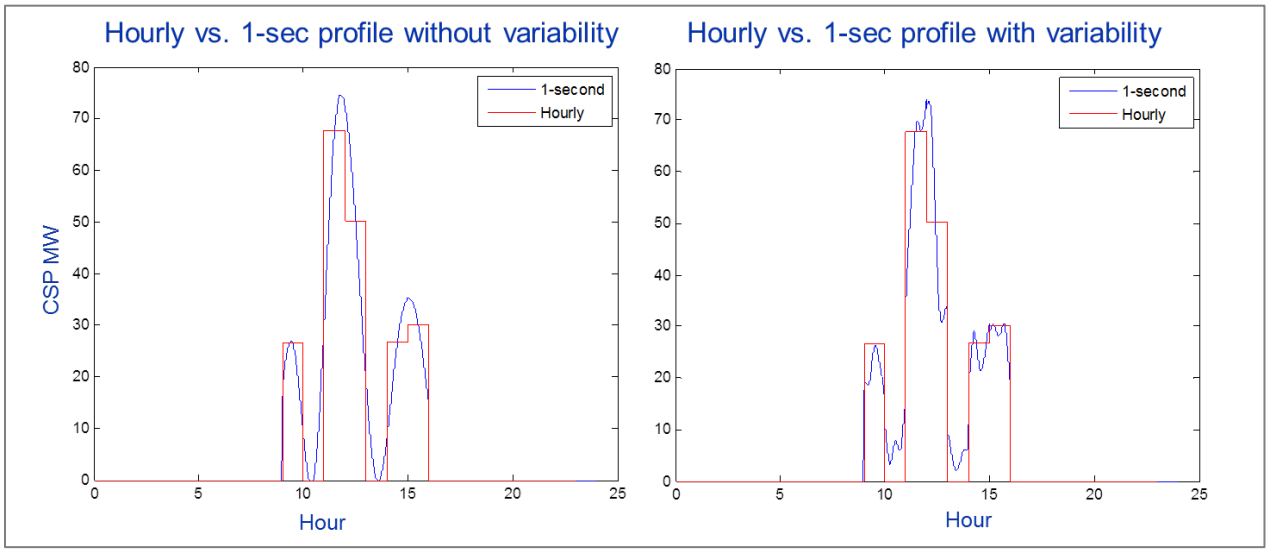

Source: DNV GL

Figure 11: Simulated Intra-Hour Variability of PV Output

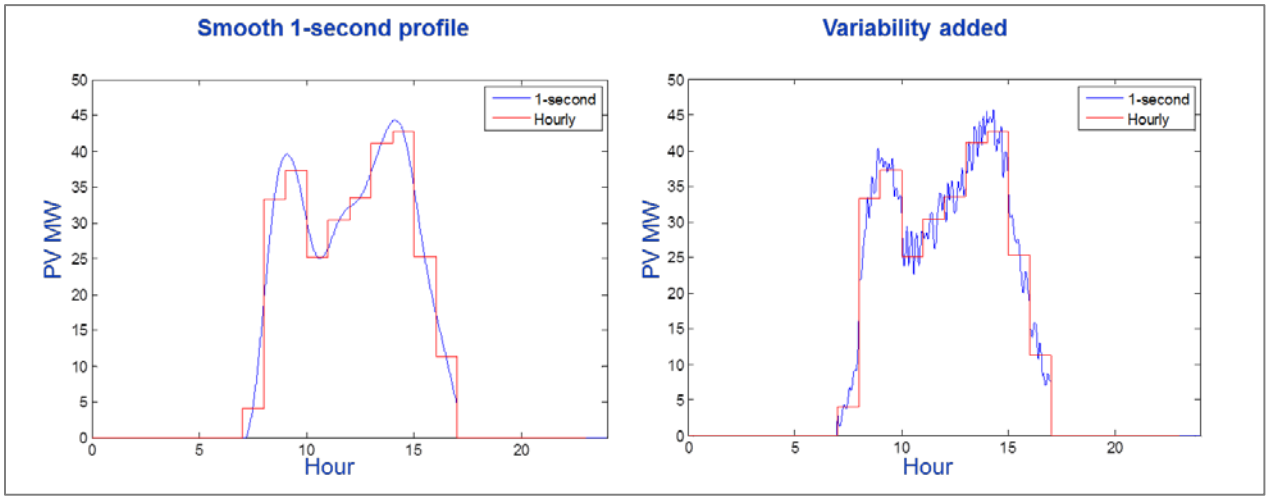

Source: DNV GL

As a next step, a generation profile reflecting forecast error, in addition to variability, was created. Hourly forecast errors were developed from the hourly schedules as a function of hourly standard deviation and a normal random noise. Figure 103 shows the CSP output derived from the hourly PLEXOS schedules (red) with an output profile with variability (blue) and a profile with both variability and an hourly forecast error of 12 percent (magenta) for a day in July and December, respectively.

Figure 12: Simulated CSP Output with 12 Percent Forecast Error and Variability

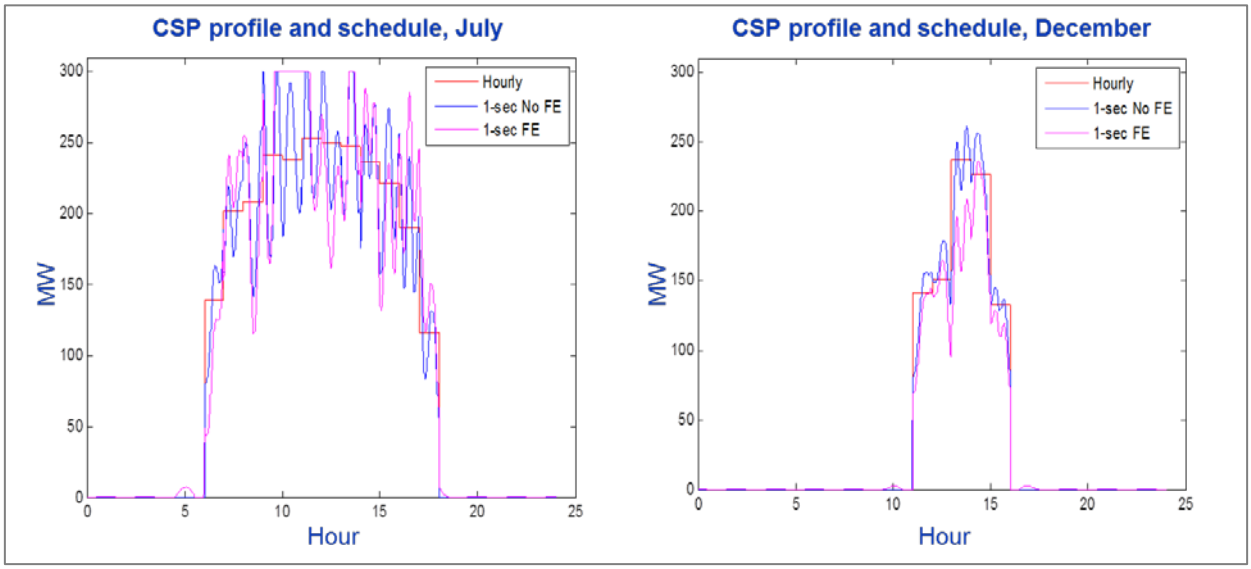

Source: DNV GL

Solar Irradiation to CSP-TES Plant

To model the dynamics of the CSP-TES plant, solar irradiation profiles were created that correspond to the hourly PLEXOS schedules and 1-second MW output profiles used for the Base Case in KERMIT. An iterative learning control (ILC) process was used to 'back-calculate' the solar irradiation from the expected MW output of the plant. For the ILC algorithm, an initial solution was assumed for the solar irradiation profile. This profile was then passed through the Simulink model of the CSP plant without storage to simulate the plant's real power output in MW. The error was calculated using the simulated output and the desired output (taken from CSP's Base Case hourly profile). The next iteration was performed by scaling this error (using a tuned scaling parameter), adding it to the initial solution, and passing the updated solar irradiation profile through the plant's model. The process was repeated until the plant's output converged to the desired hourly profile and final updated solar irradiation profile was obtained. Figure 104 shows the solar irradiation profile derived from a 1-second MW-output profile and the corresponding hourly DA schedule.

Figure 13: Solar Irradiation Profile for CSP-TES Plant

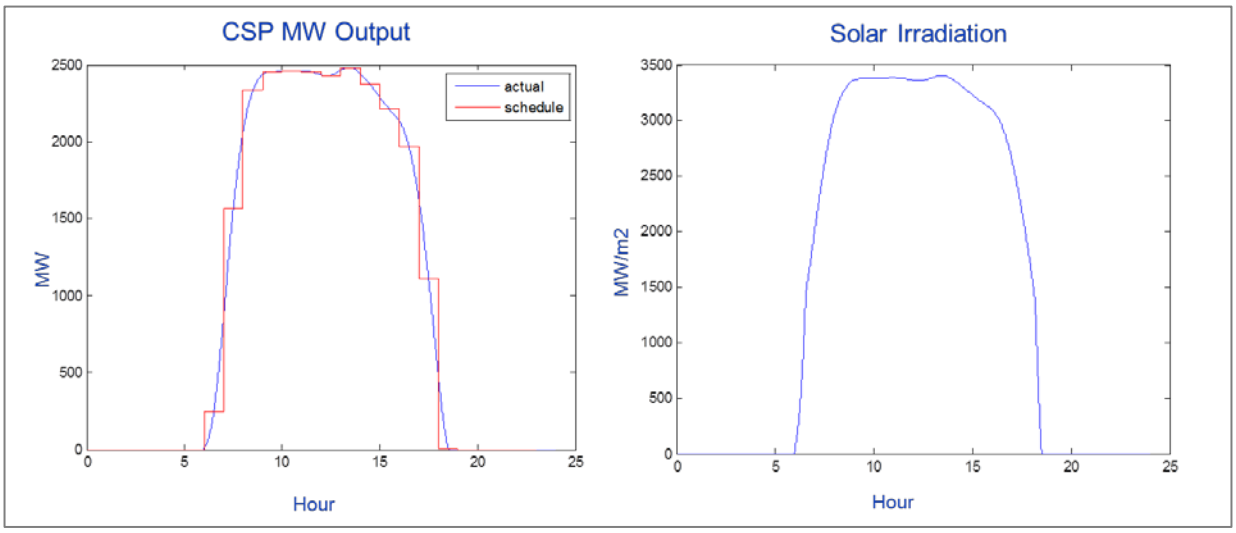

Source: DNV GL

Days Chosen for Modeling KERMIT

As mentioned, the PLEXOS model simulates a full year with 1-hour resolution. KERMIT on the other hand, simulates 24 hours with resolution of 1 second. Simulation run time and data processing limitations make running more than a handful of days in KERMIT impractical. The typical approach for annualizing results from KERMIT is to simulate 6-10 selected days, chosen to represent system challenges and seasonal variation, for an understanding of how the results would translate to the full year. The simulations in this study analyzed the following days, listed in Table 32.

Table 3: Ten Days Simulated in KERMIT

Spring	Summer	Fall	Winter
March 9	June 7	September 13	January 8
May 24	June 21	October 31	December 19
-	June 24	-	-
-	July 9	-	-

Source: DNV GL

For all these days, a full set of renewable generation data and solar irradiation were created, as inputs to KERMIT.

Renewable Profile Time Series Data

This section shows a subset of the renewable energy input profiles that were used for the KERMIT simulations. In all, 160 renewable power profiles were developed, representing PV, CSP, and Wind profiles in three regions, for 10 days across the year. All profiles were also developed to simulate the presence of forecast error versus no forecast error. All power profiles were developed from the PLEXOS hourly schedules, using DNV GL code for adding technology appropriate variability, according to the methodology described above. In addition, some simulations were done to evaluate the effect of forecast error – divergence from hourly energy schedule – according to the recommended forecast error as listed in Table 30 and Table 31.

PV Profiles without Forecast Error

All PV profiles were developed from the PLEXOS hourly schedules, using DNV GL code for adding technology appropriate variability, according to the methodology described in this appendix.

Figure 14: PV Profiles of Total MW in SDG&E Territory, No Forecast Error

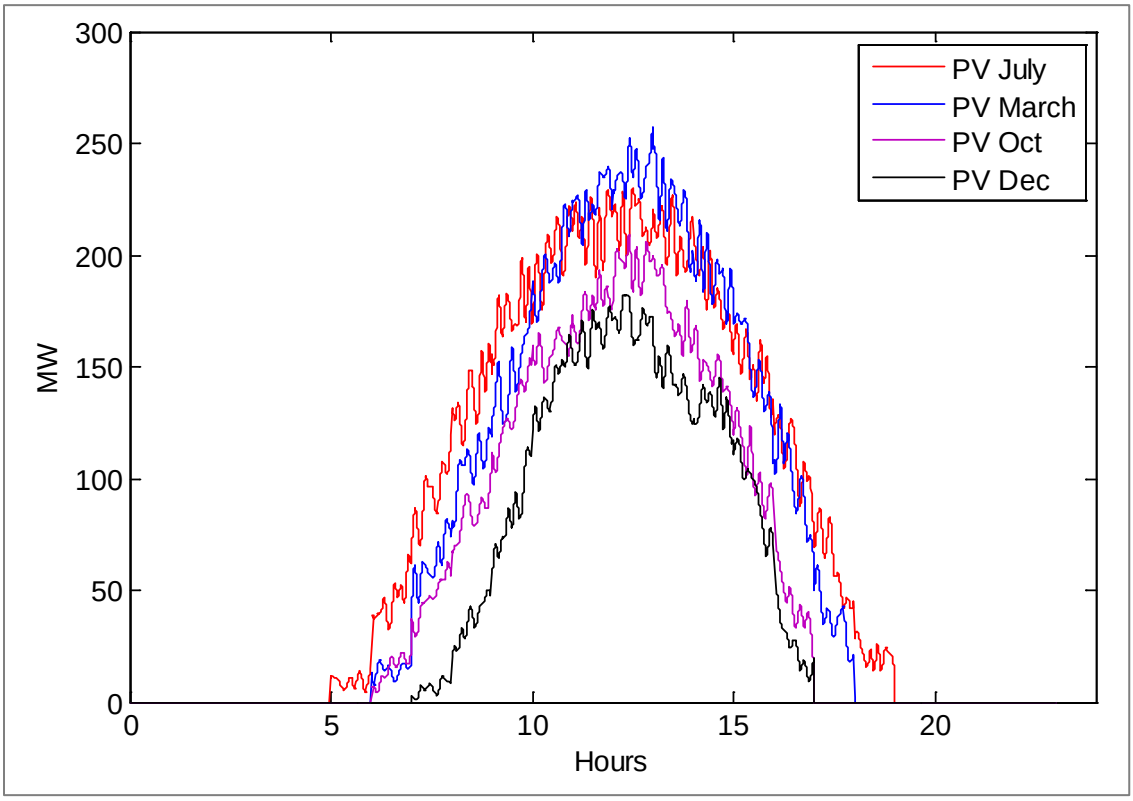

Source: DNV GL

Figure 15: PV Profiles of Total MW in Pacific Gas & Electric (PG&E) Territory, No Forecast Error

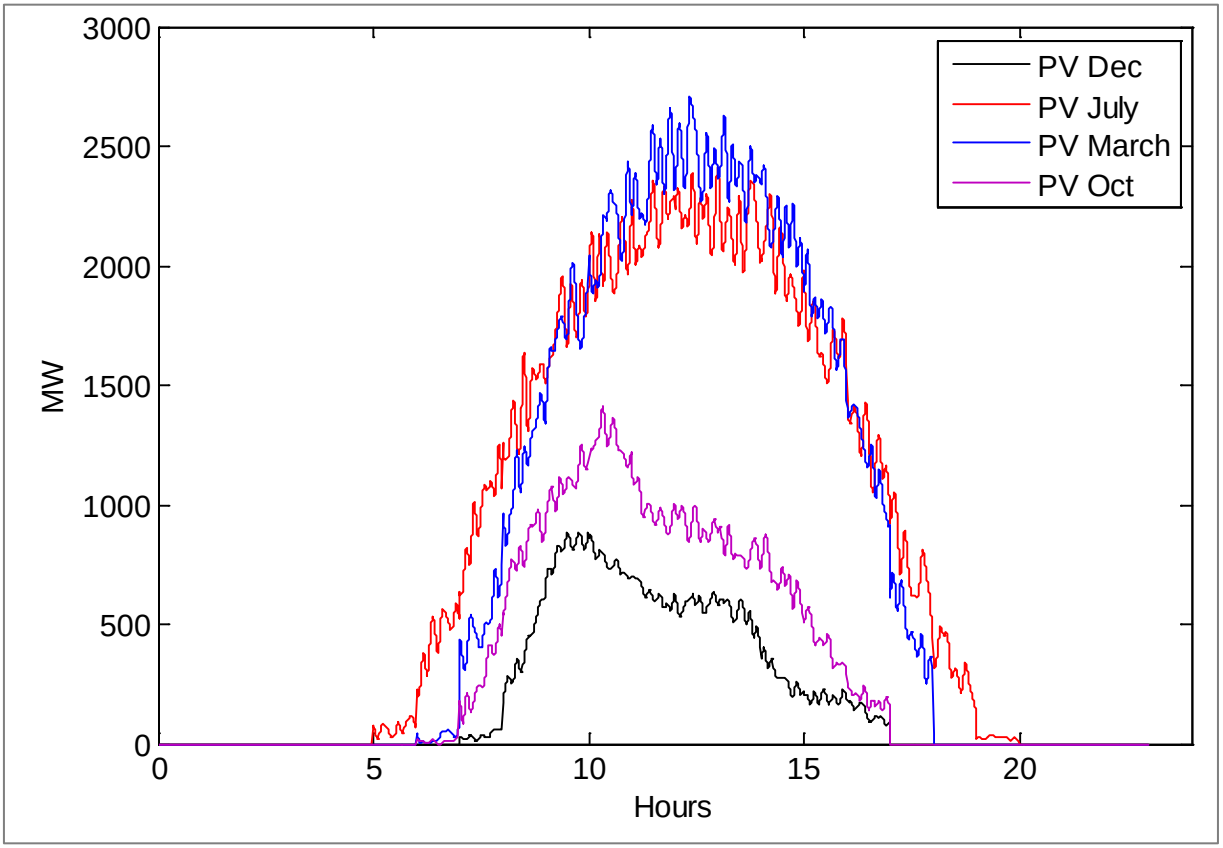

Source: DNV GL

PV Profiles with Forecast Error

All PV profiles were developed from the PLEXOS hourly schedules, using DNV GL code for adding technology appropriate variability, according to the methodology described in this appendix. In addition, these profiles have an imbedded forecast error – deviation from energy schedule, as described in this appendix – according to the recommended forecast error listed in Table 30 and Table 31.

Figure 16: PV Profiles of Total MW in SDG&E Territory, with Forecast Error

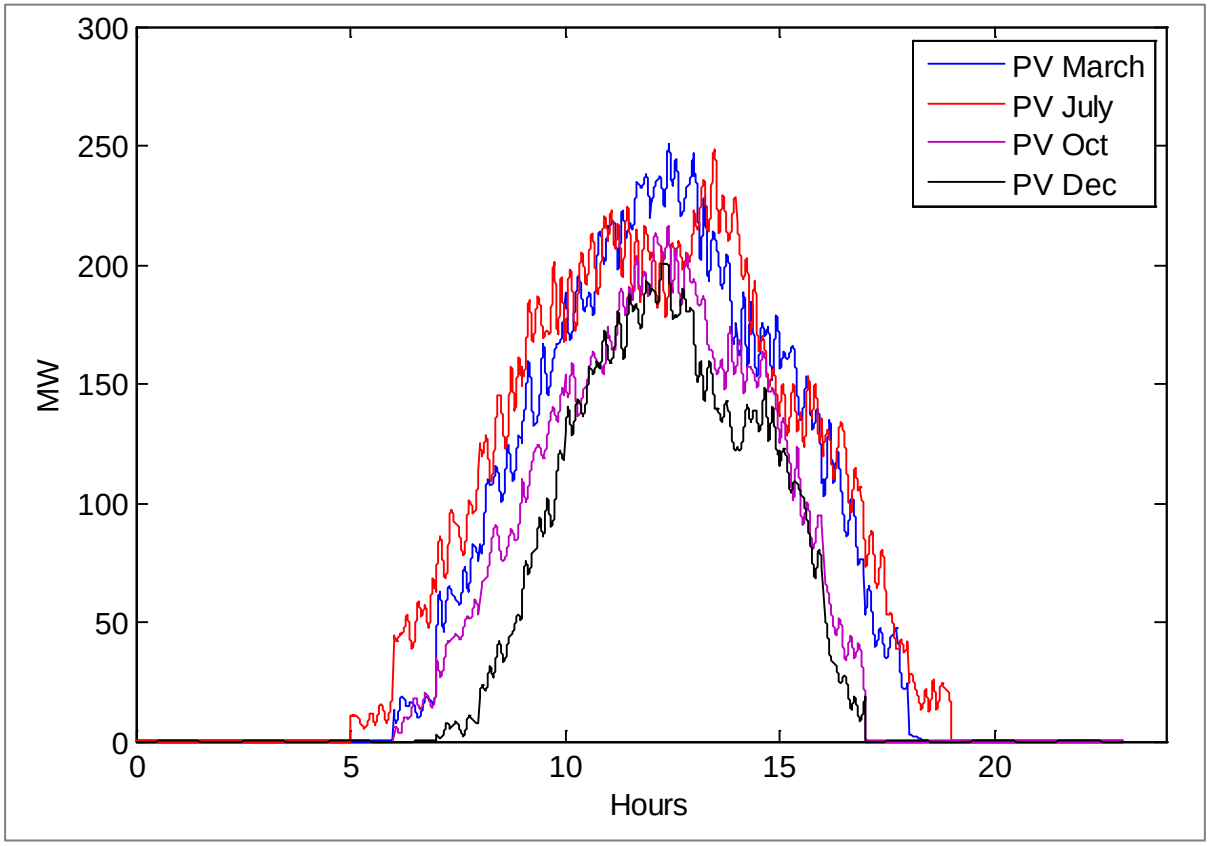

Source: DNV GL

Figure 17: PV Profiles of Total MW in PG&E Territory, with Forecast Error

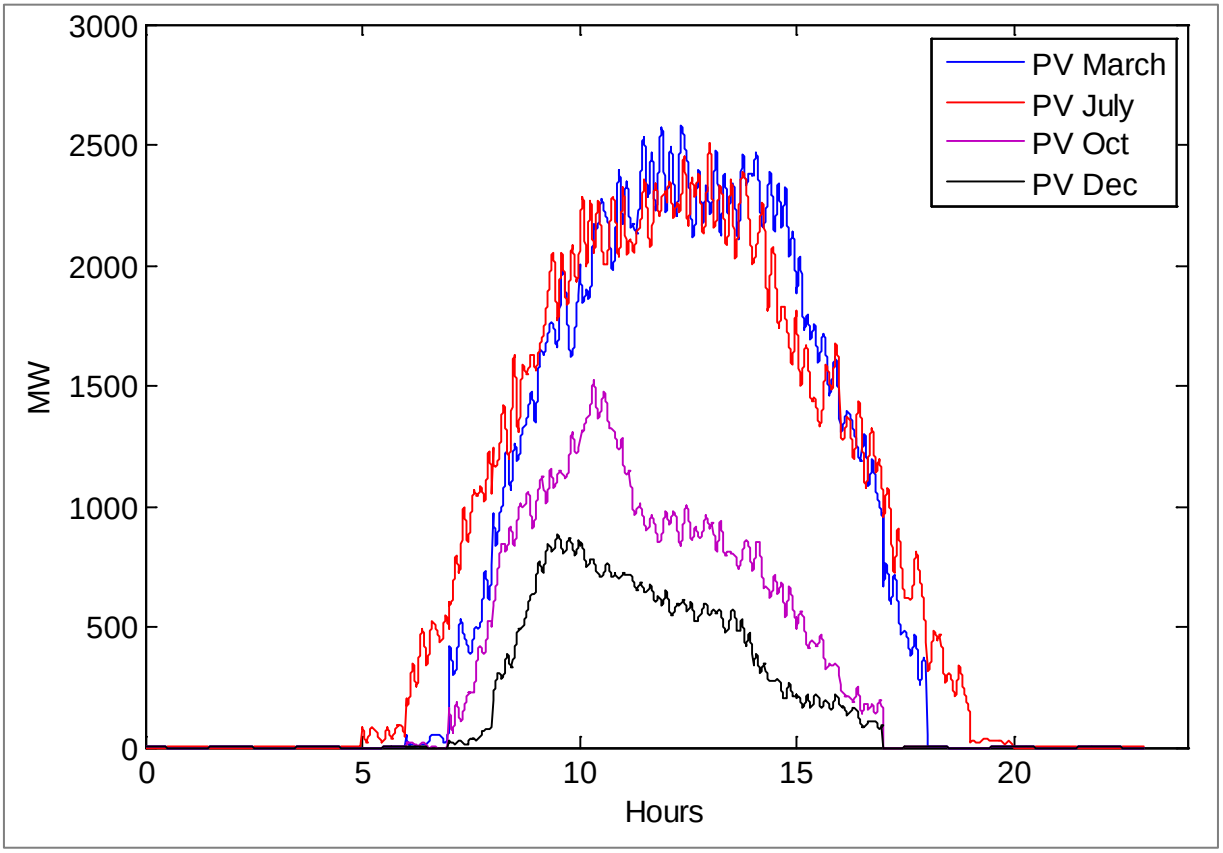

Source: DNV GL

CSP Profiles without Forecast Error

All CSP profiles were developed from the PLEXOS hourly schedules, using DNV GL code for adding technology appropriate variability, according to the methodology described in this appendix.

Figure 18: CSP Profile of Total MW in SDG&E Territory, No Forecast Error

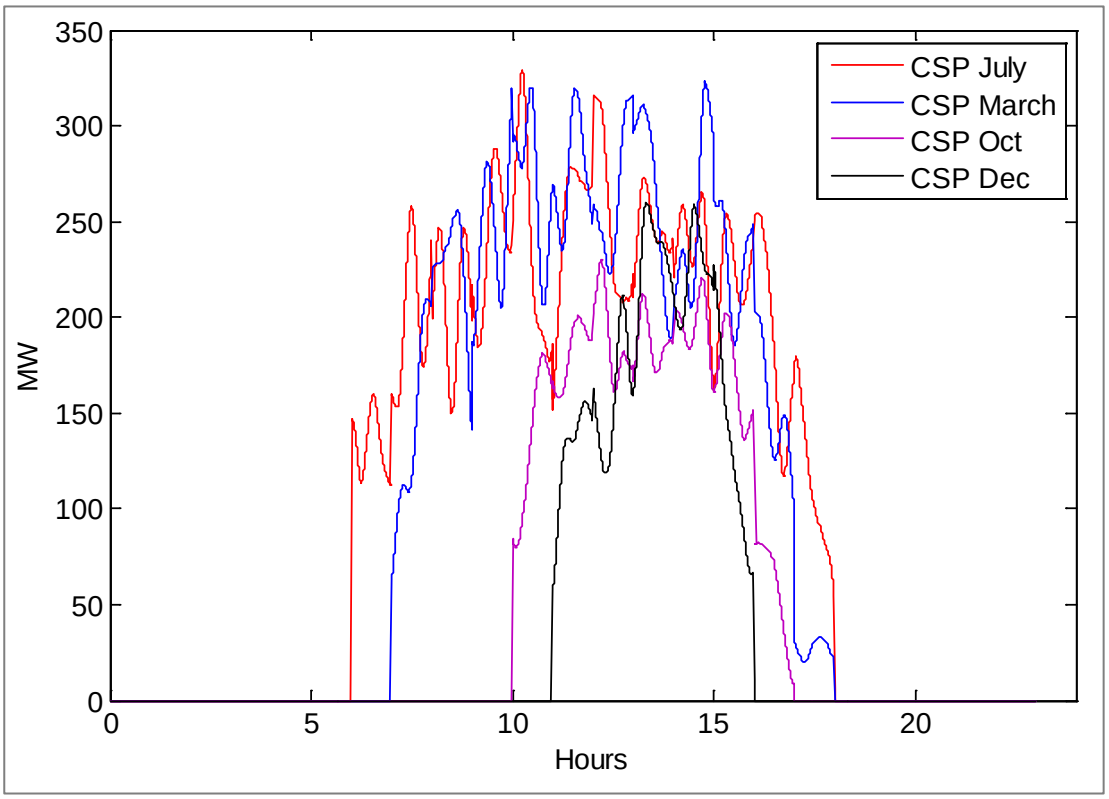

Source: DNV GL

CSP Profiles with Forecast Error

All CSP profiles were developed from the PLEXOS hourly schedules, using DNV GL code for adding technology appropriate variability, according to the methodology described in this appendix. In addition, these profiles have an imbedded forecast error – divergence from energy schedule – according to the recommended forecast error listed in Table 30 and Table 31.

Figure 19: CSP Profiles of Total MW in SDG&E Territory, with Forecast Error

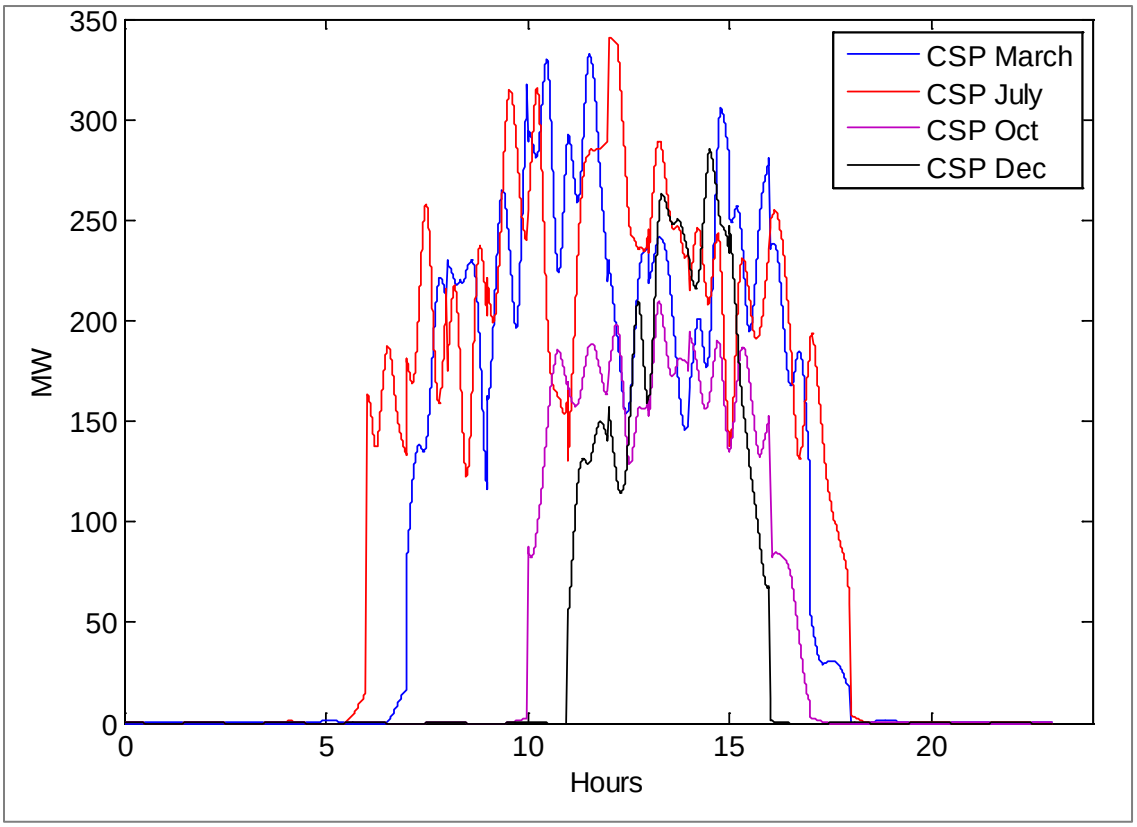

Source: DNV GL

Wind Profiles without Forecast Error

All wind profiles were developed from the PLEXOS hourly schedules, using DNV GL code for adding technology appropriate variability, according to the methodology described in this appendix.

Figure 20: Wind Profiles of Total MW in SDG&E Territory, without Forecast Error

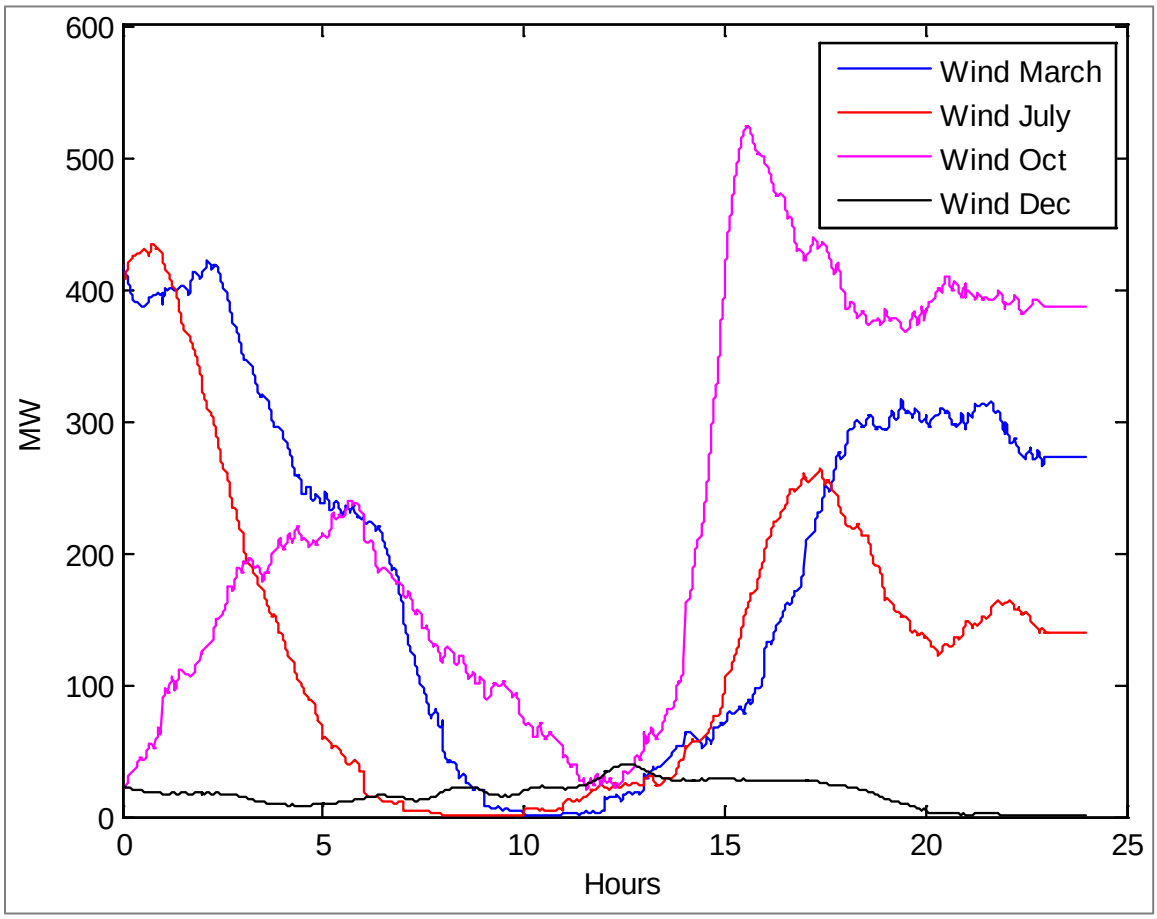

Source: DNV GL

Wind Profiles with Forecast Error

All wind profiles were developed from the PLEXOS hourly schedules, using DNV GL code for adding technology appropriate variability, according to the methodology described in this appendix. In addition, these profiles have an imbedded forecast error – divergence from energy schedule – according to the recommended forecast error listed in Table 30 and Table 31.

Figure 21: Wind Profiles of Total MW in SDG&E Territory, with Forecast Error

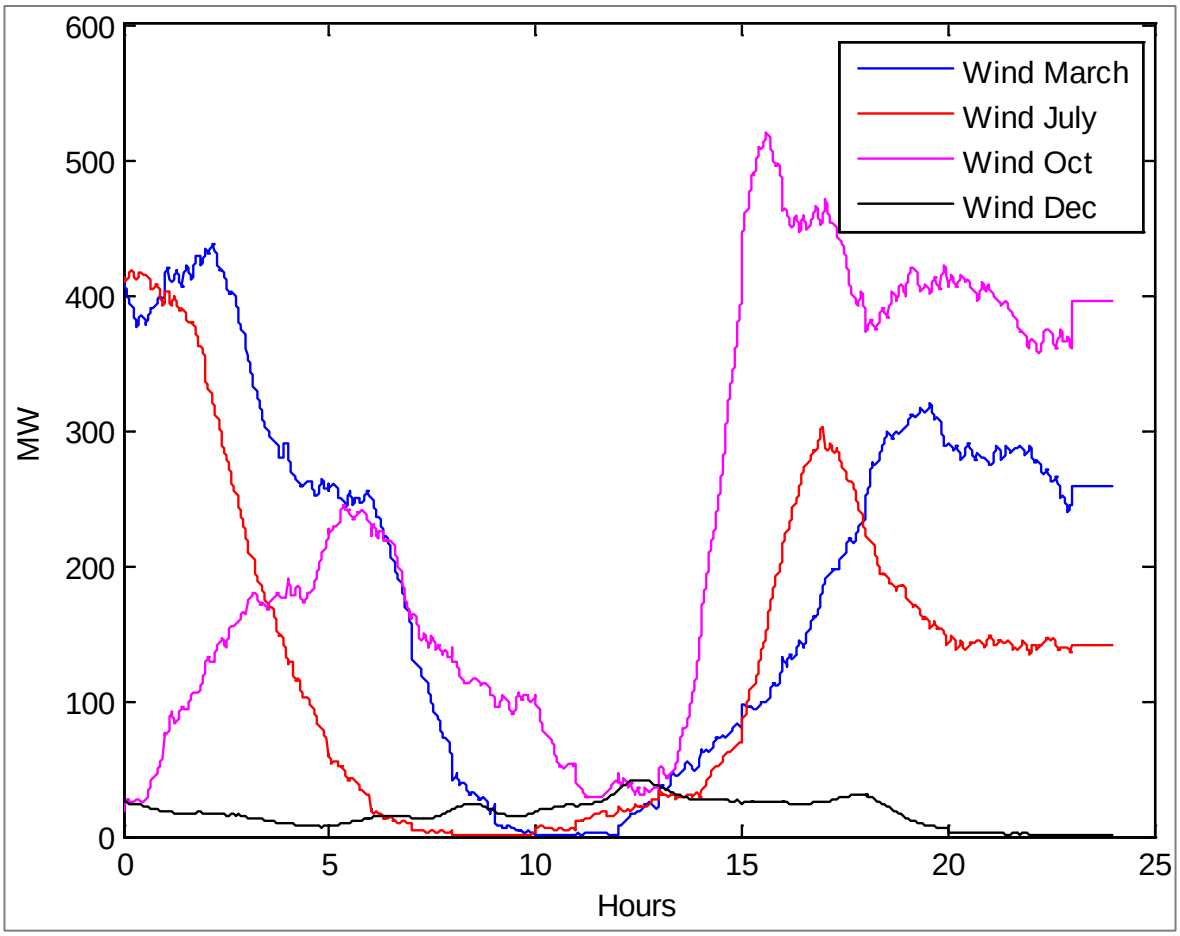

Source: DNV GL

Appendix D:
Thermodynamic Plant Models

Figure 113 shows different pieces of the modelling approach. The steps to modeling include the following:

1. Determine the system design parameters to meet the design requirements. For this, the system design model developed by Terrafore will be used.
2. Develop component models in MATLAB by coding the model equations
3. Construct a Simulink model for each configuration using the component models.
4. Integrate into the DNV GL code for grid-wise impact analysis

The models for sensible heat in hot and cold tank are straightforward and there is adequate experience with these systems to define constraints and recoverable storage volumes. Regin *et al* provide[i] a comprehensive list of models for various types of packed bed thermal storage for both sensible and phase change materials. Since these systems are still being developed to be used with CSP, a more detailed development of these equations will be done to tailor them for use with a CSP system.

Beasley *et al* [ii]provides a good analysis of thermal response of packed bed of PCM capsules. Terrafore has developed similar models for PCM storage in capsules (~5mm to 10mm diameter) to evaluate heat transfer in packed beds which is used in the analysis.

Thermal stratification has been demonstrated in laboratory scale. However, it is generally recognized that in large scale application, maintaining thermal stratification is very difficult. Thermocline degrades significantly with partial charge and discharge cycles (Terrafore' s internal study has shown that in 10 cycles the utilization factor goes from 85 percent to 40 percent). Also mixing of fluid at entrance and exit of the tank can reduce temperature and quality of heat available for discharge. To accurately model these, one needs to use a Computational Fluid Dynamics package, which is too detailed for the scope of this project. Instead, mixing is modeled using simple equations.

In an encapsulated PCM storage (not yet used in commercial CSP), the heat transfer inside the capsule can be through conduction and through convection or a combination of the two. Since there is a void inside the capsule, the heat transfer through the capsule is modeled using two-phase models.

Figure 22: Schematic View of Approach to Mathematical Modelling

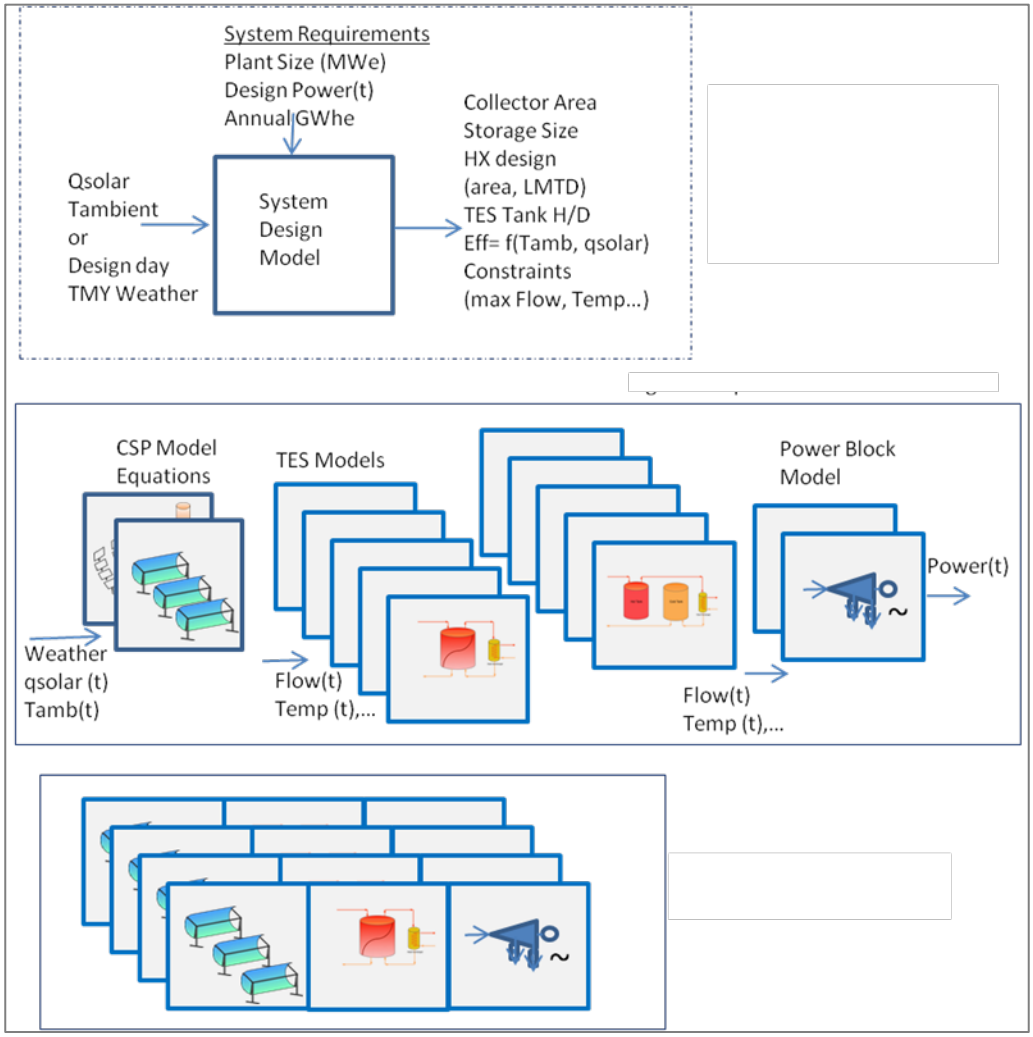

Source: Terrafore, Inc.

CSP Models

Solar Central Tower Receiver

Heat transfer fluid which enters the solar central receiver / absorber, shown in Figure 114, is spilt into the East side and West side. Each side consists of eight header groups with four panels per header group. Each panel has eighteen tubes. Along the length of each tube eight stages are defined and the following dynamic heat transfer equations are written for each stage and mixing equations at the header.

Figure 23: Solar Tower Absorber Panel Layout showing HTF Flow

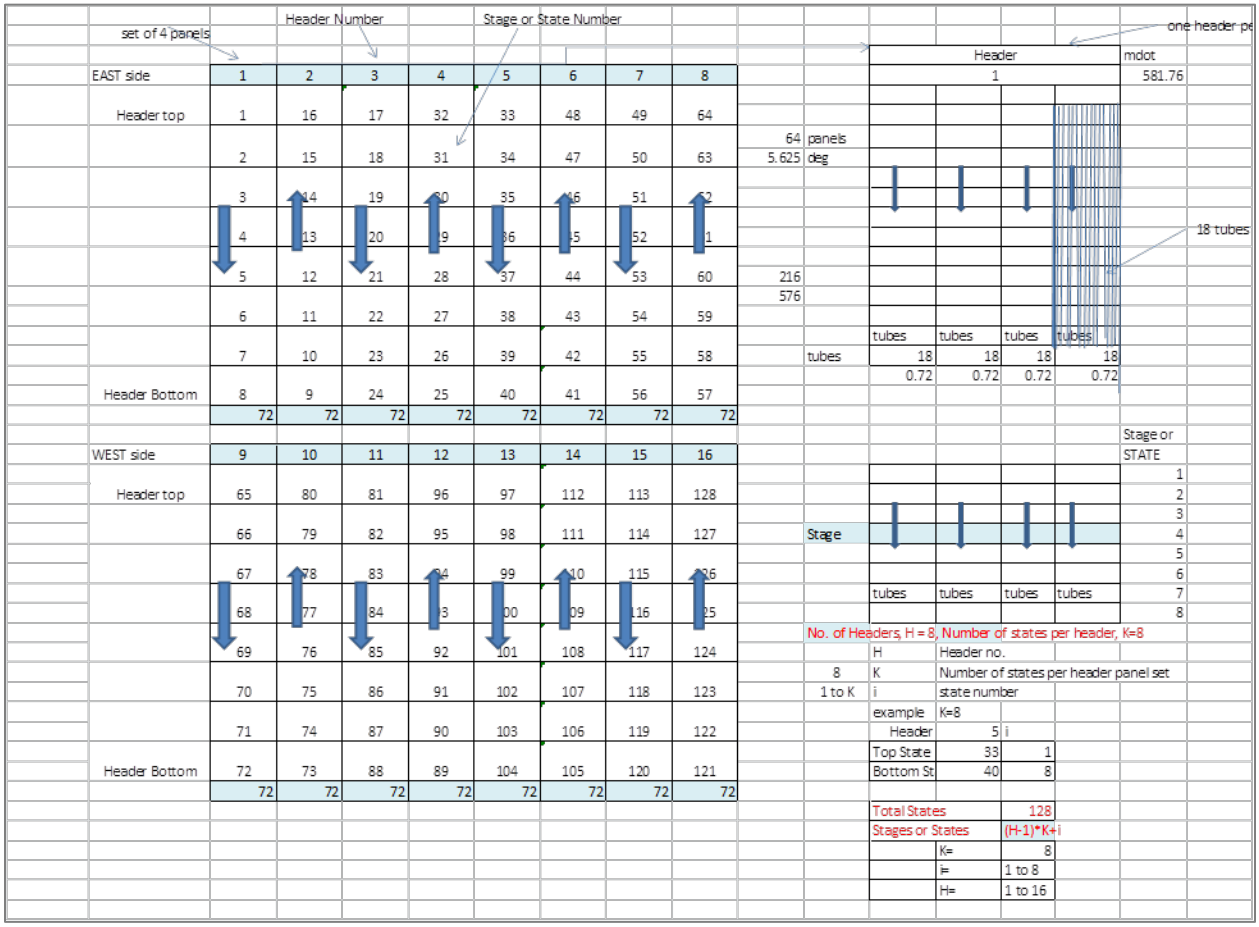

Source: Terrafore, Inc.

Energy Balance:

The receiver temperature in tube $n = 1, n_{tubs}$ is denoted by $T_{abs}(n,i,t)$, at time t and height $(1-i)\Delta z$ where $\Delta z =$ node height and $i = 1, i_{node}$. The receiver temperature satisfies:

$$\rho_{abs}\, cp_{abs} \frac{dT_{abs}(n,i,t)}{dt} = \dot{q}_{inc} - (\dot{q}_{refl} + \dot{q}_{rad} + \dot{q}_{conv}) - \dot{q}_{HTF} \qquad (1)$$

The initial conditions at $t = 0$ are $T_{abs}(n,i,0) = T_{abs,0}$

$\dot{q}_{inc}(n,i,t) =$ heat flux incident on i th node in the n th tube at time t.

$\dot{q}_{refl}(n,i,t) = (1-\alpha)\dot{q}_{inc}(n,i,t)$, $\alpha =$ absorbance = 0.96

$$\dot{q}_{rad}(n,i,t) = \sigma\,\varepsilon\left(\frac{\pi\,d}{2}n_{tubs}\Delta z\right)F\left[T_{abs}^{4}(n,i,t) - T_{amb}^{4}\right]$$

$\sigma =$ Stefan-Boltzmann = 5.67x10^{-8} W/(m^2 K^4), $\varepsilon =$ emissivity = 0.88, $d =$ tube diameter, $F =$ view factor =1.0 and $T_{amb} =$ ambient temperature.

$$\dot{q}_{conv}(n,i,t) = h_{amb}\left(\frac{\pi\,d}{2}n_{tubs}\Delta z\right)\left[T_{abs}(n,i,t) - T_{amb}\right]$$

$h_{amb} =$ convection coefficient = $f\,(wind\ speed)$

$$\dot{q}_{HTF}(n,i,t) = U\left(\frac{\pi\,d}{2}n_{tubs}\Delta z\right)\left[T_{abs}(n,i,t) - T_{HTF}(n,i,t)\right], \quad U = \frac{1}{h_{HTF}} + \frac{t^*}{k_{tub}}$$

The HTF temperature satisfies:

$$(\rho\,cp)_{HTF}\,A_{abs}\,\frac{dT_{HTF}(n,i,t)}{dt} = \dot{q}_{HTF} - (\rho\,cp)_{HTF}\,\dot{V}_{HTF}\,\frac{\left[T_{HTF}(n,i-1,t) - T_{HTF}(n,i,t)\right]}{\Delta z} \qquad (2)$$

where the ratio on the right hand side is an approximation of $\partial T_{HTF}\,/\,\partial z$. The initial and boundary conditions are $T_{HTF}(n,i,0) = T_{HTF,0}$ and $T_{HTF}(n,0,t) = T_{HTF,in}(t)$. $A_{abs} =$ area of the absorber/receiver, $\dot{V}_{HTF} =$ volumetric flow rate of $HTF = \dot{m}_{HTF}\,/\,\rho_{HTF}$.

Equations (1) and (2) are coupled by the term $\dot{q}_{HTF}$. The radiation heat loss makes them non-linear. A typical model is based on $n_{tubs} = 72$ and $i_{node} = 128$ and results in a system of 72 x 128 = 9216 coupled non-linear ordinary differential equations.

The typical heat flux map falling on the receiver absorber varies over the course of the day as the Sun moves in the sky is shown Figure 115. To obtain this heat map a detailed modelling of the solar field is required. For this analysis, a typical heat map profile is assumed, as shown in Figure 115, with normalized values shown in Table 33. The heat flux is multiplied by these values to obtain the absolute flux on each stage of the receiver. The heat flux varies as a function of the direct normal incident (DNI) radiation, which is obtained from the weather files.

Figure 24: Heat Map on Solar Absorber

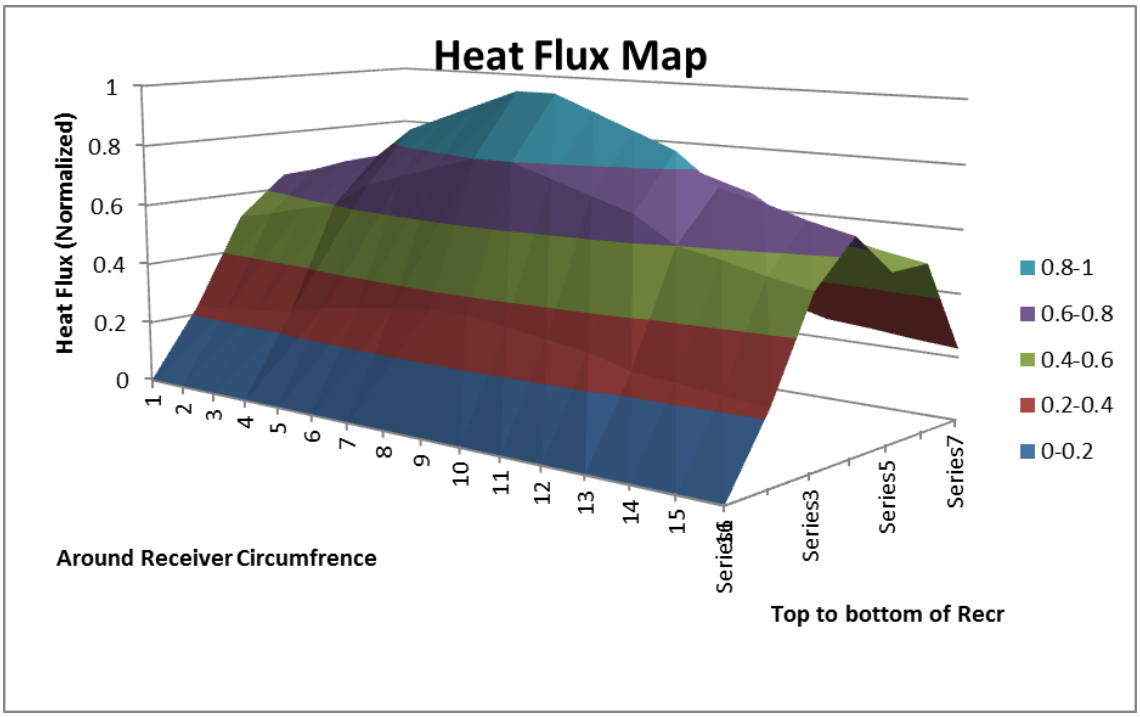

Source: Terrafore, Inc.

Table 4: Heat Map Values (Normalized)

Heat flux top to bottom

HEAT FLUX MAP

		1	2	3	4	5	6	7	8	9	10	11	12	13	14	15	16
		0.65	0.68	0.72	0.75	0.85	0.9	0.95	1	1	0.95	0.9	0.85	0.75	0.72	0.68	0.65
Top Header	0	0	0	0	0	0	0	0	0	0	0	0	0	0	0	0	0
Top of the tu	0.35	0.2275	0.238	0.252	0.2625	0.2975	0.315	0.3325	0.35	0.35	0.3325	0.315	0.2975	0.2625	0.252	0.238	0.2275
3	0.8	0.52	0.544	0.576	0.6	0.68	0.72	0.76	0.8	0.8	0.76	0.72	0.68	0.6	0.576	0.544	0.52
4	1	0.65	0.68	0.72	0.75	0.85	0.9	0.95	1	1	0.95	0.9	0.85	0.75	0.72	0.68	0.65
5	0.8	0.52	0.544	0.576	0.6	0.68	0.72	0.76	0.8	0.8	0.76	0.72	0.68	0.6	0.576	0.544	0.52
6	0.8	0.52	0.544	0.576	0.6	0.68	0.72	0.76	0.8	0.8	0.76	0.72	0.68	0.6	0.576	0.544	0.52
Bottom of th	0.35	0.2275	0.238	0.252	0.2625	0.2975	0.315	0.3325	0.35	0.35	0.3325	0.315	0.2975	0.2625	0.252	0.238	0.2275
Bottom Head	0	0	0	0	0	0	0	0	0	0	0	0	0	0	0	0	0

example table

Sum of all values	sum	53.3	
Heat Flux total	H	517	MWt
Scale 1=	H/sum	9.699812	MWt

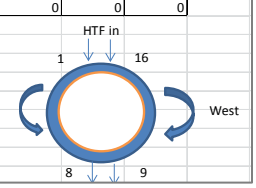

Source: Terrafore, Inc.

Table 5: Solar Tower Receiver Design Calculations

Central Receiver Design 100MWe net						
		Design hour			Design day	
Nameplate	MWe	100				
Gross Output	MWe	110				
QDNI	*W/m2*	*950*		*Wh/m2-day*	*9000*	
Solar Multiple		*1.9*				
Receiver		0.579596413		**Receiver**		
Receiver Height	m	18.8		Receiver area	m2	892.43
Receiver Diameter	m	15.11		recvr circumfrence	m	47.469465
No. of Panels		20		Tube dia	mm	40
Coating Emittance		0.88		No. of tubes		1152
Tube diameter outer	mm	40		No. of Panels		64
Tube wall thick	mm	1.25		No. of tubes/panel		18
Tube ID	mm	37.5		No. of panels to an header		4
HTF out	C	574		No. of headers		16
HTF in	C	285		No. of tubes/header		72
Coating Absorbance		0.94		sector per header	deg	22.5
Design Thermal Power	MWt	517.60				
Flow rate to Receiver	kg/s	1165.1		Flow rate total	kg/s	1165.05
	m3/s	0.6413		Flow to east side	kg/s	582.53
Constraints				Flow to west side	kg/s	582.53
Max Receiver flux	kW/m2	1000		Flow per tube	kg/s	8.09
Max Flow rate	kg/s	1602		Inner dia of tube	mm	37.50
Max HTF in	C	350		cross area	m2	0.00110
Heliostat				mass velocity	kg/m2/s	7325
Land area	acres	1508		density of fluid	kg/m3	1816.8
Heliostat Width	m	12.2		fluid velocity in tube	m/s	4.03
Heliostat Height	m	12.2		**Weights**		
Heliostat area (reflective)	m2	148.84		Metal weight of tube	kg	18.90
Reflective area	%	97%		Mass of panel	kg	340.20
Total Reflective Area	m2	144.4		Metal Mass of 4 panels (for ea hdr)	kg	1360.8
No. of Heliostats		7021		Fluid weight per panel	kg	679.03
Mirror reflectance	%	90%		Fluid weight per 4 panels	kg	2716.114595
Solar to heliostats	MWth	866.7		Header flow rate	kg/s	582.53
Cosine losses	%	17.00%			m3/s	0.32
shadowing blocking	%	0%		Header velocity design	m/s	0.75
Reflectance	%	10%		Header dia	m	0.74
Attentuation	%	5.40%		Header wt (20mm thick)	kg	54.7
Total field losses	%	32.40%		length of header (aprox)	m	3.2
Field losses, eff	%	70.7%		Header fluid weight	kg	2460.6
Solar reflected to recvr	MWth	612.4		Capacitance of header	kJ/K	3810.0
Heat rate absorbed	MWth	0		Capacitance per 4 panels	kJ/K	4855.80019

Source: Terrafore, Inc.

Parabolic Trough Model

The length of each of the n number of troughs is divided into N-nodes and heat transfer equations are written for each node as follows:

Energy Balance:

The receiver temperature in tube $n = 1, n_{tubs}$ is denoted by $T_{abs}(n,i,t)$, at time t and height $(1-i)\Delta z$ where $\Delta z =$ node height and $i = 1, i_{node}$. The receiver temperature satisfies:

$$\rho_{abs}\, cp_{abs} \frac{dT_{abs}(n,i,t)}{dt} = \dot{q}_{abs} - (\dot{q}_{glassenv}) - \dot{q}_{toHTF} \qquad (1)$$

The HTF temperature satisfies:

$$(\rho\, cp)_{HTF}\, A_{abs} \frac{dT_{HTF}(n,i,t)}{dt} = \dot{q}_{toHTF} - (\rho\, cp)_{HTF}\, \dot{V}_{HTF} \frac{\left[T_{HTF}(n,i-1,t) - T_{HTF}(n,i,t)\right]}{\Delta z} \qquad (2)$$

The initial conditions at $t = 0$ are $T_{abs}(n,0) = T_{abs,0}$

$\dot{q}_{inc}(n,i,t) =$ heat flux incident on i th absorber node in the n th tube at time t.

$\dot{q}_{abs}(n,i,t) = (\eta)\dot{q}_{inc}(n,i,t)$, η =absorbance

$$\dot{q}_{toHTF}(n,i,t) = U\left(\frac{\pi d}{2} n_{tubs}\Delta z\right)\left[T_{abs}(n,i,t) - T_{HTF}(n,i,t)\right], \quad U = \frac{1}{h_{HTF}} + \frac{t^*}{k_{tub}}$$

h_{HTF} = convection coefficient = $g(\dot{m}_{HTF})$, $t^* =$ log-mean tube thickness, k_{tub} = tube thermal conductivity, and $T_{HTF}(n,i,t) =$ HTF temperature at i th node in the n th tube, at time t.

where the ratio on the right hand side is an approximation of $\partial T_{HTF} / \partial z$. The initial and boundary conditions are $T_{HTF}(n,i,0) = T_{HTF,0}$ and $T_{HTF}(n,0,t) = T_{HTF,in}(t)$. A_{abs} = area of the absorber/receiver, $\dot{V}_{HTF}$ = volumetric flow rate of $HTF = \dot{m}_{HTF} / \rho_{HTF}$.

$$\rho_{env}\, cp_{env} \frac{dT_{glass}(n,t)}{dt} = \dot{q}_{anstoenv} - \dot{q}_{glassenv} \qquad (3)$$

$$\dot{q}_{glassenv}(n,i,t) = h_{glasstoenv}\left(\frac{\pi\, d}{2} n_{tubs} \Delta z\right)\left[T_{abs}(n,t) - T_{glass}\right]$$

The heat loss from glass envelope to environment is modeled as a single node (N is the number of stages along the length of the absorber tube (i= 1 to N).

$$\dot{q}_{loss}(n,i,t) = h_{amb}\left(\frac{\pi\, d}{2} n_{tubs} N \Delta z\right)\left[T_{glassave}(n,t) - T_{amb}\right]$$

$$h_{amb} = \text{convection coefficient} = f(wind\ speed)$$

Table 35 shows the design data for the parabolic solar trough for a plant producing 517 MW (thermal) power at the absorber. This is adequate for a 100 MW electric generating plant with six hours of storage. For a plant with lower or higher thermal storage hours or solar multiple, the total thermal power and the design of the absorber are scaled accordingly using the trough design equations from Terrafore. These design values are used to estimate the thermal capacitance of the absorber and hence the time constant and heat loss rates.

Table 6: Parabolic Trough Design Calculations

Parabolic Trough Collector Design					
		Design hour			Design day
Nameplate	MWe	100			
Gross Output	MWe	110			
QDNI	*W/m 2*	*950*		*Wh/m2-day*	*9000*
Collector					
Following calculations for SM=1					
		Design hour			Design day
Aperture area (solar multiple=1)	m2	500543.4054		m2	500543.4054
Single Collector (L=100m)	m2	470		m2	470
Qincident (SM=1)	MWt	475.5162351		MWht/day	4504.890648
Cosine effect (SM=1)		0.9928			0.8566
Optical efficiency		0.8602			0.8602
Qincident (SM=1)	MWt	406.115786		MWht	3319.426108
absorber efficiency		0.788211648			0.788211648
Qincident thermal (SM=1)	MWt	320.105193		MWht	2616.410323
Qloss absorber (SM=1)	MWt	18.64		MWht	186.3725446
Qloss Header+field	MWt	10		MWht	100
Qloss fraction		8.95%			8.95%
Qabsorbed thermal,net (SM=1)	MWt	291.4679385		MWht	2330.037779
Overall collection efficiency		61.30%			
Cycle Conversion efficiency		37.74%			37.74%
Gross Output	MWe	110			879.3562577
Thermal rate to Power block	MWt	291.4679385		MWht	2330.037779
Direct Solar generation	hours	1		hours direct	8.0
Direct SolarNet generation	MWe	100		MWhe	799.4
Collector design					
Thermal Storage hours (specified)	hours	6		hours direct	6
StoreCycle Conversion efficiency		37.74%			37.74%
TES Thermal rate to Power block	MWt	291.4679385			
TES capacity net	MWh t	1748.807631		MWht	1,749
TES losses	MWt	1.6		MWht	38.4
TES thermal rate reqd	MWt	293.0679385		MWht	1787.2
Total Generation Hours at rated cap	hours				14.0
Design Thermal Energy Required	MWt	515.0324355		MWht	4117.2
Solar Multiple Reqd		*1.767*			
Direct SolarNet generation	MWe	100		MWhe/day	1399.4
Collector Aperture reqd	m2	884475			
Collector aperture single	m2	470			
No. of collector		1882			
Length of each collector	m	100			
Total length of collector	m	188186			
No. of loop		235.2			

Absorber		
Length of receiver / collector	m	188186
OD of absorber tube	m	0.07
ID of absorber tube	m	0.066
Surf area	m2/m	0.219911486
Cross section area flow	m2	0.003421194
Weight of absorber tube	kg/m	3.39
Heat Transfer Fluid (HTF)		VP1
HTF inlet temperature	C	293
HTF outlet Temperature	C	391
HTF Delta Temp	C	98
Design Thermal Power collected	MWt	515.0324355
Average Temperature	C	342
Density of HTF (340C)	kg/m3	773
Heat capacity of HTF(340C)	kJ/kg/K	2.425
HTF flow rate	kg/s	2167.188872
No. of loops		235.2
HTF flow rate /loop	kg/s	9.21
velocity of fluid in absorber tube	m/s	3.48
Mass of HTF/length of tube	kg/m	2.6446
Minimum HTF velocity	m/s	0.4
Minimum HTF flow rate	kg/s	1.058
Maximum HTF veocity	m/s	5
Maximum HTF flow rate	kg/s	13.22
Header flow rate	kg/s	541.7972181
Header velocity	m/s	2.5
Header diameter	m	0.60
Header flow rate	kg/s	541.7971937
goal seek		0.000
wall thickness	m	0.003
Header weight	kg/m	43.92
headers/loop		4
length of headers	m	6400
Header fluid	kg	1,387,001
Headers	kg	281,099
Absorber	kg	636,688
Fluid	kg	497,182

Thermal Storage (2-Tank)			
		VP-1	Molten Salt
Storage capacity	MWht	1787.2	1787.2
Storage hot temp	C	391	386
Storage cold temp	C	293	298
Storage Delta Temp	C	98	88
Storage fluid density	kg/m3	773	1872
Storage fluid heat capacity	kJ/kg/K	2.425	1.5
Storage HTF mass	kg	27,073,206	48,742,026
Storage Volume	m3	35,024	26,037
Ullage		5%	5%
Tank volume	m3	36,867	27,408
Tank Ht	m	25	20
Tank Dia	m	43.3	41.8
H/D		0.58	0.48
Tank Surface	m2	6352.60	5365.34
Tank loss coeff	W/m2-K	0.4	0.4
Tank Loss rate/tank	MWt	0.8	0.7
Tank loss rate	MWt	1.61	1.36
Tank Loss rate/day	MWht	38.7	32.7
Tank loss rate/Store capacity	%	2.2%	1.8%
Tank Temp drop/day	C/day	2.12	1.79

Source: Terrafore, Inc.

Thermal Energy Storage Models

Two-Tank Sensible Heat Storage

Figure 116 shows a schematic of the EPCM storage.

Figure 25: EPCM Storage

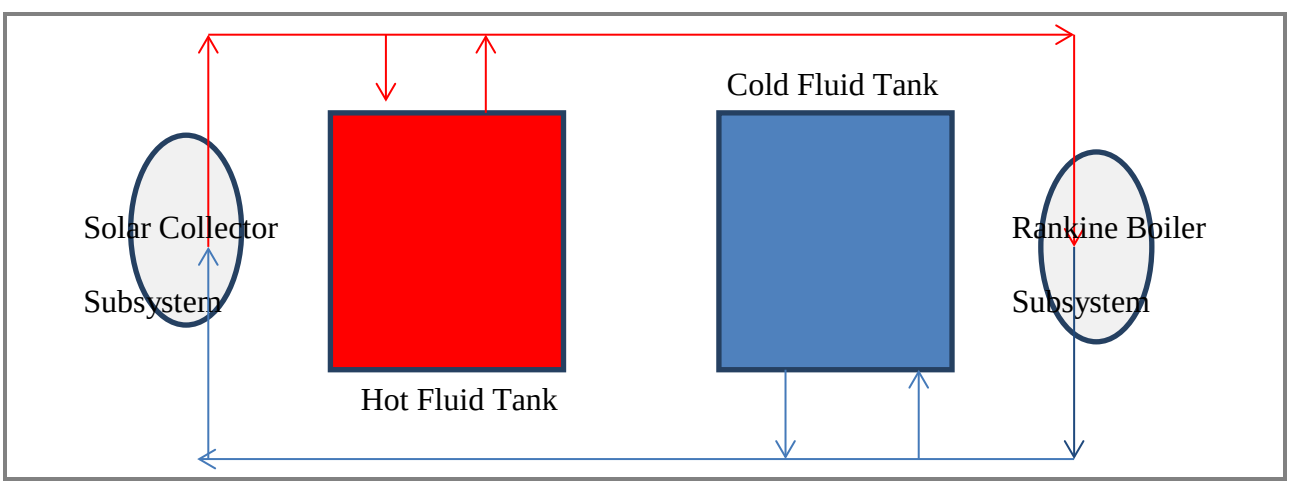

Source: Terrafore, Inc.

Dynamic Model Equations:

Charge Cycle

Hot tank

Mass Balance : $\frac{d\emptyset h}{d\tau} = u_c$

Energy Balance: $\frac{d\theta h}{d\tau} = u_c(\theta_{supply} - \theta_h)$

Cold Tank

Mass Balance : $\frac{d\emptyset c}{d\tau} = -u_c$

Energy Balance: $\frac{d\theta c}{d\tau} = 0$

Discharge Cycle

Hot tank

Mass Balance : $\frac{d\emptyset h}{d\tau} = -u_d$

Energy Balance: $\frac{d\theta h}{d\tau} = 0$

Cold Tank

Mass Balance : $\frac{d\emptyset c}{d\tau} = u_d$

Energy Balance: $\frac{d\theta c}{d\tau} = u_d(\theta_{return} - \theta_c)$

where

$\emptyset = M/M_0$, $\theta = \frac{T-Tc}{TH-TC}$, $u = \frac{m}{mdesign}$, $\tau = \frac{t}{tstore}$

T = Temperature, [K}

T_H = Design hot temperature, [K]

T_C= Design cold temperature, [K]

M = Mass of fluid in tank, [kg]

M_0 = Mass of fluid in full tank, [kg]

m = mass flow rate of heat transfer fluid, [kg/s]

m_{design} = mass flow rate of heat transfer fluid at design , [kg/s]

t=time, t_{store} = Storage time ,[s]

subscripts:

c= charge, d= discharge, 0=initial,

supply = hot fluid supply temperature from solar field,

return = cold fluid return temperature from steam cycle

design=design conditions

A Closed Form Solution for Two Tank Model Equation:

The following describes a closed-form solution to simulate the dynamic behavior of a two tank direct and indirect thermal energy storage system. The components are derived to simulate a filling tank, a draining tank and a heat exchanger. In most cases, they take the form of analytic solutions of linear ordinary differential equations. In cases when the forcing function depends on the external environment, the solutions involve integrals that may be evaluated numerically. The solutions are found using the variation of constants formula.

Single Tank:

The mass and energy balance equations are defined in terms of rates of mass transport $\dot{m}$ (kg/s) and energy exchange $\dot{q}$, or heat flow, (J/s) for a single enclosed tank as shown, diagrammatically, in Figure 117. The space above the HTF is assumed to be filled by a gas, which expands or contracts. The mass $M(t)$ (kg) changes at the rate $\dot{m}$.

Figure 26: Schematic of Mass and Energy Balance for Single Enclosed Tank

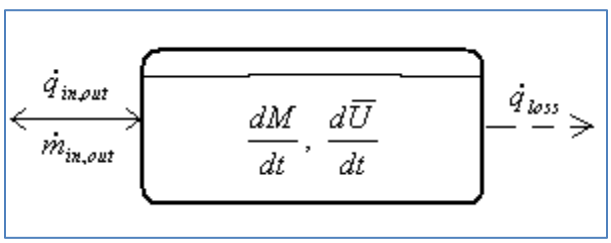

Source: Terrafore, Inc.

The inlet and outlet mass and heat flow rates are indicated by $\dot{m}_{in,out}$ and $\dot{q}_{in,out}$, respectively. The quantity $\dot{q}_{loss}$ is the rate of heat loss to the exterior. The total energy $\overline{U}$ (J), in the tank, is related to the average temperature $\overline{T}$ (°C) by the equation $\overline{U} = MC_p\overline{T}$ where C_p is the specific heat (J/kg/°C).

In the case that the tank is filling, the mass and energy balance equations are

$$\frac{dM}{dt} = \dot{m}_{in}, \qquad (1)$$

for time $t \geq 0$ and

$$\frac{d\overline{U}}{dt} = \dot{q}_{in} - \dot{q}_{loss}, \qquad (2)$$

where $\dot{q}_{in} = \dot{m}_{in} C_p T_{in}$ and T_{in} is the specified inflow temperature. The loss is $\dot{q}_{losst} = hA(\overline{T} - T_{ext})$ where h is a heat transfer coefficient [J/(m^{2}s ^{o}C)], A is area (m^2) and T_{ext} is an external temperature.

The solution for Eq. (1) is $M(t) = M_0 + \dot{m}_{in} t$ where M_0 is the initial mass. Equation (2) is converted into a differential equation for $\overline{T}$ by substituting the formulas cited above to obtain: $d[M(t)C_p\overline{T}]/dt = \dot{m}_{in} C_p T_{in} - hA(\overline{T} - T_{ext})$.

Carrying out the indicated differentiation, rearranging terms and dividing by $M(t)C_p$ yields

$$\frac{d\overline{T}}{dt} = -\frac{(\dot{m}_{in} + hA/C_p)}{M_0 + \dot{m}_{in} t}\overline{T} + \frac{\dot{m}_{in} T_{in} + (hA/C_p)T_{ext}}{M_0 + \dot{m}_{in} t} \quad . \qquad (3)$$

In addition to the mass, the surface area A would also depend on time but it is assumed to be constant to simplify the analysis. The variation of constants solution of Eq. (3) is

$$\overline{T}(t) = \alpha + (\overline{T}_0 - \alpha)\frac{(M_0)^{a/g}}{(M_0 + \dot{m}_{in} t)^{a/g}} \qquad (4)$$

where $\overline{T}_0$ is the initial temperature, $\alpha = a/b$, $a = \dot{m}_{in} + hA/C_p$, $b = \dot{m}_{in}T_{in} + (hA/C_p)$, and $g = \dot{m}_{in}$. It has been assumed that a and b are constants, Eq. (4) is valid over a short time interval.

Note that $\alpha \cong T_{in}$ when h is small. The behavior of Eq. (4) is similar to the case of a perfectly insulated tank with $h = 0$ and $a/g = 1$. The perfectly insulated solution is

$$\overline{T}(t) = T_{in} + (\overline{T}_0 - T_{in})\frac{M_0}{M_0 + \dot{m}_{in}t} \tag{5}$$

and the temperature approaches T_{in} at a linear rate. After putting the right hand side of Eq. (5) over a common denominator, it becomes clear that it is merely the mass weighted average of $\overline{T}_0$ and T_{in}.

When the tank is draining, the mass and energy balance equations are

$$\frac{dM}{dt} = -\dot{m}_{ihr}, \tag{6}$$

and

$$\frac{d\overline{U}}{dt} = -\dot{q}_{out} - \dot{q}_{loss}, \tag{7}$$

where $\dot{q}_{out} = \dot{m}_{out}C_p\overline{T}$ and $\dot{q}_{loss}$ is the same as above. The solution for Eq. (6) is $M(t) = M_0 - \dot{m}_{out}t$. Equation (7) is converted to an equation for $\overline{T}$ and yields a similar differential equation to Eq. (3):

$$\frac{d\overline{T}}{dt} = -\frac{(hA/C_p)}{M_0 - \dot{m}_{out}t}\overline{T} + \frac{(hA/C_p)T_{ext}}{M_0 - \dot{m}_{out}t} \tag{8}$$

but with T_{in} replaced by $\overline{T}$. The variation of constants solution of Eq. (8) [Eq. (A5) with $\alpha = T_{ext}$] is

$$\overline{T}(t) = T_{ext} + (\overline{T}_0 - T_{ext})\frac{(M_0)^{a/g}}{(M_0 - \dot{m}_{out}t)^{a/g}} \tag{9}$$

where $a = hA/C_p$ and $g = -\dot{m}_{in}$. The average temperature $\overline{T}$ in the draining tank is quite different from the average temperature in the filling tank. This is happens because $a/g = -\dot{m}_{out}hA/C_p$ is negative and proportional to h. When h is small, $a/g \cong 0$ so that the mass ratio in Eq. (9) stays close to one. The temperature $\overline{T}$ stays close to $\overline{T}_0$, because the T_{ext} terms in Eq. (9) nearly cancel. In the perfectly insulated case, $d\overline{T}/dt = 0$ and

$$\overline{T}(t) = \overline{T}_0 \tag{10}$$

is a constant.

Two Tank Direct:

Suppose there are two tanks, designated as hot and cold, that are used as a TES system. One tank is used to store hot HTF and the other is used as a supply of colder fluid. The behaviors of the average temperatures in the hot and cold tanks are determined by Eq. (4) or Eq. (9), depending on whether the tank is draining of filling.

During the charge cycle, fluid from the cold tank is drained and sent to the solar receiver. The cold fluid has an almost constant temperature, according to Eq. (9). After being heated in the solar receiver, the hot fluid is stored in the hot tank. The filling of the hot tank changes its average temperature according to Eq. (4).

In the discharge cycle, fluid from the hot tank is drained and sent to the steam generator. The hot fluid is at an almost constant temperature, according to Eq. (9). After cooling in the steam generator, the cooled fluid is stored in the cold tank. The filling of the cold tank changes its average temperature according to Eq. (4).

A heat exchanger is not part of the two tank direct storage system since the same HTF is used throughout. When a different HTF is used elsewhere in the system (e.g., in the steam generator), a heat exchanger needs to be incorporated with the two storage tanks for indirect TES.

Heat Exchanger Model:

First, consider only one side of the heat exchanger. It could be either the system or storage side and is, subsequently, coupled with the other side. The energy balance equation for one side of the heat exchanger is obtained by the lumped capacitance method[iii] [pp. 212-221] applied to a model with internal flow [iii] [pp. 431- 433]. It is defined in terms of the rates of energy exchange, shown diagrammatically in Figure 118.

Figure 27: Schematic of Energy Balance for One Side in Heat Exchanger

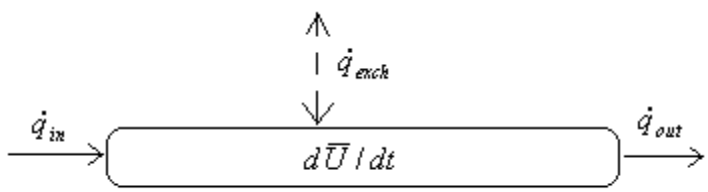

Source: Terrafore, Inc.

The notation in Figure 118 is similar to the notation used for the single tank, but there are some significant differences. The term $\dot{q}_{exch}$ is the rate of the heat exchange between one side and the other. There is a spatial separation between the inlet and outlet. This allows for different heat flow and temperature at both ends. The heat flow and temperature at inlet and outlet are related by the equation $\dot{q}_{in,out} = \dot{m} C_p T_{in,out}$ where $\dot{m}$ is the mass flow rate of the HTF. If $\dot{q}_{exch}$ is spatially constant, then the temperature changes linearly between inlet and outlet and can be lumped[iii] [p. 433] into its average $\overline{T} = (T_{in} + T_{out})/2$. The validity of this approximation is enhanced in a counter flow heat exchanger. The rate of heat transfer to the other side is then $\dot{q}_{exch} = hA(\overline{T} - \overline{T}_{other})$. The sign of $\dot{q}_{exch}$ is determined by the sign of the difference $\overline{T} - \overline{T}_{other}$.

The rate of change of the averaged energy, as shown in Fig. 2, is expressed as

$$\frac{d\overline{U}}{dt} = \dot{q}_{in} - \dot{q}_{out} - \dot{q}_{exch} \quad .$$

The spatially averaged energy is related to the temperature by the equation $\overline{U} = MC_p\overline{T}$ where the mass and specific heat are constant. The energy balance equation, in terms of the spatial averaged temperature, is

$$MC_p \frac{d\overline{T}}{dt} = \dot{q}_{in} - \dot{q}_{out} - hA(\overline{T} - \overline{T}_{other}), \tag{11}$$

for $t \geq 0$. Equation (11) can be written exclusively in terms of $\overline{T}$ by noting that

$$\dot{q}_{in} - \dot{q}_{out} = 2\dot{m}C_p(T_{in} - \overline{T}), \tag{12}$$

which is motivated by the assumption that T_{in} is known; while T_{out} can be eliminated in favor of the lumped parameter $\overline{T}$. Substituting Eq. (12) into Eq. (11) yields

$$MC_p \frac{d\overline{T}}{dt} = -(2\dot{m}C_p + hA)\overline{T} + 2\dot{m}C_pT_{in} + hA\overline{T}_{other} \quad . \tag{13}$$

Equation (13) is coupled to the other side of the heat exchanger. The two coupled equations can be expressed as a 2x2 matrix-vector differential equation, which can be solved by the matrix-vector form of the variation of constants formula. For the sake of definiteness, assume that $\overline{T}$ is the average temperature on the system side and that $\overline{T}_{other}$ is the average temperature on the storage side, of the heat exchanger.

The subscripts 1 and 2 will be used to designate the system and storage sides of the heat exchanger (i.e., $T_1 = \overline{T}$ and $T_2 = \overline{T}_{other}$). Two versions of Eq. (13) appear as

$$M_1C_{1,p} \frac{dT_1}{dt} = -(2\dot{m}_1 C_{1,p} + h_1A)T_1 + 2\dot{m}_1 C_{1,p}T_{1,in} + h_1AT_2 \tag{14}$$

and

$$M_2 C_{2,p} \frac{dT_2}{dt} = -(2\dot{m}_2 C_{2,p} + h_2 A)T_2 + 2\dot{m}_2 C_{2,p} T_{2,in} + h_2 A T_1 \qquad (15)$$

where the surface area A is the same in both equations. Solving for the temperature derivatives yields

$$\frac{dT_1}{dt} = -\alpha_1 T_1 + \beta_1 T_2 + \gamma_1 \qquad (16)$$

and

$$\frac{dT_2}{dt} = -\alpha_2 T_2 + \beta_2 T_1 + \gamma_2 \qquad (17)$$

where $\alpha_i = (2\dot{m}_i C_{i,p} + h_i A)/M_i C_{i,p}$, $\beta_i = h_i A / M_i C_{i,p}$ and $\gamma_i = 2\dot{m}_i C_{i,p} T_{i,in} / M_i C_{i,p}$ for $i = 1,2$. A 2x2 matrix-vector differential equation is obtained from Eq. (16) and Eq. (17) for the average temperature column vector $\mathbf{T} = col(T_1, T_2)$ as follows

$$\frac{d\mathbf{T}}{dt} = \mathbf{A}\mathbf{T} + \mathbf{g} \qquad (18)$$

where $\mathbf{g} = col(\gamma_1, \gamma_2)$ may depend on time, through $T_{i,in}$, but the coefficient matrix

$$\mathbf{A} = \begin{bmatrix} -\alpha_1 & \beta_1 \\ \beta_2 & -\alpha_2 \end{bmatrix}$$

has constant entries. (Usually, $\beta_1 \beta_2$ is much smaller than $\alpha_1 \alpha_2$.)

The solution of Eq. (18) is obtained using the matrix-vector form of the variation of constants formula, Eq. (A7), as follows

$$\mathbf{T}(t) = \exp[\mathbf{A}\,t]\mathbf{T}_0 + \int_0^t \exp[\mathbf{A}(t-s)]\mathbf{g}(s)ds\,. \tag{19}$$

If $\mathbf{g}(t) = \mathbf{b}$ is a constant vector, then Eq. (A8) gives the result

$$\mathbf{T}(t) = \exp(\mathbf{A}\,t)(\mathbf{T}_0 + \mathbf{A}^{-1}\mathbf{b}) - \mathbf{A}^{-1}\mathbf{b}\,. \tag{20}$$

Equations (19) and (20) are evaluated by the diagonal decomposition of the coefficient matrix $\mathbf{A}$. The decomposition has the form $\mathbf{A} = \mathbf{V}\mathbf{D}\mathbf{V}^{-1}$ where $\mathbf{D}$ is a diagonal matrix containing the characteristic values of $\mathbf{A}$ and $\mathbf{V}$ is a nonsingular matrix whose columns are the characteristic vectors of $\mathbf{A}$. Using the diagonal decomposition, Eq. (19) becomes

$$\mathbf{T}(t) = \mathbf{V}\exp[\mathbf{D}\,t]\mathbf{V}^{-1}\mathbf{T}_0 + \int_0^t \mathbf{V}\exp[\mathbf{D}(t-s)]\mathbf{V}^{-1}\mathbf{g}(s)ds\,, \tag{21}$$

which can be evaluated with scalar arithmetic. Similarly, Eq. (20) can be evaluated as

$$\mathbf{T}(t) = \mathbf{V}\exp(\mathbf{D}\,t)\mathbf{V}^{-1}(\mathbf{T}_0 + \mathbf{A}^{-1}\mathbf{b}) - \mathbf{A}^{-1}\mathbf{b} \tag{22}$$

where $\mathbf{A}^{-1} = \mathbf{V}\mathbf{D}^{-1}\mathbf{V}^{-1}$.

Two Tank Indirect:

The two tank indirect TES system is described, most simply, when the two tank are perfectly insulated.

During the charge cycle the input to the heat exchanger, on the system side, is coming from the solar receiver. The input to the heat exchanger, on the storage side, is obtained by draining the cold tank and has a constant temperature. These inputs are used in Eq. (19) to compute the output of the heat exchanger on the system and storage sides. The output on the storage side is

use to fill the hot tank using a sequence of applications of Eq. (5) with piecewise constant values for T_{in}. Alternatively, the output of the heat exchanger, on the storage side, can be used as $T_{in}(t)$ in Eq. (3), which can then be solved with Eq. (A2), using numerical integration.

In the discharge cycle, the input to the heat exchanger, on the storage side, is obtained by draining the hot tank and it has a constant temperature. The input to the heat exchanger, on the system side, is returning from the steam generator with a relatively constant temperature. The inputs are used in Eq. (20) to compute the output of the heat exchanger on the system and storage sides. The output of the heat exchanger on the system side is used to generate steam. The output of the heat exchanger on the storage side is used as T_{in} to fill the cold tank. Again this is done using a sequence of piecewise constant applications of Eq. (5), or by using Eq. (A2) to integrate Eq. (3).

Summary:

Differential equations have been derived that model the components of a two tank direct and indirect TES system. The differential equations model a filling tank with Eq. (3), a draining tank with Eq. (8) and a heat exchanger with Eq. (18). The solutions for these differential equations are found using the variation of constants formula and are given in Eq. (4), Eq. (9) and Eq. (19). These solutions may be combined to model a two tank direct and indirect TES system. The combination requires using the output of one model as input to the next, as well as input from the external environment. The solution that simulates the dynamics of the combined model sometimes requires numerical integration.

Encapsulated Phase Change Heat Storage

Figure 119 shows a schematic of the EPCM storage.

Summary of EPCM Equations: One dimensional model (dimensionless form)

$$\frac{\partial \phi}{\partial \tau} = -(\frac{1}{\lambda})\frac{\partial \phi}{\partial x} + (\frac{1}{Pe_{sx}})\frac{\partial^2 \phi}{\partial x^2} - (\frac{NTU}{\lambda})(\theta - \varphi)$$

$$\frac{\partial \mathrm{H}}{\partial \tau} = (\frac{NTU}{\lambda})(\theta - \varphi) + (\frac{k_{sx}/k_{fx}}{Pe_{sx}})\frac{\partial^2 \theta}{\partial x^2}$$

$$When,$$

$$\mathrm{H} \geq (1 + St), \phi = (\mathrm{H} - St), \varsigma = 1(Liquid)$$

$$\mathrm{H} \leq (1 + St), \phi = \Phi_f, 0 \leq \zeta \leq 1$$

$$\mathrm{H} \leq \Phi_f, \phi = \mathrm{H}, \zeta = 0(solid)$$

$$\Phi_f = \frac{T_{MPt} - T_C}{T_H - T_C}, St = \frac{H_{fusion}}{C_s(T_H - T_C)}$$

$$\theta = \frac{(T_f - T_C)}{(T_H - T_C)}, \phi = \frac{(T_s - T_C)}{(T_H - T_C)}, H = \frac{\left[C_s(T_s - T_C) + \zeta H_{fusion}\right]}{C_s(T_H - T_C)}$$

$$x = \frac{z}{L}, Pe_x = \frac{GC_f L}{k_{fx}}, NTU = \frac{h_v L}{GC_f},$$

$$\lambda = \frac{\varepsilon \rho_f C_f}{(1 - \varepsilon)\rho_s C_s + \varepsilon \rho_f C_f}$$

$$\tau = \frac{GC_f t}{\left[1 - \varepsilon)\rho_s C_s + \varepsilon \rho_f C_f\right]}\left[\frac{1}{L}\right]$$

Boundary Conditions

Charging

$$x = 0, \theta = 0$$

$$x = 1, \frac{\partial \theta}{\partial x} = 0, \frac{\partial \phi}{\partial x} = 0$$

$$\tau \leq 0, 0 \leq x \leq 1, \mathrm{H}\ \&\ \theta, \zeta, specifiedprofile$$

Discharging

$$x = 1, \theta = 1$$

$$x = 0, \frac{\partial \theta}{\partial x} = 0, \frac{\partial \phi}{\partial x} = 0$$

$$\tau \le 0, 0 \le x \le 1, \phi \,\&\, \theta specifiedprofile$$

Dimensionless Variables

$$\theta = \frac{(T_f - T_C)}{(T_H - T_C)}, \phi = \frac{(T_s - T_C)}{(T_H - T_C)}, \Phi_{fusion} = \frac{(T_{MPt} - T_C)}{(T_H - T_C)}$$

$$x = \frac{z}{L}, Pe_x = \frac{GC_f H}{k_{fx}}, NTU = \frac{h_v L}{GC_f},$$

$$\lambda = \frac{\varepsilon \rho_f C_f}{(1-\varepsilon)\rho_s C_s + \varepsilon \rho_f C_f}$$

$$\tau = \frac{GC_f t}{[1-\varepsilon)\rho_s C_s + \varepsilon \rho_f C_f]}\left[\frac{1}{L}\right]$$

Figure 28: Encapsulated Phase Change Storage Tank

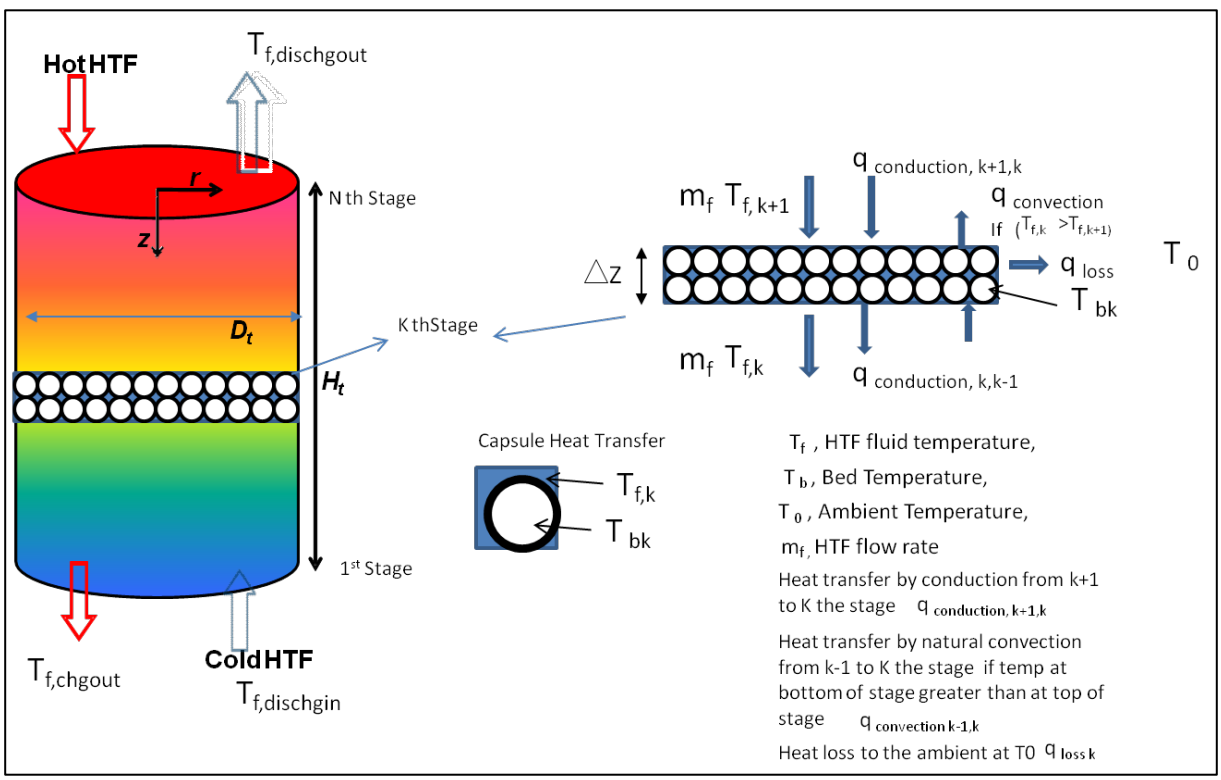

Source: Terrafore, Inc.

Cascaded Encapsulated Phase Change Heat Storage (Additional Equation)

Same equations as in 2 encapsulated phase change heat storage with following changes:

If

$$x \le \frac{L_1}{L}, then, H_{fusion} = H_{salt1}, T_{MPt} = T_{salt1}$$

$$\frac{L_1}{L} < x \le \frac{L_2}{L}, then, H_{fusion} = H_{salt2}, T_{MPt} = T_{salt2}$$

$$\frac{L_2}{L} < x \le 1, then, H_{fusion} = H_{salt3}, T_{MPt} = T_{salt3}$$

Variables:

G=mass velocity= HTF flow rate divided by tank cross section area

T = Temperature (subscripts H=design hot, C=design cold, f=fluid, s=solid or salt, MPt= melting point of salt)

L = height of tank, C =specific heat (subscript f=fluid, s=solid)

L_1= height from bottom to salt1 level; L_2 =Height from bottom to salt2 level

Salt1= salt at bottom of tank to height L_1, salt 2= salt at mid-level between L_1 and L_2, salt3 = salt at top level between L_2 and L

h_v =volumetric heat transfer coefficient = heat transfer coefficient times a_v specific area per unit volume of solid particles; a_v =6/[(1- ε) D_P]; D_P is the average particle diameter

ρ = density (subscripts: s=solid, f= fluid)

t = time, k=thermal conductivity (subscript: sx=solid, fx=fluid)

Pe= Peclet number

St= Stanton number

H = dimensionless enthalpy of capsule (subscript: fusion =heat of fusion)

Φ_{fusion} = dimensionless fusion temperature

ζ = liquid fraction (1=liquid, 0=frozen solid)

Dual Media Thermocline Heat Storage

Figure 120 shows a schematic of the thermocline thermal storage.

Figure 29: Dual Media Thermocline Tank with Trough Collector and Steam Rankine Turbine

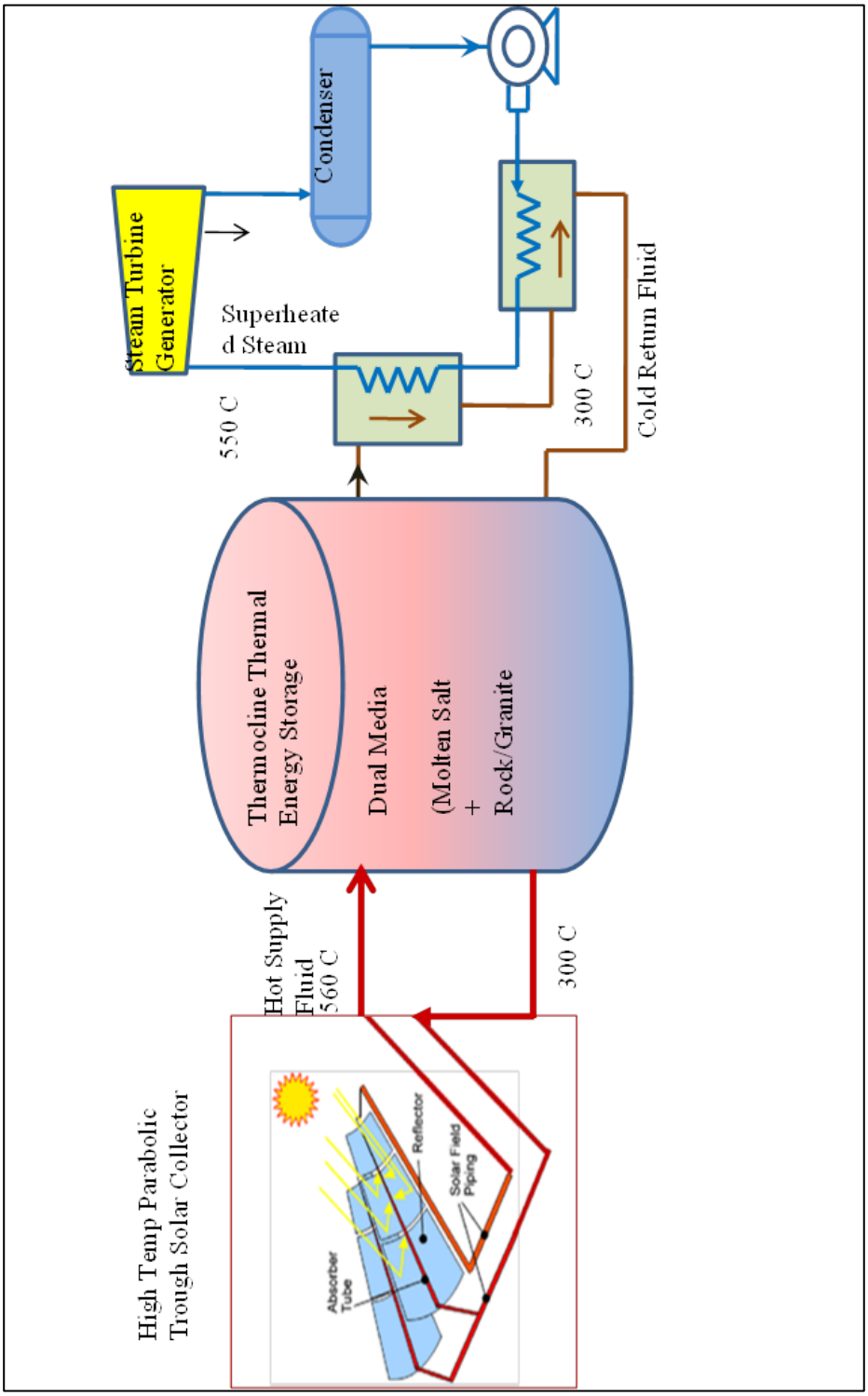

Source: Terrafore, Inc.

Summary of Equations One-Dimensional Model (dimensionless form)

$$\frac{\partial \phi}{\partial \tau} = -(\frac{1}{\lambda})\frac{\partial \phi}{\partial x} + (\frac{1}{Pe_{sx}})\frac{\partial^2 \phi}{\partial x^2} - (\frac{NTU}{\lambda})(\theta - \varphi)$$

$$\frac{\partial \theta}{\partial \tau} = (\frac{NTU}{\lambda})(\theta - \varphi) + (\frac{k_{sx}/k_{fx}}{Pe_{sx}})\frac{\partial^2 \theta}{\partial x^2}$$

Boundary Conditions

Charging

$$x = 0, \theta = 0$$
$$x = 1, \frac{\partial \theta}{\partial x} = 0$$
$$x = 1, \frac{\partial \phi}{\partial x} = 0$$
$$\tau \le 0, 0 \le x \le 1, \phi \;\&\; \theta specifiedprofile$$

Discharging

$$x = 1, \theta = 1$$
$$x = 0, \frac{\partial \theta}{\partial x} = 0$$
$$x = 0, \frac{\partial \phi}{\partial x} = 0$$
$$\tau \le 0, 0 \le x \le 1, \phi \;\&\; \theta specifiedprofile$$

$$\theta = \frac{(T_f - T_C)}{(T_H - T_C)}, \phi = \frac{(T_s - T_C)}{(T_H - T_C)}$$

$$x = \frac{z}{L}, Pe_x = \frac{GC_f L}{k_{fx}}, NTU = \frac{h_v L}{GC_f},$$

$$\lambda = \frac{\varepsilon \rho_f C_f}{(1-\varepsilon)\rho_s C_s + \varepsilon \rho_f C_f}$$

$$\tau = \frac{GC_f t}{\left[(1-\varepsilon)\rho_s C_s + \varepsilon \rho_f C_f\right]}\left[\frac{1}{L}\right]$$

Explicit Finite Difference Method to Solving Dual Media Equations:

This section provides an example of applying an explicit finite difference method to solve a heat storage problem. The finite difference method converts the partial differential equations for temperature into algebraic equations that can be applied, sequentially, to obtain the time histories of the temperatures as a function of the spatial variable.

Accuracy and efficiency of two finite difference schemes are discussed. Center-spaced differencing, applied to the fluid convection term, is more accurate and less efficient while upwind differencing is less accurate and more efficient.

The following is based on the dual media model, with one spatial dimension, used by Ismail and Stuginsky [iv] [Eq. (3) and (4), p.762]. The partial differential equations for the temperatures $\overline{T}(t,x)$ (of the fluid) and $\overline{\theta}(t,x)$ (average in the solid particles) are

$$\varepsilon \rho_f c_f \frac{\partial \overline{T}}{\partial t} + Gc_f \frac{\partial \overline{T}}{\partial \overline{x}} = k_{fx} \frac{\partial^2 \overline{T}}{\partial \overline{x}^2} + h_v(\overline{\theta} - \overline{T}) \qquad (1)$$

$$(1-\varepsilon)\rho_s c_s \frac{\partial \overline{\theta}}{\partial t} = k_{sx} \frac{\partial^2 \overline{\theta}}{\partial \overline{x}^2} + h_v(\overline{T} - \overline{\theta}) \qquad (2)$$

where $0 \le t$ and $0 \le \overline{x} \le L$. The wall heat transfer coefficient has been set to zero and $h_v = h_p a_p$. The dual media parameters in Eq. (1) and Eq. (2) are described in Tab. 1 and Tab. 2 with associated units and values for a molten salt and concrete example.

The boundary conditions for Eq. (1) are $\overline{T}(t,0) = T_H$ and $\partial \overline{T}(t,L)/\partial \overline{x} = 0$ for $t \ge 0$. The boundary conditions represent a specified hot inlet temperature T_H, at $\overline{x} = 0$ and the lack of any

temperature gradient at outflow, at $\bar{x} = L$. The initial temperature $\bar{T}(0,\bar{x})$ is assumed to be some colder temperature T_C, except at $\bar{x} = 0$ where $\bar{T}(0,0) = T_H$. The boundary conditions for Eq. (2) are $\partial\bar{\theta}(t,0)/\partial\bar{x} = 0$ and $\partial\bar{\theta}(t,L)/\partial\bar{x} = 0$ for $t \geq 0$.

The non-dimensional variables to be used here are

$$x = \bar{x}/L, \quad \tau = \frac{Gc_f t}{[(1-\varepsilon)\rho_s c_s + \varepsilon\rho_f c_f]L}, \quad T = \frac{(\bar{T} - T_C)}{(T_H - T_C)} \quad \text{and} \quad \theta = \frac{(\bar{\theta} - T_C)}{(T_H - T_C)}.$$

This choice yields the following set of non-dimensional equations

$$\lambda\frac{\partial T}{\partial \tau} = \frac{k_{fx}}{Gc_f L}\frac{\partial^2 T}{\partial x^2} - \frac{\partial T}{\partial x} + \frac{h_v L}{Gc_f}(\theta - T) \tag{3}$$

$$\gamma\frac{\partial \theta}{\partial \tau} = \frac{k_{sx}}{Gc_f L}\frac{\partial^2 \theta}{\partial x^2} + \frac{h_v L}{Gc_f}(T - \theta) \tag{4}$$

where $\lambda = \dfrac{\varepsilon\rho_f c_f}{(1-\varepsilon)\rho_s c_s + \varepsilon\rho_f c_f}$ and $\gamma = \dfrac{(1-\varepsilon)\rho_s c_s}{(1-\varepsilon)\rho_s c_s + \varepsilon\rho_f c_f}$. These non-dimensional equations are a variation of the set of equations found in Ismail and Stuginsky **Error! Bookmark not defined.**[Eq. (26) and (27), p.768]. They are based on a different choice of non-dimensional time, τ.

The non-dimensional boundary conditions for Eq. (3) are $T(\tau,0) = 1$ and $\partial T(\tau,1)/\partial x = 0$ for $\tau \geq 0$. The initial fluid temperature $T(0,x)$ is assumed to be zero, except at $x = 0$ where $T(0,0) = 1$. The boundary conditions for the solid temperature in Eq. (4) are $\partial\theta(\tau,0)/\partial x = 0$ and $\partial\theta(\tau,1)/\partial x = 0$ for $\tau \geq 0$. The initial solid temperature $\theta(0,x)$ is assumed to be zero.

Finite Difference Method:

Equations (3) and (4) are rewritten as

$$\lambda \frac{\partial T}{\partial \tau} = a \frac{\partial^2 T}{\partial x^2} - \frac{\partial T}{\partial x} + c(\theta - T) \tag{5}$$

and

$$\gamma \frac{\partial \theta}{\partial \tau} = b \frac{\partial^2 \theta}{\partial x^2} + c(T - \theta) \tag{6}$$

where $a = k_{fx} / (Gc_f L)$, $b = k_{sx} / (Gc_f L)$ and $c = h_v L / (Gc_f)$. The finite difference method is based on introducing a discrete grid in time and space: $\tau_n = n\Delta\tau,\ n = 0,1,\cdots$ and $x_j = j\Delta x,\ j = 0,1,\cdots,J$ where $\Delta x = 1/J$. The values of the non-dimensional temperatures are designated by $T_{n,j} = T(\tau_n, x_j)$ and $\theta_{n,j} = \theta(\tau_n, x_j)$. The partial derivatives in Eq. (5) are approximated with difference quotients as follows (forward central for time and space derivatives respectively):

$$\frac{\partial T}{\partial \tau} \cong \frac{T_{n+1,j} - T_{n,j}}{\Delta \tau},$$

$$\frac{\partial T}{\partial x} \cong \frac{T_{n,j+1} - T_{n,j-1}}{2\Delta x} \quad \text{or} \quad \frac{\partial T}{\partial x} \cong \frac{T_{n,j} - T_{n,j-1}}{\Delta x},$$

and

$$\frac{\partial^2 T}{\partial x^2} \cong \frac{1}{\Delta x}\left\{\left(\frac{T_{n,j+1} - T_{n,j}}{\Delta x}\right) - \left(\frac{T_{n,j} - T_{n,j-1}}{\Delta x}\right)\right\} = \frac{T_{n,j+1} - 2T_{n,j} + T_{n,j-1}}{\Delta x^2}\ .$$

Similar finite difference approximations for $\partial\theta / \partial\tau$ and $\partial^2\theta / \partial x^2$ will be used in Eq. (6). The spatial difference approximation for $\partial T / \partial x$ that is symmetric about $T_{n,j}$ is called center-spaced. The alternative asymmetric approximation for $\partial T / \partial x$ is called the upwind difference, since the index j increases in the same direction as the flow of the HTF. The substitution of

these approximations into Eq.'s (5) and (6) give explicit formulas for $T_{n+1,j}$ and $\theta_{n+1,j}$ in terms of $T_{n,j}$ and $\theta_{n,j}$. These finite difference schemes have stability requirements, on the size and relationship between $\Delta\tau$ and Δx. The stability requirements are discussed in the next section.

The explicit formulas, to advance the temperature forward in time, are:

$$\lambda\frac{T_{n+1,j}}{\Delta\tau} = \lambda\frac{T_{n,j}}{\Delta\tau} + a\frac{T_{n,j+1} - 2T_{n,j} + T_{n,j-1}}{\Delta x^2} - \frac{T_{n,j+1} - T_{n,j-1}}{2\Delta x} + c(\theta_{n,j} - T_{n,j})$$

or

$$\lambda\frac{T_{n+1,j}}{\Delta\tau} = \lambda\frac{T_{n,j}}{\Delta\tau} + a\frac{T_{n,j+1} - 2T_{n,j} + T_{n,j-1}}{\Delta x^2} - \frac{T_{n,j} - T_{n,j-1}}{\Delta x} + c(\theta_{n,j} - T_{n,j})$$

and

$$\gamma\frac{\theta_{n+1,j}}{\Delta\tau} = \gamma\frac{\theta_{n,j}}{\Delta\tau} + b\frac{\theta_{n,j+1} - 2\theta_{n,j} + \theta_{n,j-1}}{\Delta x^2} + c(T_{n,j} - \theta_{n,j})$$

for $j = 1, J-1$. For the purpose of implementation, the explicit formula for the fluid temperature is rewritten as

$$T_{n+1,j} = \alpha_f T_{n,j-1} + \delta_f T_{n,j} + \beta_f T_{n,j+1} + \xi_f \theta_{n,j} \qquad (7)$$

where, using center-spaced differencing,

$$\alpha_f = \frac{\Delta\tau}{\lambda}\left(\frac{a}{\Delta x^2} + \frac{1}{2\Delta x}\right),\ \delta_f = \frac{\Delta\tau}{\lambda}\left(\frac{\lambda}{\Delta\tau} - \frac{2a}{\Delta x^2} - c\right),\ \beta_f = \frac{\Delta\tau}{\lambda}\left(\frac{a}{\Delta x^2} - \frac{1}{2\Delta x}\right);$$

or, using upwind differencing,

$$\alpha_f = \frac{\Delta\tau}{\lambda}\left(\frac{a}{\Delta x^2} + \frac{1}{\Delta x}\right),\ \delta_f = \frac{\Delta\tau}{\lambda}\left(\frac{\lambda}{\Delta\tau} - \frac{2a}{\Delta x^2} - \frac{1}{\Delta x} - c\right),\ \beta_f = \frac{\Delta\tau\, a}{\lambda\,\Delta x^2}\ ,$$

and $\xi_f = \Delta\tau\, c/\lambda$, in both cases. The explicit formula for the solid temperature is rewritten as

$$\theta_{n+1,j} = \alpha_s\theta_{n,j-1} + \delta_s\theta_{n,j} + \beta_s\theta_{n,j+1} + \xi_s T_{n,j} \qquad (8)$$

where

$$\alpha_s = \frac{\Delta\tau\, b}{\gamma\,\Delta x^2},\ \delta_s = \frac{\Delta\tau}{\gamma}\left(\frac{\gamma}{\Delta\tau} - \frac{2b}{\Delta x^2} - c\right),\ \beta_s = \frac{\Delta\tau\, b}{\gamma\,\Delta x^2} \text{ and } \xi_s = \frac{\Delta\tau\, c}{\gamma}$$

for $j = 1, J-1$.

The boundary conditions on the fluid temperature, which apply for $j = 0$ and $j = J$, require that the inflow temperature is fixed and that the discrete approximation of the outflow gradient is zero. These conditions take the form $T_{n+1,0} = 1$ and $T_{n+1,J} = T_{n+1,J-1}$. The conditions on the solid temperature are $\theta_{n+1,0} = \theta_{n+1,1}$ and $\theta_{n+1,J} = \theta_{n+1,J-1}$.

Stability Requirements:

While implicit finite difference schemes can be unconditionally stable, explicit schemes usually have requirements on the size and relationship between $\Delta\tau$ and Δx to assure stability. For the purpose of this discussion, Eq. (5) is converted to the standard convection-diffusion equation**Error! Bookmark not defined.** [p. 157]. This is accomplished by dividing Eq. (5) by λ and ignoring coupling to obtain

$$\frac{\partial T}{\partial\tau} + b_f\frac{\partial T}{\partial x} = a_f\frac{\partial^2 T}{\partial x^2}$$

where $b_f = 1/\lambda$ and $a_f = a/\lambda$. The stability requirement for forward-time center-spaced differencing is $2a_f \Delta\tau / \Delta x^2 < 1$, which makes the accuracy of the scheme second order in space. The elimination of oscillations [2, p. 158], in the center-spaced differencing scheme, yields the convection-diffusion requirement $\Delta x < 2a_f / b_f$ where a_f / b_f is the ratio of the diffusion coefficient to the convection coefficient.

The use of upwind differencing alleviates the convections-diffusion requirement at the expense of producing a scheme that is only first order accurate in space[v] [p. 160-161]. Upwind differencing, implicitly, adds numerical diffusion so that the convections-diffusion requirement is satisfied. The stability requirement then becomes $(2a_f + b_f \Delta x)\Delta\tau / \Delta x^2 \leq 1$.

A simpler stability analysis, without convection, applies to Eq. (6), after ignoring the effect of coupling between Eq. (5) and Eq. (6).

Plant Model in Simulink

Models developed for various CSP and TES technologies are implemented in Simulink. The models of solar field, thermal storage and other components such as steam generation system (boiler/heat exchanger) and steam turbine are integrated to simulate the entire plant model. A PID controller is also designed and tuned to control the output of the plant according to the instructed set-points. A block diagram of the Simulink model is shown in Figure 121.

Figure 30: Overview of Plant Model in Simulink

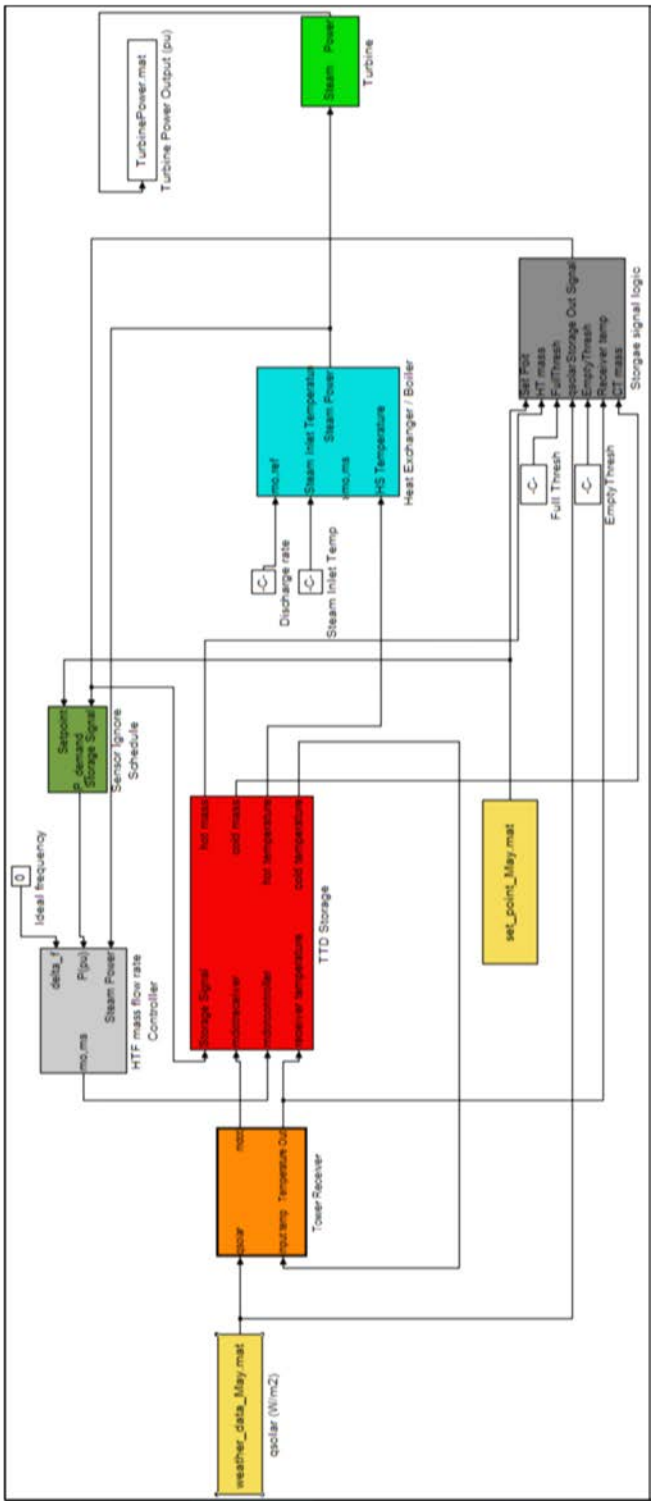

Source: DNV GL

[i] **A. Felix Regin, S.C. Solankia and J.S. Sainia.** Heat Transfer Characterisitcs of thermal energy storage system using PCM capsules: A Review. *Renewable and Sustainable Energy Reviews.* 2008, Vol. 12, 9 pages 2438-2458.

[ii] **Beasley, D.E, Ramanarayan, C., Torab, H.** Thermal Response of a packed bed of spheres containing a phase change material. *International Journal of Energy Research.* 1989, Vol. 13, 3 pages 253-265

[iii] **F. P. Incropera and D. P. DeWitt**, Fundamentals of Heat and Mass Transfer, 4th Edition (John Wiley and Sons, New York, NY, 1996).

[iv] **K. A. R. Ismail, and R. Stuginsky Jr.** A parametric study of possible fixed bed models for pcm and sensible storage. *Applied Thermal Engineering.* 1999, Vol. 19, 7, pages 757-788.

[v] **F. Brauer and J A. Nohel,** Ordinary Differential Equations: A First Course, 2nd Edition (W. A. Benjamin, Inc. Menlo Park. California, 1973).

Appendix E:
Detailed Results from Thermodynamic Plant Model Simulations

System-Level Analysis

This subsection verifies the performance of CSP and TES technologies, using the detailed thermodynamic models (Appendix D), when following day-ahead schedules obtained from the production costing simulations in PLEXOS. These schedules were optimized for system-level benefits as described in Chapter 3.

Following Day-Ahead Energy Schedules

In the Day-Ahead Energy market, plant schedules are optimized to meet load at minimum cost of production. Technology constraints such as ramp limits, minimum and maximum capacity and other parameters are considered in the optimization, but the generators are assumed capable of producing the set MW level each hour and ramp within the allowed time window (typically 10 minutes before the hour) to the set-point for the next hour. For a CSP-TES plant operator, following a Day-Ahead schedule means assuring there is enough energy stored or solar production forecast to meet the schedule each hour and that ramping capabilities are adequate and predictable. Generators submit bids and receive an hourly dispatch schedule depending on how they are selected in the loading order. Payments depend on market prices and ability to follow the dispatch schedule and penalties are paid if a generator does not meet its schedule.

The ability of the CSP-TES technologies to follow a Day-Ahead Energy schedule is tested using the detailed thermodynamic models in combination with set-points derived in the system-level analysis. Figure 122 shows results for a CSP-TES plant with a central tower receiver and a two-tank direct thermal storage system using molten salt (Tower/TTD configuration): The storage net charging rate (on the left), and the plant output in response to the hourly day-ahead schedule for a July day (on the right). Note that simultaneous charging (from the solar field) and discharging (to the steam turbine) is allowed and indeed “normal” for thermal storage. Hence, positive net charging rate implies that the storage charging rate exceeds its discharge rate and vice versa. The chart shows that this technology is capable of following day-ahead schedules within the acceptable. Simulation results for multiple days and other configurations (Tower/EPCM, Trough/TTD, and Trough/EPCM) confirm this capability for other technologies as well. In conclusion, the system-level analysis results for Day-Ahead Energy participation of CSP-TES plants are considered achievable.

Figure 31: Tower/Two-Tank Direct Configuration – Storage Net Charging Rate and Plant Output

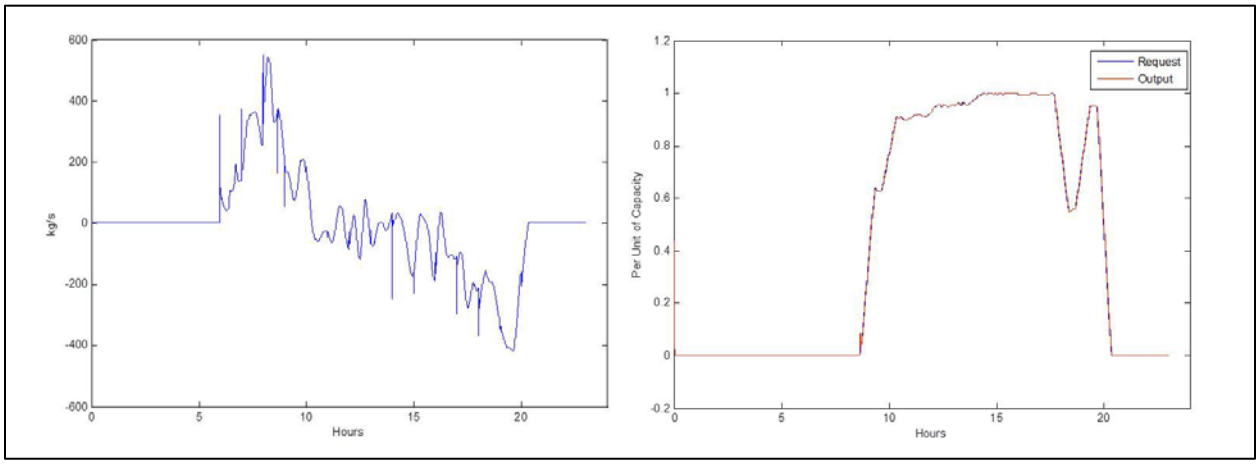

Source: DNV GL

Following Day-Ahead Regulation Schedules

In addition to participating in the Day-Ahead Energy market, plants can opt to bid into the ancillaries market, such as the regulation market. Regulation (also called AGC) consists of power output increases and decreases in response to up and down control signals. These signals are sent from a central system that senses the frequency in the grid and any variations in power flowing into and out of the control area on transmission lines (tie lines), and adjusts generator set-points to match load and restore the frequency. The control signal for regulation changes rapidly – every 4 seconds – and plants need to be flexible in order to follow this signal. In other words, performance requirements for the CSP-TES plant are higher when participating in the regulation market, including higher ramp rates and an ability to switch between charging and discharging rapidly.

For other ancillary market products, such as Spinning Reserves, dynamic performance requirements are similar to the Day-Ahead market, and it is assumed that if the plant is capable of following a regulation signal it is also fit to participate in other markets. However, participating in Spinning Reserves may imply other operational strategies and design choices. This is discussed in Chapter 6.

Tower and Two-Tank Direct Storage Model

The outputs of a Tower/TTD plant are shown in Figure 123 when the plant is providing both day-ahead energy and regulation services for days in May, July, October, and December. The initial level of energy in the hot tank is 4 percent of its capacity in the beginning of the day. While the plant is capable of following the rapid swings in the regulation set-point, it falls short in a couple of situations:

For the July day, the plant is not able to follow the set-point in the early morning hours. The early output is requested but not enough incoming solar energy in the morning is available.

On the December day, the plant is falling short at the end of the day. This is due to not enough solar energy being collected during the day, for the requested output.

Storing over-night and starting with more energy (for example, 10 percent of capacity) in the storage tank would solve this issue, as seen in Figure 0-33, which shows the plant output versus the requested set-point following day-ahead energy and regulation schedules, but with initial storage levels at 10 percent of storage capacity, for a July day. As long as the thermal storage is reaching the same level at the end of the day, this strategy will ensure enough energy is available in the early morning for regulation and ramping. However, for the December all energy from the sun should have been gained during this day, in other words, the schedule requests more energy than the energy input. Storing over-night would fix it for this one day, but the storage cannot be replenished on this day to be ready for early hours of next day.

Figure 32: Tower/Two-Tank Direct Configuration – Plant Output for DAE & Regulation

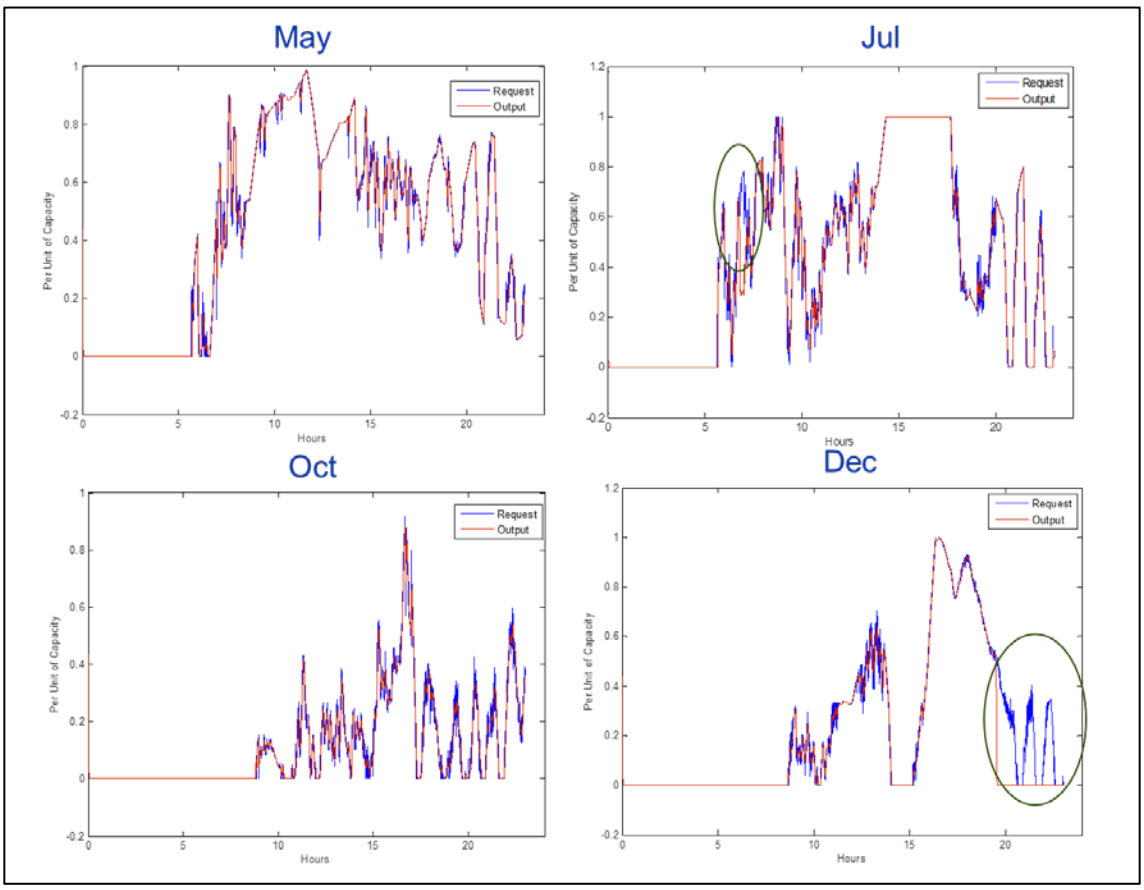

Source: DNV GL

Figure 33: Tower/Two-Tank Direct – Plant Output with 10 Percent Initial TES Energy Level

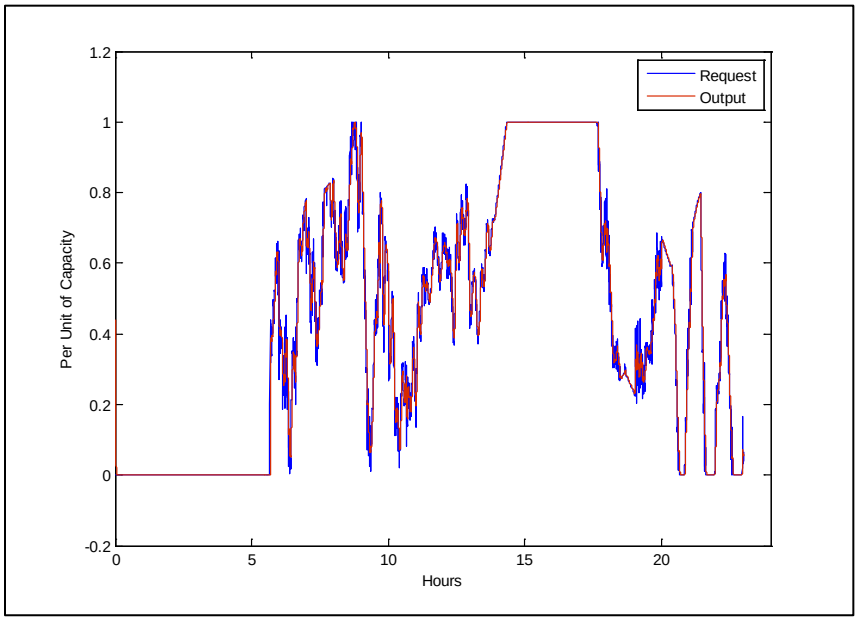

Source: DNV GL

Trough and Two-Tank Direct Storage Model

The same analysis was done for a CSP plant using the trough technology, coupled with two-tank direct thermal storage. Figure 125 depicts the outputs of Trough/TTD in response to day-ahead energy and regulation schedules. The same phenomenon can be observed for the May and July days, as was seen for the tower model: available solar energy is not sufficient in the morning, preventing the plant from following the set-points after it runs out of the energy it stored over-night (4 percent of capacity). For the December day, the plant is again falling short in the evening. Starting with higher energy levels in the tank would solve the issue; however, as noted in the results for the Tower/TTD model, this strategy is not sustainable, unless there is excess energy from the sun the following day. Figure 126 shows how increasing the initial storage level to 11 percent of the thermal storage capacity improves the performance, but does not totally eliminate the issue. For the trough model, 15 percent of initial storage would enable the plant to fully follow the set-points over the course of day.

Figure 34: Trough/Two-Tank Direct – Plant Output for DAE and Regulation Schedules

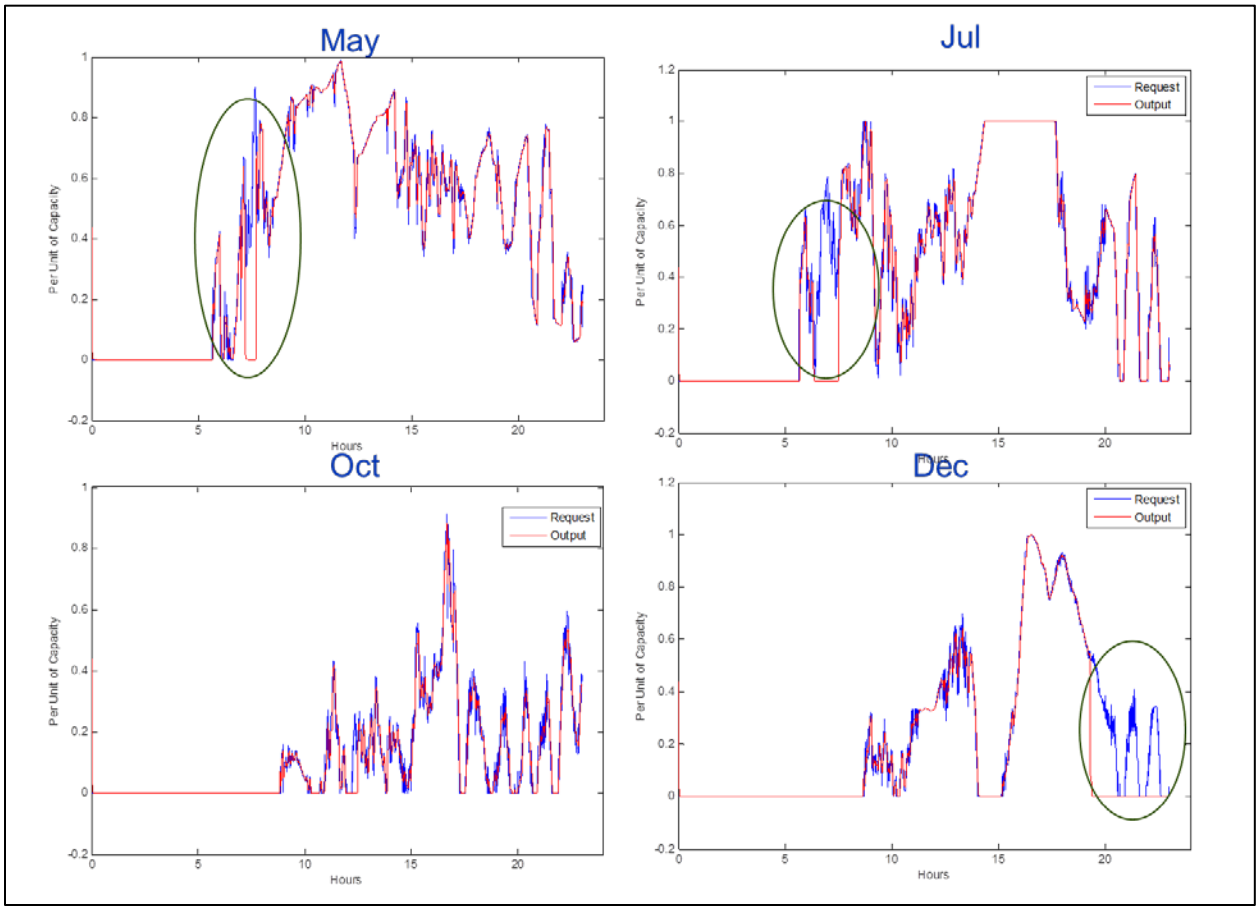

Source: DNV GL

Figure 35: Trough/Two-Tank Direct – Plant Output with 11 Percent and 15 Percent Initial TES Energy Levels

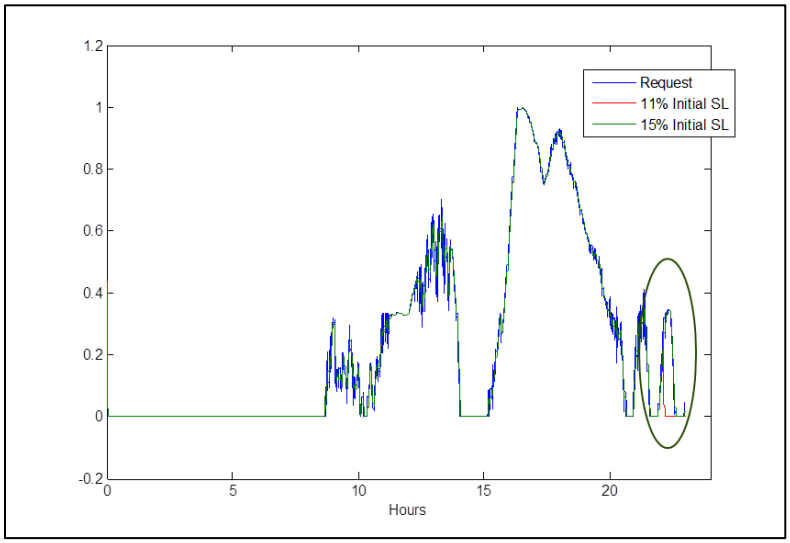

Source: DNV GL

Comparing the results of the two configurations suggests that there may be a difference in the performance of the two CSP technologies, trough and tower. The solar irradiation profiles for the same four days are shown in Figure 127. The same solar irradiation inputs are used for both Tower/TTD and Trough/TTD. Figure 128 illustrates the temperature profiles of HTF in the Tower model (left) and the Trough model (right). The simulation results suggest that it takes longer for the trough technology to heat up the HTF. This explains why the plant with trough requires more energy in the storage during early hours of morning and points to a difference in operational strategy and optimal storage configuration between the tower and trough technologies.

Figure 36: Solar Irradiation Profiles

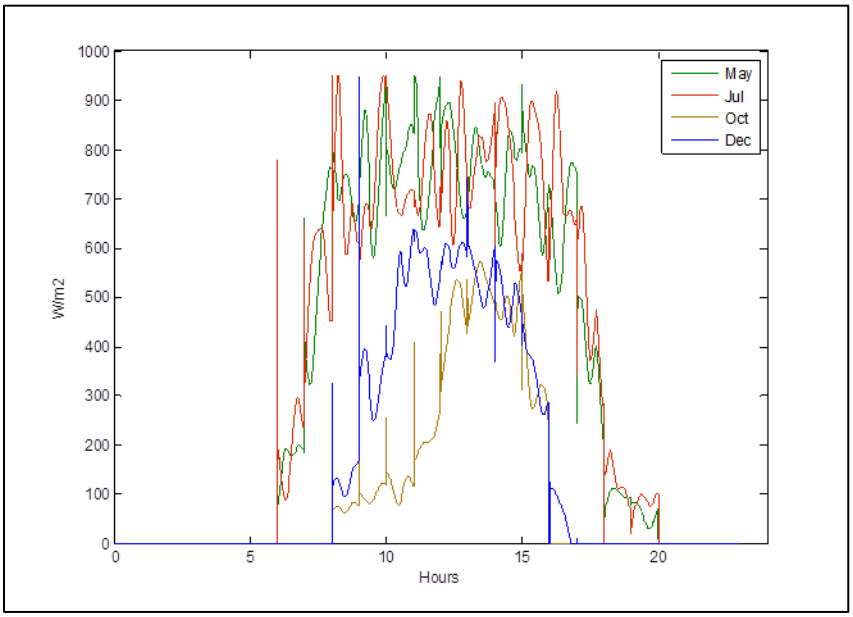

Source: DNV GL

Figure 37: HTF Temperature Profiles for Tower (Left) and Trough (Right)

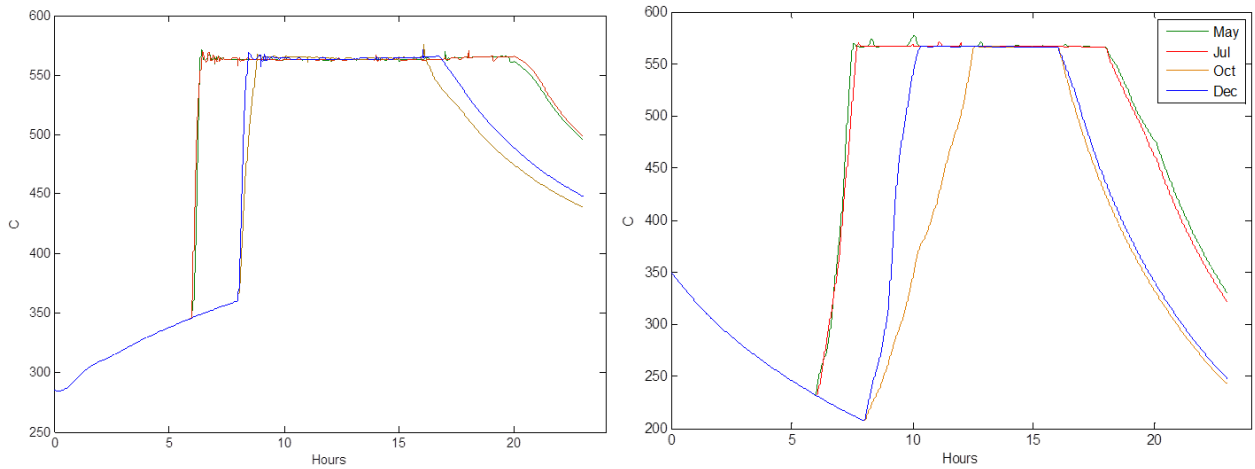

Source: DNV GL

The performance of additional thermal storage technologies was tested in similar simulations. Results show no significant difference in the dynamic performance of different storage technologies. Figure 129 depicts the output of a Tower/EPCM plant responding to day-ahead energy and regulation schedules for a day in July, suggesting dynamic behavior similar to that of the two-tank direct thermal storage tested above.

Figure 38: Tower/EPCM Configuration – Plant Output for DAE & Regulation

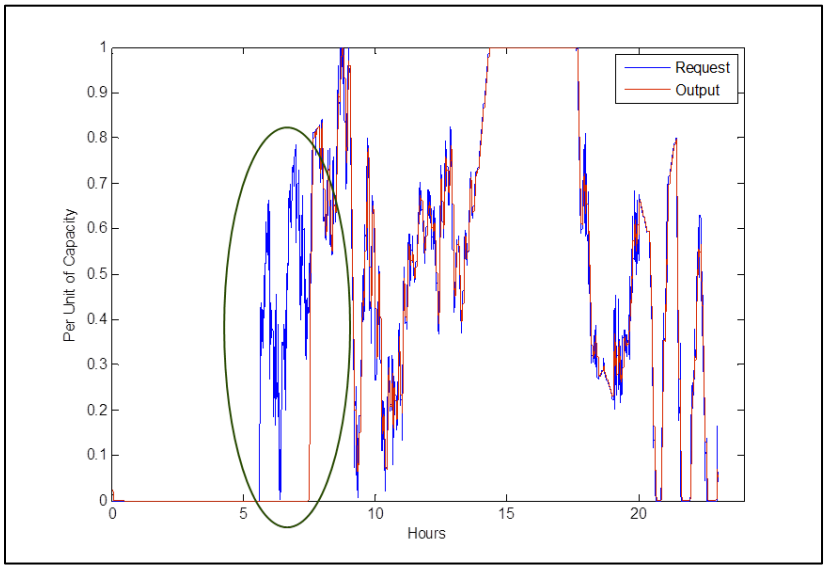

Source: DNV GL

Plant-Revenue Optimization Simulations

This subsection verifies the performance of CSP and TES technologies, using the detailed thermodynamic models (Appendix D), when following day-ahead schedules obtained from the market participation optimization simulations in in MGO. These schedules were optimized for highest plant revenue when participating in day-ahead markets, as described in Chapter 5.

Viability of Market Participation Schedules

The CSP-TES plant's optimal market participation model does not account for detailed dynamics of any components. The model guarantees the maximum revenue stream for the plant by participating in a specific combination of markets (energy and ancillary services), and obtains the optimal hourly commitment to each market. However, some operational constraints might exist due to dynamic behavior of the plant including the thermodynamics of the solar field and TES as well as the flexibility of the steam turbine. For instance, the input to the market participation model is hourly energy output of the solar field and the model dispatches resources based on available energy from the solar field and thermal storage tank, as well as available capacity of the steam turbine. It also considers efficiency losses of storage and turbine. The thermodynamic models on the other hand, operate based on solar irradiation profiles and deploy the thermodynamic models of solar field and thermal storage to simulate the temperature profiles and the resulting energy flows throughout the system. It also considers dynamics of the turbine and relevant time delays for different components within the system. Therefore, some discrepancy is expected between the performances of different devices across the two models, but any major differences would indicate that the optimized dispatch schedules may be technically unfeasible.

In order to evaluate the viability of the schedules obtained from the plant market participation model the schedules are input to the thermodynamic models of the CSP-TES system, developed and described in Chapter 4 and Appendix D. The results of these simulations suggest that the schedules obtained from the market participation optimization are viable.

Figure 133 illustrates the viability of the schedules for a plant participating in the day-ahead energy market. The revenue-optimal schedules for a May day are input to a stand-alone thermodynamic Simulink model of a CSP-TES plant using the Tower/Two-Tank Direct technologies. The plant consists of a 100 MW steam turbine (with a solar multiple of 1) and 6-hour thermal storage. Figure 131 and Figure 132 show the charging and discharging behavior of the thermal storage to be consistent across the two models, verifying the technical feasibility of the dispatch schedule. Since the market participation model takes the energy gain profile from the solar field that is simulated by the dynamic model as input, storage charging profiles are in close agreement in both models (Figure 130). There is an average of 5 percent discrepancy in discharge profiles simulated by the two models, which is considered to be acceptable given all dynamic effects that are ignored in the market participation model (Figure 131).

Figure 39: Plant Output versus Requested Set-Point, May Day

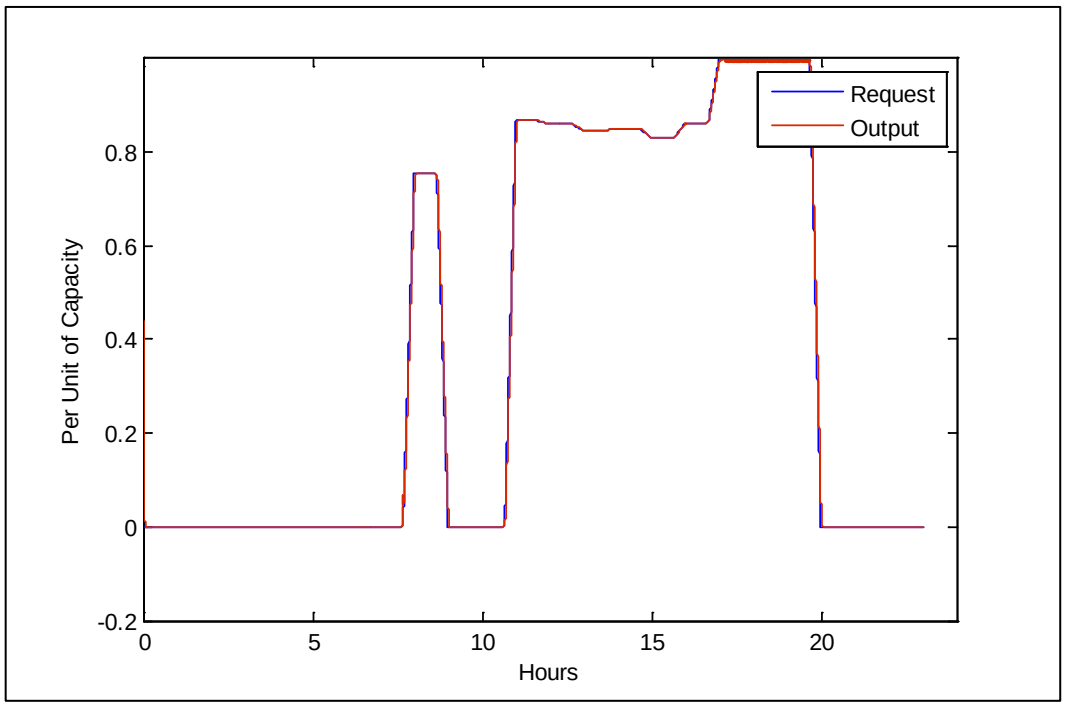

Source: DNV GL

Figure 40: Hot Tank Storage Charging Profiles, May Day

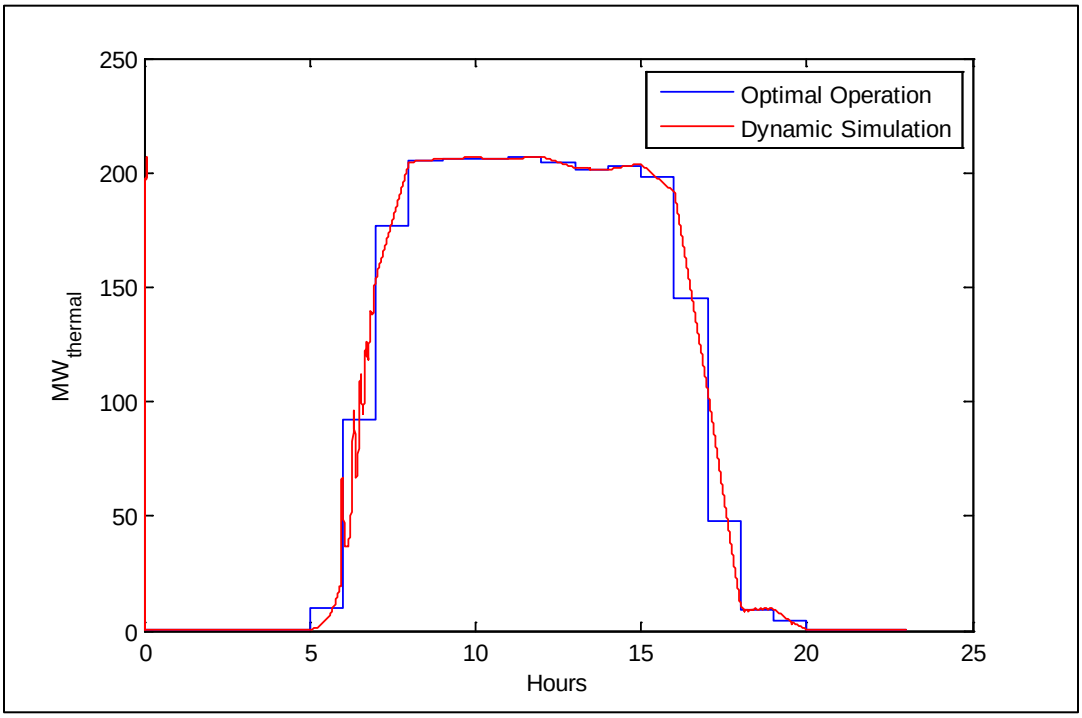

Source: DNV GL

Figure 41: Hot Tank Storage Discharging Profiles, May Day

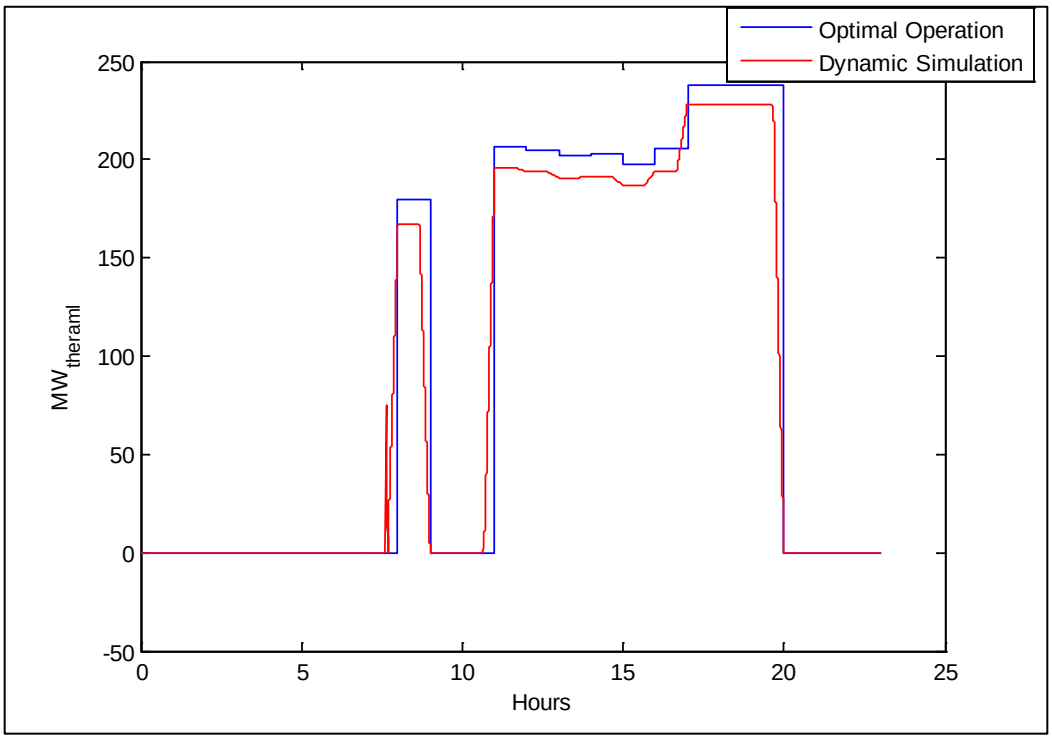

Source: DNV GL

Appendix F:
MGO – Operational Optimization Model

Linear Programming Formulation

The hourly optimization is formulated as a Mixed Integer Linear Program (MILP) problem. The mathematical formulation of the problem is described in the following sections.

Input Variables

Consider the time horizon of optimization $T = 24$ hours and $T = k.h$ where k is one hour and h = 24. The remainder of the document follows the notation listed below:

- S is a $h \times 1$ vector denoting the hourly energy production of solar collectors in MWhr.
- R_{Gen} is the ramp rate of the turbine generator in percent capacity/min
- G_{Cap} is the maximum capacity in MW of the steam turbine generator and $G_{\min}$ is the minimum capacity in MW. η_G is the efficiency of the steam turbine generator.
- B_{Cap} is the maximum capacity of the gas burner in MW and η_B is the efficiency of the burner.
- P_{DAE} is a $h \times 1$ vector denoting the hourly Day Ahead Energy (DAE) market clearing prices in \$/MWhr. Similarly, P_{RegU}, P_{RegD} and P_{SP} are $h \times 1$ vectors denoting the day ahead clearing prices of regulation up, regulation down and spinning reserve markets in \$/MW.
- P_G is the price of gas in \$/MWhr.
- H_{Cap} is the power capacity of thermal storage device in MW and H_{Dur} is its duration in hours. The energy capacity of the thermal storage device is $H_{En} = H_{Cap}.H_{Dur}$ in MWhr. η_H is the round-trip efficiency of the thermal storage device.
- l_{Init} is the state of charge of the thermal storage device at the beginning of the first time interval in MWhr
- m_{DART} denotes the ratio of the mean real time energy price over an hour to the day ahead energy market clearing price at that hour.
- m_{RegUE} is the energy produced over an hour in MWhr while following a regulation up signal when the capacity committed to the day-ahead regulation up market is one MW.
- m_{RegDE} is the energy produced over an hour in MWhr while following a regulation down signal when the capacity committed to the day-ahead regulation down market is one MW.

Decision Variables

The vectors of decision variables are as listed below. The decision variables are of dimension $h \times 1$ unless otherwise stated.

- δ_{GEN} is a binary vector where 1 implies that the turbine-generator is ON and 0 implies that the turbine-generator is OFF.
- g_{SFTS} denotes the energy output of the solar field used for charging thermal storage in MWhr
- g_{SFST} denotes the energy output of the solar field going directly to the steam turbine generator in MWhr
- g_{TSST} denotes the energy discharged from thermal storage device to the steam turbine generator in MWhr
- g_{GBST} denotes the energy transfer from the gas burner to the steam turbine generator in MWhr
- l_{TS} is the state of charge of the thermal storage device at the end of every hour in MWhr
- p_{STDAE} is the commitment of the steam turbine generator to the day ahead energy market in MW
- $p_{ST\,RegU}$ is the capacity in MW of the steam turbine generator committed to the regulation up market
- $p_{ST\,RegD}$ is the capacity in MW of the steam turbine generator committed to the regulation down market
- p_{STSP} is a $(h/2)\times 1$ vector denoting the capacity in MW of the steam turbine generator committed to the spinning reserve market. Each element of p_{STSP} has a dimension of 2k.

The vectors of decision variables are as listed below. The decision variables are of dimension $h \times 1$ unless otherwise stated.

- δ_{GEN} is a binary vector where 1 implies that the turbine-generator is ON and 0 implies that the turbine-generator is OFF.
- g_{SFTS} denotes the energy output of the solar field used for charging thermal storage in MWhr
- g_{SFST} denotes the energy output of the solar field going directly to the steam turbine generator in MWhr
- g_{TSST} denotes the energy discharged from thermal storage device to the steam turbine generator in MWhr

- g_{GBST} denotes the energy transfer from the gas burner to the steam turbine generator in MWhr
- l_{TS} is the state of charge of the thermal storage device at the end of every hour in MWhr
- p_{STDAE} is the commitment of the steam turbine generator to the day ahead energy market in MW
- $p_{ST\,RegU}$ is the capacity in MW of the steam turbine generator committed to the regulation up market
- $p_{ST\,RegD}$ is the capacity in MW of the steam turbine generator committed to the regulation down market
- p_{STSP} is a $(h/2)\times 1$ vector denoting the capacity in MW of the steam turbine generator committed to the spinning reserve market. Each element of p_{STSP} has a dimension of 2k.

Objective Function

The cost terms are as follows:

- Revenue in $ from committing to the day ahead energy market, $D_{DAE} = p_{STDAE} P_{DAE}$
- Revenue in $ from committing to the day ahead regulation up market consists of revenue from capacity committed as well as settlement on the spot market price of the energy discharged while providing the regulation up service

$$D_{RegU} = p_{ST\,RegU} P_{RegU} + p_{ST\,RegU} m_{RegUE} P_{DAE} m_{DART}$$

- Revenue in $ from committing to the day ahead regulation down market consists of revenue from capacity committed as well as the compensation for deficit in energy delivered from the day ahead energy commitment.

$$D_{RegD} = p_{ST\,RegD} P_{RegD} - p_{ST\,RegD} m_{RegDE} P_{DAE} m_{DART}$$

- Revenue in $ from committing to the spinning reserve market, $D_{SP} = p_{STSP} P_{SP}$
- Operational cost of the gas burner in $, $D_B = (g_{GBST} / \eta_B) P_G$

The objective function is then given by equation (1).

$$\min\left(\sum_{T}\left(-D_{DAE}-D_{RegU}-D_{RegD}-D_{SP}+D_{B}\right)\right) \tag{1}$$

Constraints

The energy output from the solar collectors is less than equal to the energy input to the solar collectors

$$g_{SFTS}+g_{SFST}\leq S \tag{2}$$

Equations (3) - (4) denote the constraints related to the capacity committed to the regulation up market. If the energy committed to the day ahead market is zero, equation (3) holds, else equation (4) holds. In general, the most restrictive bounds hold at any time.

$$p_{ST\,RegU}\leq G_{Cap}-G_{\min} \tag{3}$$

$$p_{ST\,RegU}\leq G_{Cap}-p_{STDAE} \tag{4}$$

Equation (5) denotes that the capacity committed to the regulation down market at any hour is less than equal to the capacity corresponding to the energy committed to the day-ahead energy market

$$p_{ST\,RegD}\leq p_{STDAE} \tag{5}$$

The capacity committed to spinning reserve is less than equal to the operational capacity of the steam turbine generator

$$p_{STSP}\leq G_{Cap}-G_{\min} \tag{6}$$

The change in the state of charge of the thermal storage device over any time interval is less than

$$l_{TS}\left(i\right)-l_{TS}\left(i-1\right)\leq g_{SFTS}\left(1-\frac{\left(1-\eta_{H}\right)}{2}\right)-g_{TSST}\left(1+\frac{\left(1-\eta_{H}\right)}{2}\right),\ i=1,\ldots,h \tag{7}$$

The state of charge of the thermal storage device at the end of the final time interval is greater than equal to its state of charge at the beginning of the first time interval i.e.

$$l_{TS}\left(h\right) \geq l_{Init} H_{en} \tag{8}$$

The energy output of the steam turbine generator is less than equal to its energy input

$$p_{STDAE} + p_{ST\,\mathrm{Re}\,gU} m_{\mathrm{Re}\,gUE} - p_{ST\,\mathrm{Re}\,gD} m_{\mathrm{Re}\,gDE} \leq \left(g_{SFST} + g_{GBST} + g_{TSST}\right)\eta_G \tag{9}$$

The total committed capacity of the steam turbine generator is less than equal to its maximum capacity

$$p_{STDAE} + p_{ST\,\mathrm{Re}\,gU} + p_{TSST} \leq G_{cap} \tag{10}$$

Thermal storage state of charge at the beginning and end of an hour is less than equal to the energy required to deliver the committed capacity to the spinning reserve market. Equation (11) denotes the energy at the end of hour *i* and equation (12) denotes the energy at the beginning of that hour.

$$p_{STSP}\left(i\right) \leq l_{TS}\left(i\right)\eta_G,\ i = 1,\ldots,h \tag{11}$$

$$p_{STSP}\left(i\right) \leq l_{TS}\left(i-1\right)\eta_G,\ i = 1,..,h \tag{12}$$

The upper and lower bounds of the decision variables are given by

$$
\begin{aligned}
&0 \le g_{SFTS} \le S \\
&0 \le g_{SFTS} \le H_{CAP} \\
&0 \le g_{SFST} \le S \\
&0 \le g_{TSST} \le G_{Cap} \\
&0 \le g_{TSST} \le H_{Cap} \\
&0 \le g_{GBST} \le B_{Cap} \\
&0 \le l_{TS} \le H_{En} \\
&G_{\min} - \left(1 - \delta_{GEN}\right) G_{\min} \le p_{STDAE} \le G_{Cap} - \left(1 - \delta_{GEN}\right) G_{Cap} \\
&0 \le p_{ST\,\mathrm{Re}gU} \le R_{Gen} G_{Cap} \left(5/60\right) \\
&0 \le p_{ST\,\mathrm{Re}gD} \le R_{Gen} G_{Cap} \left(5/60\right) \\
&0 \le p_{ST\,\mathrm{Re}gU} \le G_{Cap} - \left(1 - \delta_{GEN}\right) G_{Cap} \\
&0 \le p_{ST\,\mathrm{Re}gD} \le G_{Cap} - \left(1 - \delta_{GEN}\right) G_{Cap} \\
&0 \le p_{STSP} \le G_{Cap} - \left(1 - \delta_{GEN}\right) G_{Cap}
\end{aligned}
\tag{13}
$$

The optimization problem is then expressed as (1) subject to constraints (2) - (13).

Appendix G:
Input Data for MGO 2020 simulations

Energy and Gas Prices

Hourly 2020 data for day-ahead energy and ancillary market prices are derived from a production costing simulation of the CAISO system in PLEXOS. The simulation is based on CPUC 2010 Long Term Procurement Plan, with the 2020 trajectory scenario assuming 4 GW of CSP-TES with 6 hours of thermal storage installed in the CAISO system. The unit under consideration is assumed to be installed in the Southern California Edison (SCE) region. The following price signals are used as inputs to the optimization: day-ahead energy, regulation up, regulation down and spinning reserves. The monthly gas prices are consistent with the RPS scenario and vary between $5.5 and $6.3 per MMBtu, as shown in Figure 133.

Figure 42: 2020 Natural Gas Forecast

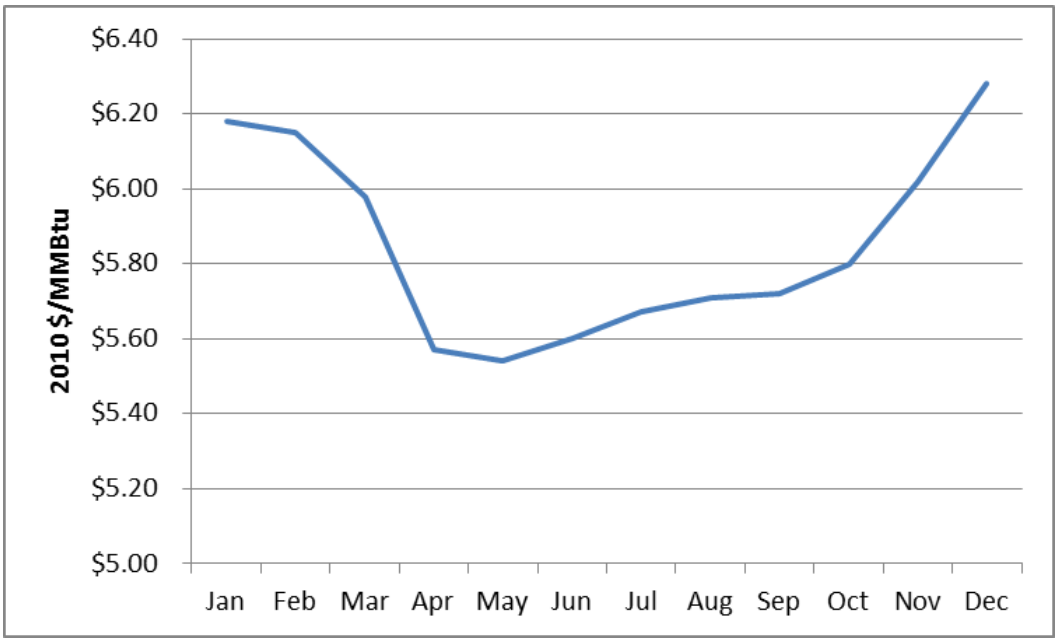

Source: CAISO Trajectory Scenario

Figure 43: Average Day-Ahead Energy Prices, January – December 2020

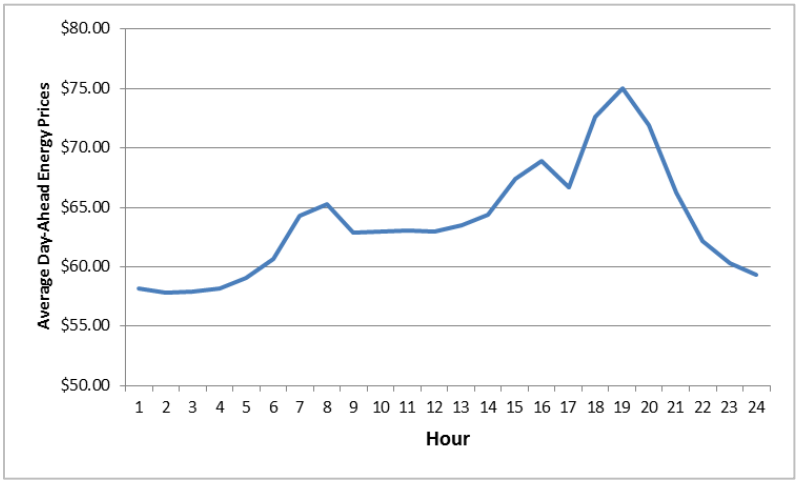

Source: DNV GL

Figure 44: Average Day-Ahead Regulation Prices, January – December 2020

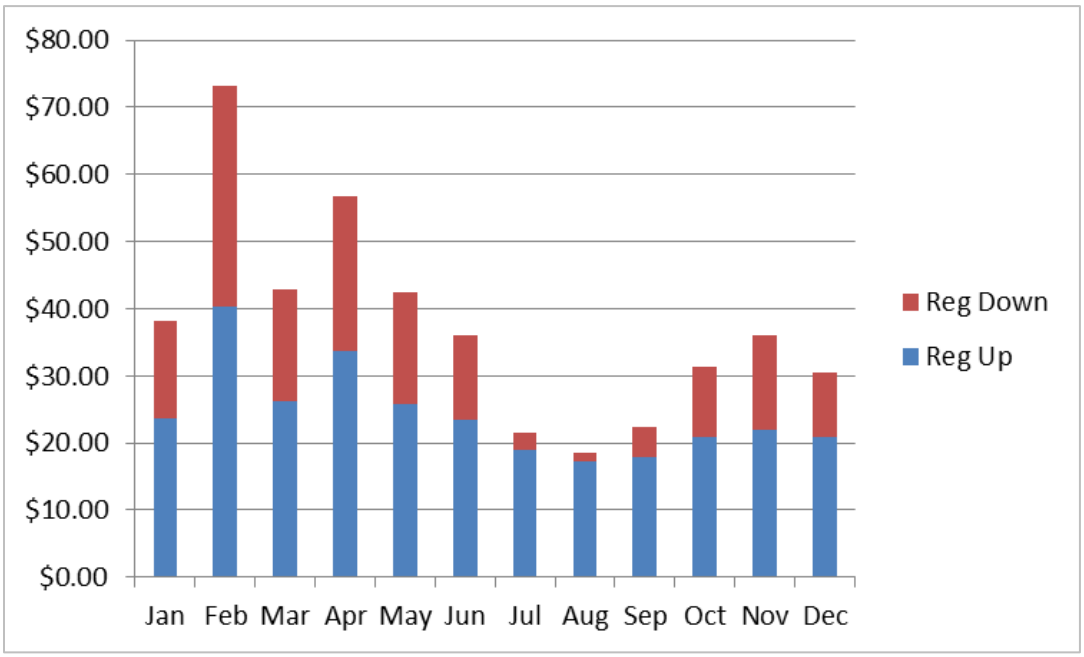

Source: DNV GL

Figure 45: Average Day-Ahead Hourly Regulation Prices, January – December 2020

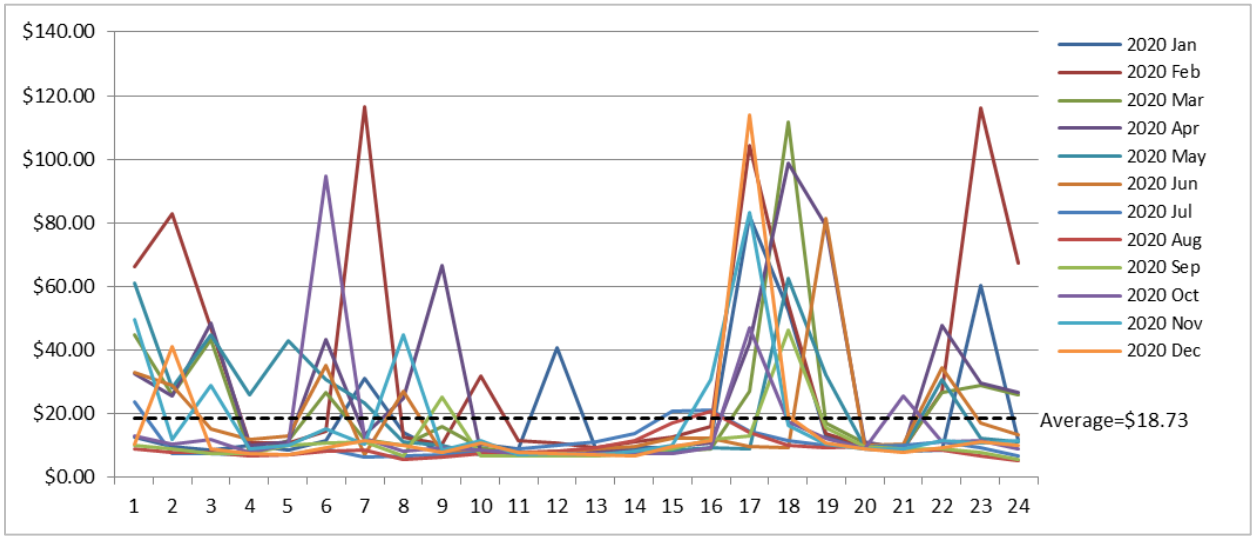

Source: DNV GL

Figure 46: Spinning Reserves Prices by Month, January – December 2020

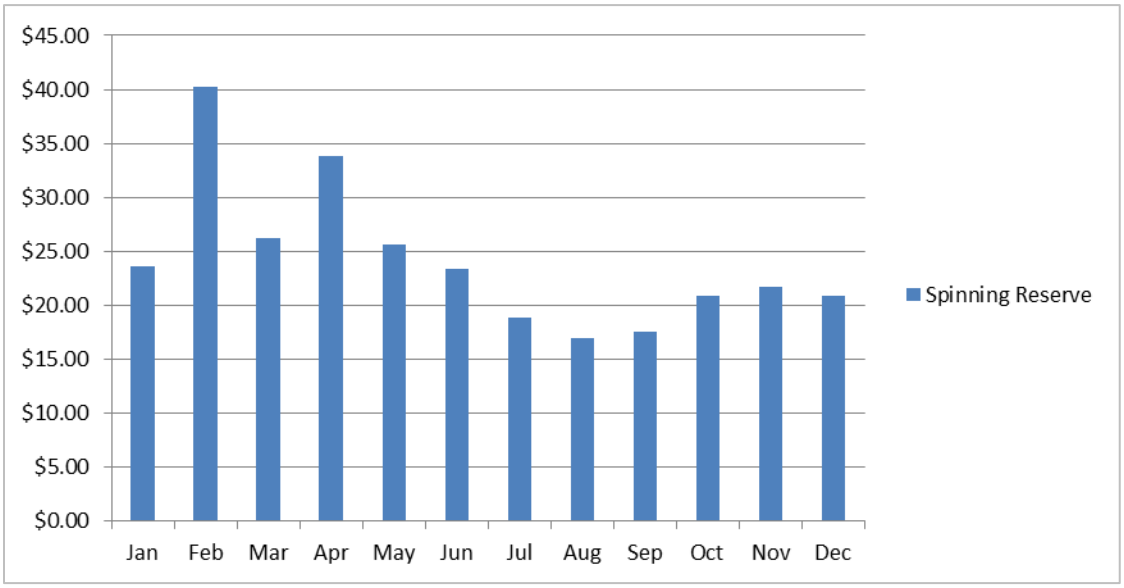

Source: DNV GL
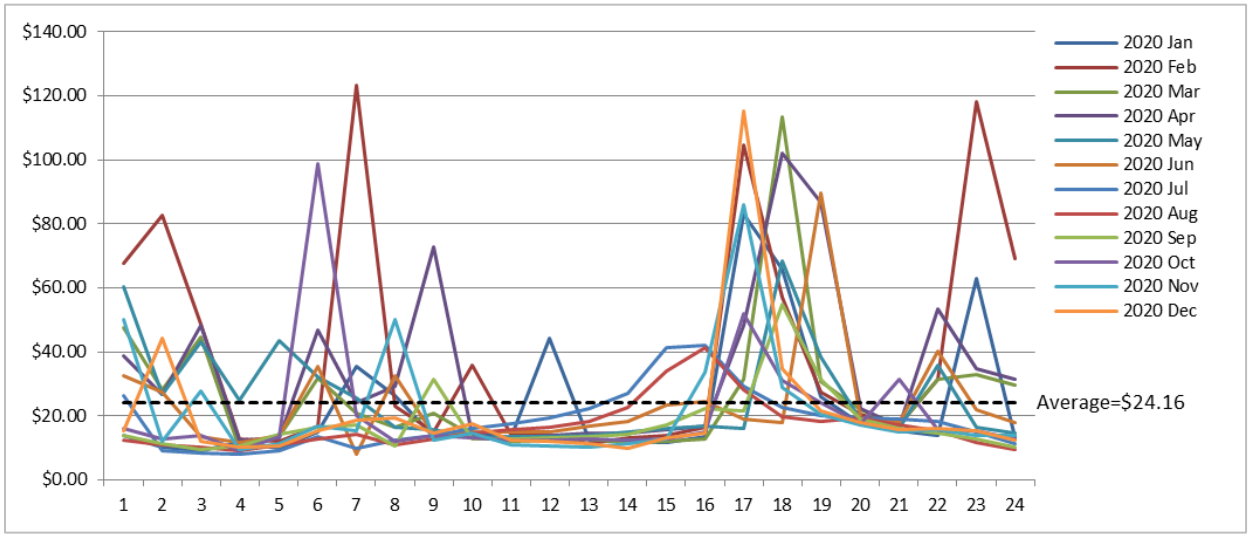
Figure 47: Spinning Reserve Prices by Hour, January – December 2020